Up-scaling of froth flotation equipment

Thesis for a master degree in Resource Engineering at the Delft University of Technology, The Netherlands

07/07/2014
C.R. Boeree

Please print this document in colour for optimal readability.

TUDelft Delft University of Technology

NEW **BOLIDEN**

Challenge the future

Title	:	Up-scaling of froth flotation equipment
Author(s)	:	C.R. Boeree
Date	:	July 2014
Supervisor(s)	:	Dr. M.W.N. Buxton
		Dr. J.H.L. Voncken
Report number	:	AES/RE/14-08
Postal Address	:	Section for Resource Engineering
		Department of Geoscience & Engineering
		Delft University of Technology
		P.O. Box 5028
		The Netherlands
Telephone	:	(31) 15 2781328 (secretary)
Telefax	:	(31) 15 2781189

NEW BOLIDEN

Abstract

The up-scaling of flotation equipment has been investigated based on comparisons between laboratory, pilot and industrial scale flotation tests and a characterization study of large-scale industrial flotation cells in Boliden's Aitik copper mine in Northern Sweden. The use of high volume flotation cells has nowadays become more and more common to deal with the production of high capacity, low-grade open pit mines, which are typically copper or gold mines. Implementation of large flotation cells in the mineral beneficiation process holds several financial benefits, but gives no guarantee of an equal or improved metallurgical performance.

From a historical point of view, flotation plants have been designed based on the results of laboratory tests, multiplied with a time up-scaling factor at which recovery was expected to be above a certain value on the industrial scale. Due to the uniqueness of each ore, such an experience-based factor has often resulted into under- or overestimations of the total required cell volume. One of the main differences between lab and industrial flotation in this research is found the be the behaviour of fine particles (-45 μm), which are shown to have slower flotation kinetics and poor recovery on the industrial scale in comparison to the lab scale, but are also accompanied by a relatively high degree of gangue mineral entrainment in lab tests.

A characterization of the industrial flotation equipment was done to acquire more information on the sub-processes that take place within the cells. Sampling on different depths in 160 m^3 rougher and scavenger cells revealed a well-mixed regime in the lower cell half, decreasing homogeneity above a depth of 2,5 m under the froth, and an accumulation zone of fine-grained copper-rich minerals directly under the pulp-froth interface. The effectiveness of the low-turbulent zone in the top half of the industrial flotation cell is questioned, while the general trend in flotation cell design of increasing volume even shows an increasing height-to-diameter ratio, which could eventually lead to a larger fraction of the cell volume being low turbulent.

To obtain more insight in the functioning of these flotation cell sub-zones, the use of a bubble load measurement is proposed to determine the recovery of both valuable and gangue minerals as a profile of cell height. Furthermore test work in a laboratory pilot scale cell with adjustable height is discussed, in which the volume fractions of the mixing zone, quiescent zone and froth zone can be varied. Combination of these two investigations is expected to allow better understanding of how an industrial flotation cell functions.

Author contact details

C.R. (Ruben) Boeree

Email:
c.r.boeree@student.tudelft.nl
ruben_boeree@hotmail.com

LinkedIn:
https://www.linkedin.com/pub/ruben-boeree/33/9aa/251

List of symbols

A list of the most important symbols used in this research.

C_A — Carrying capacity [-].

C_R — Carrying rate [-].

d_b — Mean bubble diameter [m].

d_{32} — Sauter mean bubble diameter [m].

EF_i — Entrainment factor for size class i [-].

ER — Enrichment ratio [-].

J_g — Superficial gas velocity [m/s].

k_n — n^{th}-order flotation rate constant [1/s].

P — Floatability component [-].

P_{80} — Particles size [μm] at which 80% of the material is smaller than this size.

Q — Flow rate [m^3/s]

$R(t)$ — Recovery as a function of time in batch flotation processes [-].

$R(\tau)$ — Recovery as a function of residence time in continuous flotation processes [-].

R_∞ — Maximum recovery [-].

R^2 — Coefficient of determination [-].

S_b — Bubble surface area flux [1/s].

Greek symbols

ε_g — Flotation cell gas holdup [-].

η — Dimensionless recovery [-].

μ — Dynamic viscosity [Pa·s].

ρ — Density [kg/m^3].

σ — Standard deviation.

τ — Continuous flotation cell residence time [s].

φ_s — Bubble surface coverage [-].

$\psi_{s,x}$ — Dimensionless metal distribution [-] for particle size class s and metal x.

BOLIDEN

List of terms

ANOVA table: Analysis of Variation table; a statistical test to determine if specific data sets are equal or different. More thoroughly explained in appendix C.

Bootstrapping: A statistical method to determine the accuracy in the comparison of sample estimates.

Bubble surface area flux: The rate at which bubble surface area moves through the flotation cell per unit of cell horizontal cross-sectional area.

Carrying capacity: Maximum carrying rate, i.e. the maximum mass transport rate of solids by bubbles per time unit per cell horizontal cross-sectional area.

Carrying rate: Mass transport rate of solids by bubbles per time unit per cell horizontal cross-sectional area.

CFD: Computational Fluid Dynamics; numerical method to analyse fluid flows, for example in flotation equipment.

Cleaner flotation: Stage of the flotation process aiming to reach a final concentrate with an acceptable grade for further processing.

Enrichment ratio: Ratio describing the enrichment of the concerning mineral or metal, defined as the concentrate grade divided by the feed grade.

Entrainment: Particles recovered by the flow of the pulp, instead of selective attachment to air bubbles. Typical for fine particles.

Entrapment: Particles recovered by physical entrapment between air bubbles. Typical for coarse particles.

Factorial design: Statistical method to compare the influence of test variables on the test results.

Factors: Test variables under investigation in a factorial design test.

Flotation rate constant: Constant describing the rate at which the concerning mineral or metal is recovered in the flotation process.

Froth zone: Zone in the top of the flotation cell consisting of froth loaded with mainly valuable minerals, which provides extra separation between valuable minerals and gangue minerals.

Gangue minerals: Unwanted, barren minerals, without valuable mineral or metal content.

Gas holdup: The volume fraction of a flotation cell occupied by gas.

Lip: Top of the flotation cell wall, where concentrate can overflow the cell.

Mixing zone: Zone around the impeller of the flotation cell, in the test work of this research located in the cell bottom.

Quiescent zone: Laminar flow zone of pulp between the mixing and froth zones of the flotation cell, through which loaded bubbles rise to the top of the cell.

Responses: Test results being compared in a factorial design test.

Rougher flotation: First stage of the flotation process, aiming for a low grade of the valuable metal in the tailings, and an acceptable grade for cleaner flotation.

Scavenger flotation: Stage of the flotation process aiming to recover as much valuable minerals as possible.

Superficial gas velocity: A measure of the aeration ability of the flotation cell, defined as the volume of air passing through a certain horizontal cross-sectional area of a flotation cell per unit of time.

Table of contents

List of figures

4. Experimental procedure

5. Experimental results

6. Conclusions and recommendations

List of tables

NEW BOLIDEN

1. Introduction

This research focuses on aspects of up-scaling laboratorial and pilot cell froth flotation tests to a full scale industrial flotation operation and identifying the roots of these differences. It has been performed in the context of a master degree thesis in Resource Engineering at the Delft University of Technology in the Netherlands, and was supported by Boliden Mineral in Sweden.

Boliden Mineral operates in a total of four mining sites, of which three are located in Sweden and one in Ireland (Boliden, 2014). The Garpenberg site, located in the southern part of Sweden, is currently the smallest in terms of production with a yearly ore production of 1,4 million tonnes. The Boliden Area, around the Northern Swedish town of Boliden, has five operating mines, with a total production of around 1,8 million tonnes. Recently also the production of tellurium concentrate was commenced at its processing plant. The Tara mine in Ireland is the largest zinc mine of Europe, and produces roughly 2,5 million tonnes of ore. Finally, Boliden's largest mine is Aitik, a large scale open pit mine located in Swedish Lapland with a production of 37 million tonnes in 2012. A production overview is given in table 1.1, and a map with operations and office locations is given in figure 1.1.

Table 1.1: Boliden's operating mines and their products (Boliden, 2014).

Mining site	Ore production (2013)	Concentrate products
Boliden Area	1809 ktonnes	Cu, Zn, Ag, Au, Pb, Te
Garpenberg	1495 ktonnes	Cu, Zn, Ag, Au, Pb
Aitik	37070 ktonnes	Cu, Ag, Au
Tara (Ireland)	2493 ktonnes	Zn, Pb

Figure 1.1: Boliden operations and office locations (Boliden, 2014).

In 2010 an expansion project at the Aitik mine was completed, which doubled the total capacity of the mine and processing plant from 18 to an estimated 36 million tonnes of ore per year, while 2013 already resulted into a higher mine production. The 2013 concentrate production was 292.000 tonnes, which a metal content of 70.861 tonnes of copper, 54 tonnes of silver and over 2 tonnes of gold. An expansion project is also planned for the Garpenberg site, which will raise the ore production from 1,4 to 2,5 million tonnes. Full capacity is expected to be reached at the end of 2015.

During the last decades, the size of both individual flotation cells and flotation circuits as a whole has encountered a significant change in size, driven by the mining industry's continuous search for lower operational costs, better metal recoveries and a more efficient use of energy. The advance of the flotation process began with the flotation of zinc ore gravity separation tailings in Australia in 1904, with an initial capacity of 46,8 kt per year (Arbiter, 2000). In 2005, it was reported that annually nearly 2 billion tonnes of ore are treated by flotation processes around the world (Yianatos et al., 2005a). This development is accompanied by reducing metal grades in ores, which calls for larger flotation cells in order to meet the demand for high capacities. The use of cells with a larger volume holds several advantages:

1. Lower capital costs for the same effective flotation volume.
2. Lower operational costs; less maintenance, reagent and energy costs.
3. Less floor space required.

Inherently, there are a number of disadvantages that come with larger cell volumes:

1. No guarantee of equal or improved performance; reduced recovery or concentrate grades can quickly nullify the capital and operational costs saved by the choice for larger cells.
2. Poor operation of a certain cell has a larger effect on overall flotation performance.
3. A higher chance of valuable mineral particles reporting to the tailings due to 'short-circuiting' within the flotation cell, i.e. floatable particles from the feed by-passing to the tailings without being floated. With more cells in a bank, the chance is higher that these particles will be floated in the subsequent cells, before ending up in the bank tailings.
4. Less cells often translates into less flotation banks. When a bank of flotation cells has to be shut down, for example due to mill maintenance, the negative effect on production will be larger.

Figure 1.2 gives the maximum flotation cell volumes at several points of time since 1972. The numbers until 1998 were reported by Arbiter in 2000, who states that there is a minimal number of 12 flotation cells in a bank to sufficiently avoid short-circuiting of flotation feed. This would limit the maximum volume of flotation cell to the 100 to 200 m^3 range.

However, advancing technology allowed the further increase of cell volume, and also a reduction in the number of cells per bank. The introduction of round instead of square flotation cells came in the 1990s to reduce production costs of large cells (Euston, 2011). Cells with an effective volume of 300 m^3 are now common practice at the concentrators of Codelco in Chile, the world's largest copper producer (Yianatos et al., 2010a). In 2012 FLSmidth launched the SuperCell-600 series (Govender et al., 2014), the largest flotation cell type currently on the market, with an effective volume of 660 m^3 in the largest model.
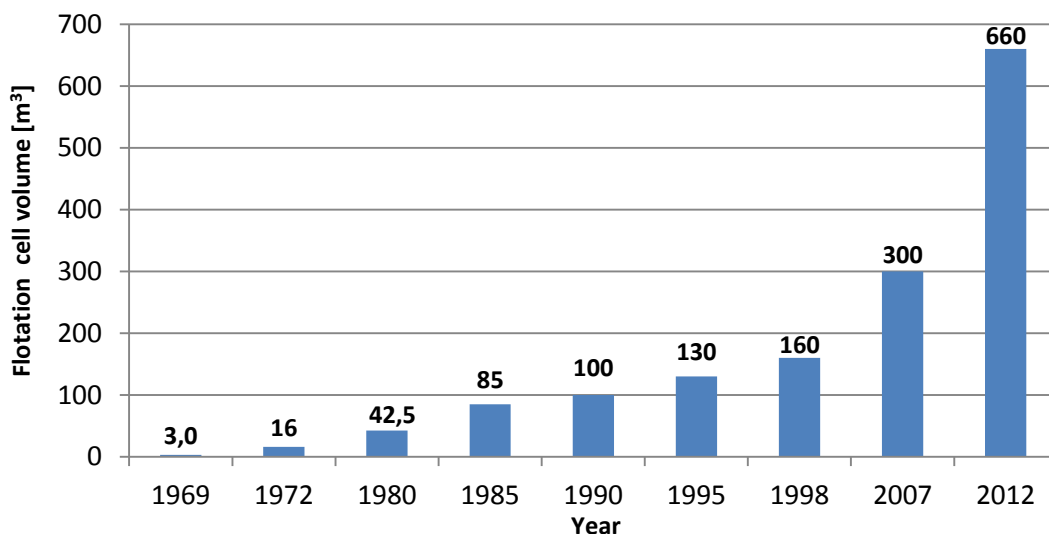
Figure 1.2: Largest available mechanical flotation cell volumes on the market since 1972. (Arbiter, 2000; Govender et al., 2014).

1.1 Motivation

To secure the future of Boliden as a company, continuous exploration and feasibility studies are done to investigate mining possibilities on new locations. Part of these feasibility studies is the mineralogical research, in which the methods to process the ore into an adequate concentrate are examined. Since Boliden's operations are focussed on sulphide ores, froth flotation is the main concentrating method used in the processing plants.

Laboratorial batch flotation tests can be performed in order to estimate the behaviour of a full scale flotation operation. The obtained results can be used to enlarge the test work to a pilot plant, and eventually to design the full scale operation. However, experience has shown that lab tests give distinctly better results than for the same material in an industrial operation. Especially the recovery of the valuable metal is faster and higher than what can be expected from an industrial flotation cell. This makes it especially complicated to scale-up the flotation results and estimate the proper total cell volume requirements and cell arrangements for the design of a new processing plant. Additionally, the application of even larger industrial cells brings mining companies into an unfamiliar area where the effects and consequences of further up-scaling are relatively unknown.

Publication of previous research on the up-scaling of flotation cells in public sources is relatively limited, while also confidential research by companies working in the field of mineral processing is suspected to be small. One explanation for the lack of research is the separation of mining companies and flotation equipment manufacturers. Most mining companies have less advanced research capabilities or a limited influence on the design of flotation equipment, whereas manufacturers do not own mines where detailed phenomena for different types of ore in their equipment can be tested and characterized. In addition, the largest flotation cell models are generally only used at high capacity open pit mines with low metal grades, which are typically copper and gold deposits.

From a historical point of view, an experience-based time factor in the order of 2 to 4 is often mentioned to scale-up from batch flotation kinetic rates to a full-scale operation. Such a factor is however strongly situation dependent and an especially risky estimation in case of a greenfield project. Additionally, the performance of industrial flotation equipment is hard to measure since the feed grade and mineralogy frequently changes, and performance measurements have to be done over a multitude of cells. The tendency is to over-dimension flotation plants to account for situations like an increased throughput, for example in times of high metal prices or a better than expected mine production, inexperienced operators, or to be "on the safe side". However, in some cases this has led to large sections of the flotation plant to become stand-by, causing unnecessary capital and operational expenses. This emphasizes the need for a substantiated and confident up-scaling methodology.

1.2 Research questions

A well-known feature in mineral processing is that each ore is unique, and processing results can practically never be copied to another ore. Therefore it is expected that no single 'factor' exists that can directly predict the results of an industrial operation, based on laboratorial test work. The main research question is defined as:

How can a better estimation of industrial flotation performance be made based on lab tests?

Since experience has shown that for the same feed material the rate at which the valuable minerals float is slower on an industrial scale, it appears that certain variables are changed during up-scaling and cause the results to the different. A better understanding of these variables may help to either perform lab test work in a different way to obtain a better estimation, or look at flotation as a combination of several sub-processes that all influence the results instead of one process as a whole. The first partial research question is therefore defined as:

1. What causes the differences in results between laboratory and industrial flotation?

The flotation process is known to involve several sub-processes that each have their own influence on the total cell performance, such as the attachment of minerals to air bubbles, transport of the loaded bubbles through the pulp, and the recovery of minerals by the froth zone. Since the functioning of these and other sub-processes may vary on different scales, the second partial research question is defined as:

2. What are the influences of the different sub-processes of the flotation cell on its performance?

Furthermore, it is likely that future Boliden operations will operate with larger cells than the currently largest cell of 160 m³ at the Aitik mine. During the construction of new processing plant it has to be considered if a larger, unfamiliar cell type, or if a familiar model that has been applied before will be used. A larger model will have its own way of operation and it will be useful to know what the consequences of using a larger cell type can be. Considering that the volume of individual flotation cells has strongly grown over the last decades, this leads to the third and final partial research question:

3. What could happen during further up-scaling of industrial flotation cells?

1.3 Aim and objectives

The aim of this research is to find the causes of the differences in flotation results between an industrial flotation circuit and laboratorial test work, with the underlying objective of making a better estimation of industrial flotation performance. A more accurate estimation will be valuable during the design of a new processing plant for future operations. Since many different ores exist and results will be different for each ore, a practical methodology will take years to develop and this research can only be a small part of the entire picture. Therefore it is also meant as a starting point for further research, in which the differences between lab and industrial flotation can be tested for other ores. Furthermore, once specific phenomena on the industrial scale are found, specialized measurements can be done to provide more insight as to why these phenomena occur, and how they can be predicted or prevented.

A total of three objectives has been determined for this research:

1. Identify any kind of differences in flotation cells of increasing sizes, such as segregation phenomena or dissimilar behavior of particles of different sizes.
2. Make a theoretical prediction of the possible consequences of further up-scaling.
3. Provide a basis for further research on the specific phenomena that are identified as the causes of varying flotation results.

These objectives all serve to answer the main research question on how a better estimation of an industrial flotation circuit can be made. Figure 1.3 gives an overview of the relations between the objectives and the previously given research questions.

1.4 Hypothesis

It is expected that the performance of flotation cells on the industrial scale is strongly influenced by consequences of its size, such as the longer transportation distances from the impeller zone to the froth zone, and through the froth zone into the concentrate launder. The laboratory cell is suspected to be more homogeneous in the pulp zone and has a relatively thin froth layer, leading to a fast recovery of the valuable minerals. Previous internal research by Boliden has also shown segregation of magnetic minerals in desulphurization flotation cells at the Aitik mine, and such segregation phenomena are expected to exist in the copper flotation cells and possibly to obstruct the cell´s performance.
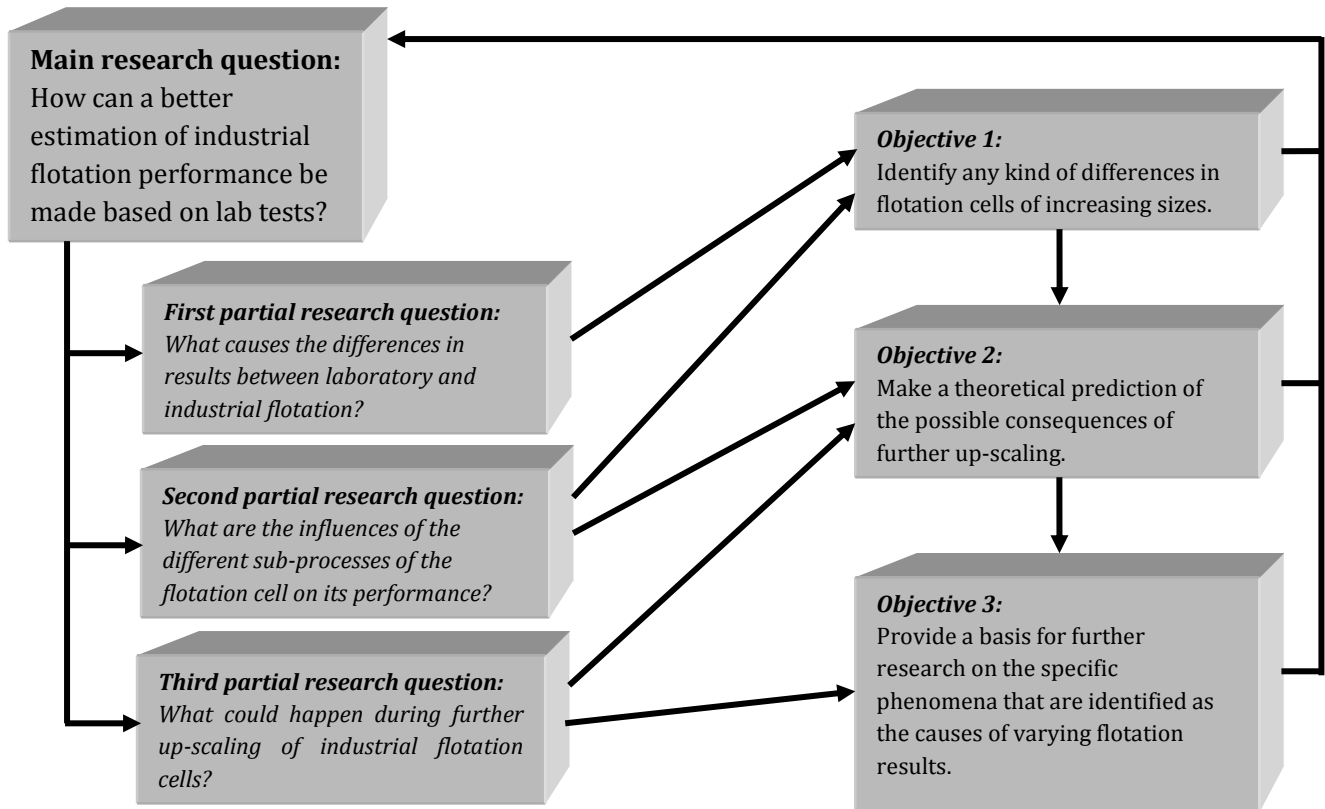
Figure 1.3: Relations between the research questions and objectives.

1.5 Report outline

The structure of this report is given in figure 1.4. Chapter 2 will cover the essential theorical background and modelling methods of the flotation process. Chapter 3 covers several aspects of flotation up-scaling. Firstly, different cell designs and their influence on the process are explained, including an explanation of the different zones that are normally distinguised in a flotation cell. Next, the available research that has previously been done on up-scaling is covered. Finally, the expansion method that has been used at the processing plant of the Aitik mine is shown. Chapter 4 gives the experimental procedures of this research, and the results are shown in chapter 5. The experiments are sub-divided into the following four sections:

- A comparison of laboratorial flotation tests in different cells, to find differences on a small scale.
- A factorial design of laboratory test operating parameters, to determine the influence of operating parameters on lab test results.
- A characterization of the industrial flotation cells at the Aitik mine; to identify possible segregation phenomena that may influence the cell's performance.
- A simulaneous test work in a lab cell, pilot cells and industrial cells, to directly compare flotation results and eliminate any influence of variation in the feed material.

Finally, chapter 6 will give conclusions based on the test work of chapter 5, and a number of recommendations for future test work.
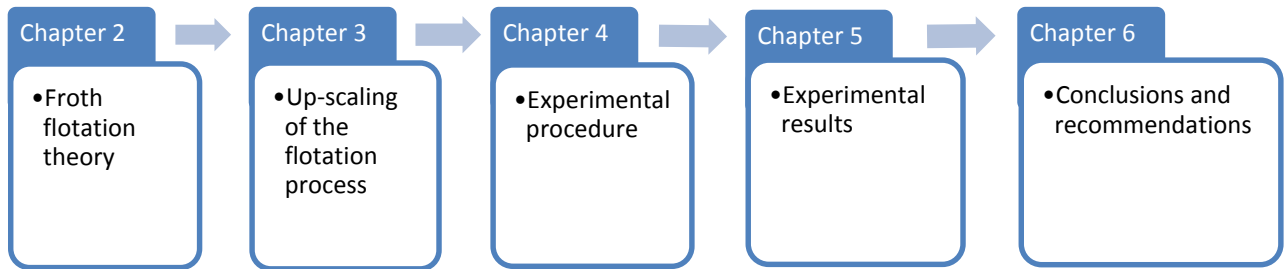
Figure 1.4: Structure of this report, with the subjects of each chapter.

1.6 Research and scope

The test work in this research on up-scaling has been done on a relatively coarse grained porphyry copper ore, and results may well be different for other ore types. Also the type of flotation cell will have an important influence on any findings, thus this research is limited to conventional bottom-driven flotation cells. Table 1.2 gives an overview of what is included in and excluded from this research.

Table 1.2: Research scope and limitations.

Subject	Included	Excluded
General		
Ore type	• Aitik porphyry copper ore (relatively coarse grained).	• Finer ores, and ores of different genesis and commodities
Flotation cell types	• Conventional bottom-driven flotation cells.	Unless otherwise indicated: • Centre- or top driven flotation cells. • Self-aerating cells. • Flotation columns.
Analytical methods	• Sieving for size-by-size analysis and particle size distributions. • X-ray fluorescence (XRF). • Density pycnometer.	• Qemscan / MLA (due to a time limitation). • Microsieving / cyclosizer
Experimental work		
Laboratory batch flotation (sections 4.1 & 5.1)	• Any differences in metal recovery, metal grades and concentrate particle sizes as a result of the flotation cell size.	• Sampling inside the batch cell itself. • Influence of lab test operating conditions.
Factorial design (sections 4.2 & 5.2)	Influence of the • lab cell size, • grinding time, and • pulp weight percentage solids on the lab test flotation results.	• Influence of all other operating conditions.
Characterization study of industrial flotation equipment (sections 4.3 & 5.3)	• Sampling of the cells to investigate segregation and enrichment phenomena as a profile of depth. • Gas holdup measurements.	• Bubble surface area flux measurements. • Bubble load measurements. • Turbulence and energy dissipation measurements.
Comparison of lab, pilot plant and industrial plant flotation results (sections 4.4 & 5.4)	• Recovery calculations of copper minerals and sulphide minerals in general for different size classes. • Water recovery and entrainment calculations.	• Behaviour of ultrafine particles (45 µm is the smallest split size). • Comparison of hydrodynamic conditions.

2. Froth flotation theory

2.1 Fundamentals of froth flotation

Froth flotation is a vital method for the physico-chemical separation of mineral particles, based on the differences in surface properties of the valuable and unwanted particles to be separated (Wills, 2006). The method was first applied in 1904 in Australia (Arbiter, 2000) and has permitted the mining of ore bodies with low metal grades and complex mineralogies, which would otherwise have been considered uneconomical. Flotation is not only common in the mining industry, but also has its applications in industries like wastewater treatment and recycling, for example the de-inking of paper.

The basis of flotation lies in differences in wettability of the valuable and gangue minerals. In normal flotation air is bubbled through the suspension of water and mineral pulp, where the water-repellent, *hydrophobic* minerals will attach to the air bubbles and float to the surface, while the water wettable, *hydrophilic* minerals will sink to the cell bottom. The froth layer on the top surface will consist of a concentrated product of valuable minerals. Coal is an example of a naturally hydrophobic material, but for most industrial applications chemicals are used to induce hydrophobicity to the surface of the valuable minerals.

According to Wills (2006), the recovery of material from the feed pulp consists of three mechanisms:

1. Selective attachment to air bubbles (also called 'true flotation').
2. Entrainment, generally of the finer particles, in the water which passes through the froth zone.
3. Physical entrapment between particles in the froth attached to air bubbles.

Of these three mechanisms, the attachment of valuable minerals to the air bubbles plays the most important role in the recovery to the concentrate. Whereas true flotation is based on mineral surface properties, both gangue and valuable minerals can also be recovered by entrainment and entrapment. This is the main reason why a single flotation stage is insufficient, and several stages, known as 'circuits' are needed to reach the desired grade and recovery of the valuable mineral.

Evidently, the metal grade is decreasing when recovery is improved, since an extra fraction of the gangue minerals will end up with the concentrate. Identically, improving the metal grade will reduce the recovery since more valuable minerals end up in the tailings. For this reason most concentrators aim for a fixed acceptable metal grade for smelters and aim to improve the recovery for this grade.

Basic flotation circuits consist of a number of cells in series, also called a *bank*. The output of the milling circuit enters the first flotation cell, generally after classification by hydrocyclones or spiral classifiers and a conditioning tank for mixing with reagents and recycle streams in between. In the first cell part of the valuable minerals is collected in the froth and overflows the cell as concentrate. The remainder of the pulp continues to the next cell, where more valuable minerals are removed, and this continues until the remaining pulp in the last cell is discharged as tailings.

Most flotation plants are divided into at least three banks (Wills, 2006). The new feed enters the *roughers*, where the objective is to create a low grade tailing and a concentrate of acceptable grade for the next stage, the *cleaners*. This is generally achieved by allowing a large retention time, mainly depending on the slow floating particles. In the cleaners the main objective is to reach the target grade, while keeping the cleaner tailings as low grade as possible. These tailings are most often recirculated to the rougher feed, while the cleaner concentrate forms the final flotation concentrate. The tailings of the roughers are fed to the *scavengers*, where recovery is maximized by removing as much valuable minerals as possible. The scavenger tailings form the final flotation tailings, or continue as feed for a subsequent flotation process that is optimized to recovery another valuable mineral. Scavenger concentrate and cleaner tailings often contain many insufficiently liberated *middling particles*, which can be reground to liberate the minerals and more efficiently separate gangue from valuable minerals. Figure 2.1 gives an example of a simple flotation circuit consisting of roughers, scavengers and cleaners.
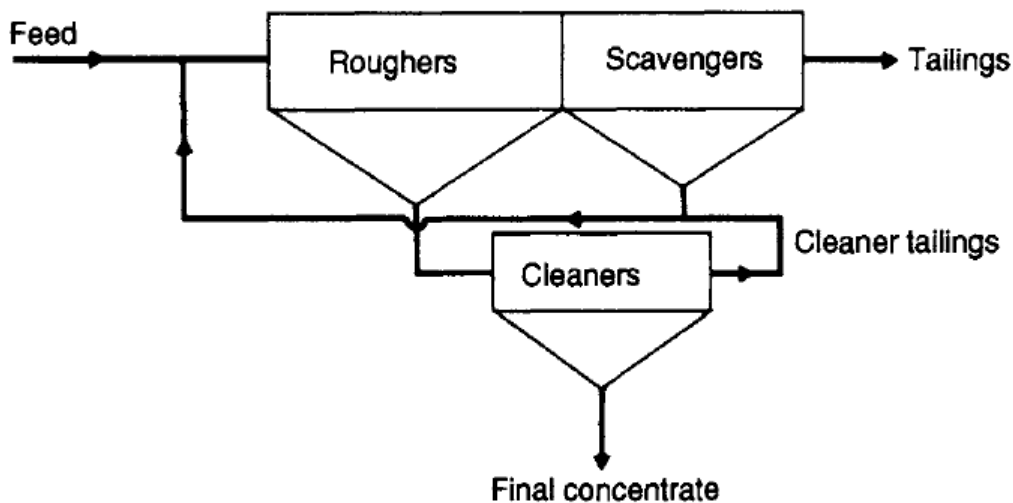
Figure 2.1: Example of a basic flotation system with roughers, scavengers and cleaners (Wills, 2006).

The pulp level of flotation cells is an important operational parameter, since this directly controls the froth thickness and the froth is able to reject entrained or entrapped gangue minerals from the concentrate, as mentioned previously. A thicker froth allows more gangue minerals to be released from the air bubbles back into the pulp since the residence time of the particles in the froth is longer. A thicker froth will therefore improve the concentrate grade, but reduce recovery, since also more middling particles are rejected. The first cells of a bank generally have thicker froths as there are plenty of hydrophobic minerals to float. Cleaner cells have relatively thick froths in order to increase the final concentrate grade, whereas scavengers have thin froths to maximize recovery.

2.2 Copper ore flotation

The introduction of froth flotation as a method to efficiently separate sulphide minerals has had an enormous impact on the production of copper, since it has provided a method of concentration for chalcopyrite ($CuFeS_2$), the most abundant copper ore mineral. Before froth flotation copper was mainly won from oxide minerals in the oxidized zones of ore bodies (Wills, 2006). These deposits were often high-grade, with sometimes even over 5% of copper, but relatively small scale. The majority of the current copper production originates from porphyry chalcopyrite deposits, which consist of disseminated veins of enriched ore zones. These veins are formed by hydrothermal activity during the cooling of magma to rock. The most obvious example is the Chilean copper industry, which accounts for approximately 35% of the world's production (Yianatos et al., 2003). Common by-products of porphyry copper deposits are molybdenum, silver and gold. By-products often play an important role in copper production, as the expenses for the large-scale mining operations and high-tonnage concentrating processes are high in comparison to most other metals. Even low grades of gold or silver can have a strong impact on the profitability of the mine.

Besides chalcopyrite, copper sulphide minerals like bornite (Cu_5FeS_4), chalcocite (Cu_2S) and covellite (CuS) can occur in an ore body. Copper sulphide minerals are known to respond well to anionic collectors, of which xanthates are by far the most used in the industry, with a market share of around 83% (Wills, 2006). Lime is used to control the alkalinity of the solution and depress pyrite (FeS_2).

2.3 The kinetics of flotation and methods for modelling

The kinetics of flotation on all scales ranging from laboratory batch cells to full-scale industrial cells are affected by many factors in the flotation system, of which the most prominent are (Wills, 2006):

- Reagent type and dosage
- Eh/pH system
- Hydrodynamic conditions in the cell
- Air flow rate
- Bubble size and distribution
- Particle size and distribution
- Ore mineralogy and degree of liberation

To express the transferring rate of a floatable particle transfer into concentrate per unit of time, the *rate equation* is commonly used. The rate equation for the flotation process is expressed as:

$$\frac{dW}{dt} = -W^n \cdot k_n \tag{2.1}$$

in which W is the weight of floatable material left in the flotation pulp after time t, n is the order of the reaction, and k_n is the nth-order rate constant (Wills, 2006).

The majority of researchers classify flotation as a first order process, although it has also been classified as a second order process in the case of fluorite flotation (Mori, 1985). For copper ore flotation, Dowling et al. (1985) attempted to fit thirteen models to laboratory test data, for which the first order models showed the best fit. Also Yianatos et al. (2010a) compared several flotation rate models by applying these to batch and plant tests of low-grade copper ore flotation at Codelco's El Teniente mine in Chile. It was found that the first order rate equation gave a suitable fit for both processes, although other models were also found to be applicable. Since this research deals with copper ore flotation, the process will be regarded as first order from here on. According to Burstein and Filippov (2010) a first order model is valid under the assumption that particles do not 'compete' for space on the bubble surface, and the system is steady-state. The first order recovery equation can be expressed as:

$$R(t) = R_\infty \cdot \int_0^\infty \int_0^\infty (1 - e^{-kt}) \, F(k)E(t) \mathrm{d}k \mathrm{d}t \tag{2.2}$$

in which $(1 - e^{-kt})$ represents the recovery of the floatable mineral according to a first order process as a function of time, $F(k)$ represents the kinetic distribution function for mineral species with a different flotation rates, and $E(t)$ is the residence time distribution function for continuous processes with different mixing characteristics (Polat and Chandler, 2000). The constant k is known as the *first order flotation rate constant*, given in 1/s. For batch flotation tests equation 2.2 is often simplified by considering a single, non-distributed rate constant for the whole ore sample and therefore using the Dirac delta function, giving $F(k) = \delta(k)$. By definition the residence time in batch flotation is not distributed, thus obtaining $E(t) = \delta(t)$. Evaluating the integral of equation 2.2 gives:

$$R(t) = R_\infty \cdot (1 - e^{-kt}) \tag{2.3}$$

in which $R(t)$ stands for the recovery at time t, and R_∞ for the maximum recovery (for $t = \infty$). However, equation 2.3 is an averaged function, since flotation kinetics are distributed over different particle sizes, particles with different degrees of liberation, different mineralogies, et cetera. A multi-component model derived from equation 2.3 was given by Imaizumi and Inoue (1965):

$$R(t) = R_\infty \cdot \sum_{i=1}^n m_i \, (1 - e^{-k_i t}) \tag{2.4}$$

9

in which m_i is the mass fraction of the floatability component i, and k_i is the first order rate constant of this component. Another recovery model assuming perfect mixing is most commonly used for full scale flotation processes, based on the continuous process residence time τ (Imaizumi and Inoue, 1965):

$$R(t) = R_\infty \cdot \left(\frac{k\tau}{1 + k\tau}\right) \tag{2.5}$$

This model was found to be more applicable for continuous processes since only a small fraction of the total material leaves the cell as concentrate overflow at the top. Like in equation 2.4, the flotation kinetics are distributed, and the equation can be rewritten for a continuous flotation process as:

$$R(t) = R_\infty \cdot \sum_{i=1}^{n} m_i \left(\frac{k_i \tau}{1 + k_i \tau}\right) \tag{2.6}$$

Another multi-component floatability model was proposed by Kelsall (1961), who splits equation 2.3 into a fast and slow floating component:

$$R(t) = (1 - \varphi)\left(1 - e^{-k_f t}\right) + \varphi\left(1 - e^{-k_s t}\right) \tag{2.7}$$

in which k_f and k_s are the rate constants for the fast and slow floating components, respectively, and φ is the mass fraction of slow floating components. No term for maximum recovery is taken into this equation, and thus it assumes that eventually all of the valuable minerals are recovered as a slow floating component for infinite time. Jowett (1974) multiplied equation 2.7 with a maximum recovery term, but this often leads to a negligible slow floatability component ($k_s \to 0$ for $t \to \infty$) and thereby virtually obtaining equation 2.3. This can be prevented by assuming that k_s is, for example, one tenth of k_f ($k_s = k_f/10$), although this assumption is not based on any experimental findings.

Another approach is for selecting fast and slow floating components is by appointing the collected concentrate before and after a certain time period as fast floating and slow floating, respectively. Runge (2010) proposed a multiple stage batch flotation process in which 0 to 2 minutes is performed under rougher conditions, and 2 to 8 minutes under scavenger conditions. The 'rougher' concentrate is then refloated under cleaner conditions. The mineral content of the cleaner concentrate, combined scavenger concentrate and cleaner tailings, and scavenger tailings is denoted as fast, slow and non-floating, respectively.

Although certain models fit reasonably well to batch flotation, the predictive power towards industrial flotation is most often poor. Heiskanen (2013) noted that some of the problems arise from the assumptions that are made, such as k being time independent while chemical conditions may change with time, and the reaction volume being constant while it may change slightly in reality.

In a stable flotation operation with more or less constant operation and chemical conditions, the particle size and degree of liberation of the valuable minerals have the largest influence on the flotation kinetics (Wills, 2006). Particle size is the main factor influencing downward gravitational force and is known to have several other effects on flotation (Kowalczuk et al., 2010), which will be explained more thoroughly in section 2.4. The degree of liberation refers to the fraction of the valuable mineral in the ore that is present as free particles in relation to the total valuable mineral content (Wills, 2006), and is strongly dependent on the combination of ore type and grind size.

Before the introduction of analysis methods like Qemscan and MLA, measurement of particle liberation was not possible, and thus its influence could not be related to flotation kinetics. Jameson (2012) proposed an empirical flotation liberation function to relate flotation kinetics to the liberation of minerals:

$$L = axe^{bx^c} \tag{2.8}$$

in which L is the ratio of the rate constant for a given particle size and liberation class and the rate constant for a fully liberated particle in the same size class ($L = k/k_{max}$), x is the fractional liberation ($0 \leq x \leq 1$), and a, b and c are constants to fit the model. Figure 2.2 gives rate constant curves for various liberation classes as a function of particle size. Note the logarithmic scales on the axis; the rate constants of the fully-liberated particles are in many cases several orders of magnitude larger than the badly liberated particles.
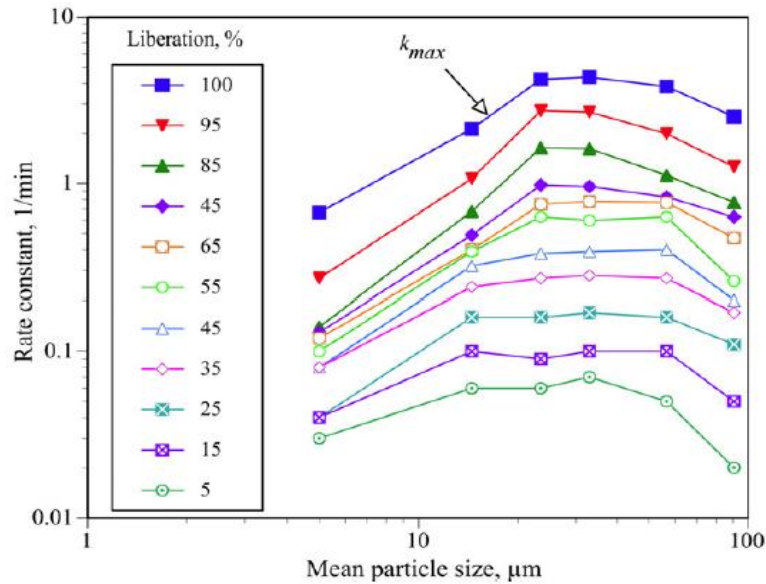
Figure 2.2: Flotation rate constants as a function of particle size
for different liberation classes (Jameson, 2012).

Apart from the time-dependent approach of flotation performance, a number of researchers prefer a probabilistic approach to determine the rate constant. Lambert (2003) states that *"the concept of residence time is wrong, flotation is a probability exercise and the frequency of particle bubble collision controls the performance"*. Since the use of this approach is very limited in literature, based on many assumptions and requires measurement techniques unavailable in this research, it will not be further discussed. Additional reading and a practical example are available from Derjaguin and Dulkin (1961) and Duan et al. (2003), respectively.

2.4 Gas dispersion in flotation cells

The role of the air bubbles in a flotation cell has been reported to be one of the most critical components in the science of flotation (Wills, 2006). In the first place this is influenced by the cell design, which sets the basis for the hydrodynamic conditions, dispersion regime and turbulence inside the cell. During operation, several factors have a direct influence on gas dispersion, for example the air flow rate, impeller speed and frother type and concentration. Frother lowers the surface tension of the solution and therefore generally allows smaller bubbles. The effect of gas dispersion is often represented in relation to the first order rate constant*:*

$$k = P \cdot R_f \cdot S_b \tag{2.9}$$

in which k stands for the first order rate constant [1/s], P stands for the floatability component [-], R_f stands for the froth recovery [-], and S_b stands for the bubble surface area flux [1/s].

The floatability (P) is a dimensionless parameter that represents the ability to float of a certain component in the ore, and is found by fitting equation 2.9 to test results. The froth recovery is defined as the mass fraction of floatable particles that pass into the froth at the pulp-froth interface, which is transported to the concentrate (Ata, 2012). The bubble surface area flux is the rate at which bubble surface area moves through the flotation cell per unit of cell horizontal cross-sectional area. One can measure this value directly in a cell, by regarding the superficial gas velocity and the mean bubble size:

$$S_b = 6 \cdot \frac{J_g}{d_b} \tag{2.10}$$

in which J_g stands for the superficial gas velocity [m/s], and d_b stands for the mean bubble diameter [m].

The superficial gas velocity represents the velocity at which gas moves upward in a flotation cell and is a measure of the aeration ability of a cell. It has been reported to have a direct influence on flotation kinetics, for example by Ahmed and Jameson (1989). When J_g is too high, the entrainment of unwanted material into the concentrate is increased and the stability of the froth-pulp interface is reduced.

Collisions between particles and bubbles are also affected by the size of the particles in relation to the bubbles. Too small bubbles will not have enough buoyant force to raise the particle to the top of the cell, while too large bubbles result into a lower total number of bubbles, and a more turbulent fluid regime around the bubble that prevents attachment (JKTech, 2007). Therefore each particle size distribution will have a corresponding optimal bubble size distribution for flotation purposes.

The most commonly used measure for the mean bubble diameter is the Sauter mean bubble diameter (d_{32}), defined as the diameter of a sphere with the same volume/surface area ratio as the bubble of interest. Smaller bubbles can generally be produced by increasing the impeller rotation speed in air-induced cells, or by increasing frother dosage to reduce the surface tension of the pulp.

Flotation cell gas dispersion is additionally characterized by the gas holdup (ε_g), which is the volume fraction of air within the flotation cell. Gas holdup is often represented globally, i.e. over the whole cell volume, or locally in a certain location within the cell. In an ideally mixed cell the global and local values should be equal at the same depth. A higher gas holdup increases flotation kinetics due to the higher air volume per unit of cell volume, up to certain point where the slurry residence time is too negatively affected. The relation between the gas holdup and superficial gas velocity is given by (JKTech, 2007):

$$J_g = v_g(z) \cdot \varepsilon_g(z) \tag{2.11}$$

in which $v_g(z)$ stands for the rising velocity of bubbles at depth z in m/s. The superficial gas velocity can also be related to the air flow rate and cross-sectional area of the cell:

$$J_g = \frac{Q_{air}}{A} \tag{2.12}$$

in which Q_{air} stands for the air flowrate in m³/s, and A for the cell's cross-sectional area in m². Note that these are global values; the local superficial gas velocity can differ per location in a cell.

2.5 Influence of particle size on flotation performance

The particle size of minerals is an important influence on the flotation process. In general, a too large particle size will signify insufficient liberation of the valuable minerals, and the particles may be too heavy for bubbles to lift. Too small particles will lead to increased entrainment of gangue minerals, increased oxidation of the mineral surface, possible slime coating of mineral surfaces, and high costs for grinding and reagents consumption.

With increasing energy costs, especially for the grinding process, recovery of minerals at a coarser size range can have a significant beneficial effect on operational costs. The primary condition to make a particle float is that the attractive forces between particle and bubble have to be greater than the detachment forces. This leads to a certain size limit above which a particle is no longer floatable, because downward forces like gravity and inertia become too large. Kowalczuk et al. (2011) derived equation 2.13, which gives the maximum size of a floatable particle:

$$d_{max} = \sqrt{\frac{6\sigma \cdot sin^2\left(\frac{\theta_d}{2}\right)}{(\rho_p - \rho_l)g + \rho_p a}} \qquad\qquad (2.13)$$

in which d_{max} stands for the maximum diameter of a floatable particle, σ stands for the surface tension of the liquid, θ_d stands for the detachment contact angle, ρ_p and ρ_l stand for the density of particles and liquid respectively, g stands for the gravitational acceleration, and a stands for the acceleration of the particle. The detachment contact angle is determined by the hydrophobicity of the mineral surface, and can thus be influenced by reagents, as well as the liquid surface tension.

The response of minerals to the chemical environment has also been shown to change for different particle sizes. Trahar (1981) reported a higher sensitivity to changes in the pulp acidity for coarse particles than for fine particles. Crawford and Ralston (1988) performed tests on flotation of quartz of various particle sizes, and reported that coarse particles require a significantly larger fraction of the surface covered by collector than fine particles at the same recovery.

Furthermore, particle size influences the behaviour of the froth phase. Szatkowski and Freyburger (1985) reported that fine quartz particles increase the stability of the froth, whereas Tao et al. (2000) reported strong froth-destructive behaviour for coal particles under 30 μm. The physical and chemical causes behind these phenomena were not well understood, but the researches agree that a particle range exists at which froth stability is optimal.

Rahman et al. (2012) investigated the effects of operational flotation variables on the recovery of different particles size fractions of silica in a flotation column, with dodecyclamine as a collector. The recovery of coarse particles from the pulp zone was improved by increasing collector concentration, while the recovery in the froth zone was greatly reduced due to a destabilized froth phase, leading to an overall decrease in recovery of coarse particles. Collector concentration did not significantly influence fine particle recovery. An increase of the air flow rate improved coarse particle recovery and did not significantly influence fine particle recovery.

A notable result was that the presence of fine particles is essential for a good recovery of coarse particles in both the froth zone and collection zone. This effect is shown in figure 2.3. The froth stability is improved by the presence of fine particles due to reduced bubble coalescence and thus the preserving of more bubble surface area. Coarse particles on the other hand can rupture bubbles due to their higher mass. Also in the collection zone is the recovery of coarse particles enhanced by the presence of fine particles. The suggested reason for this is that fine particles on the surface of bubbles are able to stabilize the air-liquid interface by restricting the three phase contact line, and thereby reduce bubble deformation or break-up.

NEW BOLIDEN
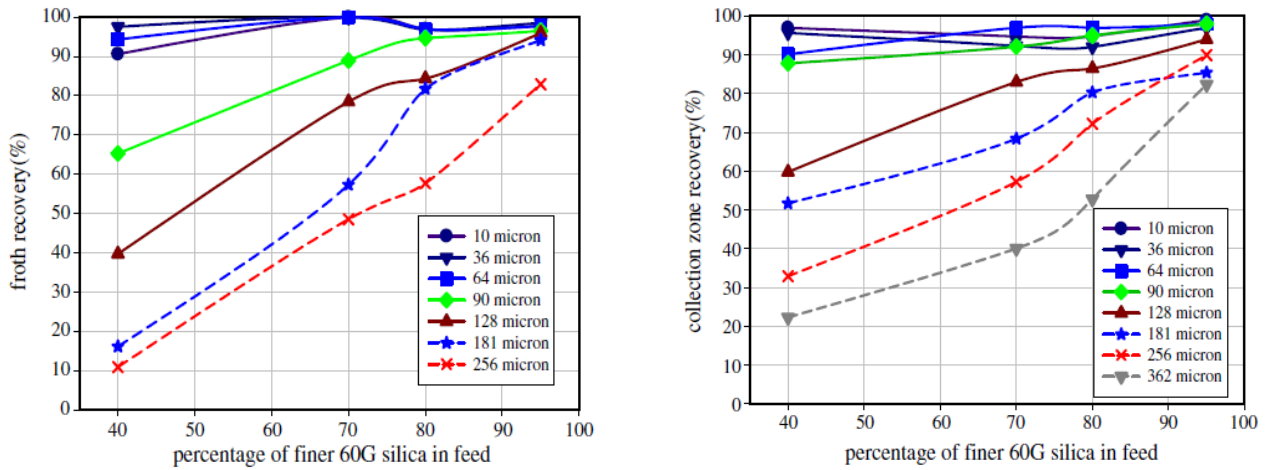
Figure 2.3: Recovery of different particle sizes of silica as a function of the percentage of 60G silica (P_{80} = 72 µm) in the froth zone (left) and pulp zone (right) of a flotation column (Rahman et al., 2012).

Ata and Jameson (2013) investigated the recovery of coarse particles in the froth of chalcopyrite flotation. A specially designed continuous operation flotation cell with a diameter of 300 mm was fed with feed material of the industrial scale rougher and cleaner banks, with P_{80} values of 220 and 76 µm respectively. Cleaner bank feed is introduced into the pulp zone of the flotation cell, and bubbles loaded with particles are guided to a froth column. Any particles washed down in the froth are collected in a dropback lid. Rougher bank feed is introduced to the top of the froth zone. The design is shown in figure 2.4.
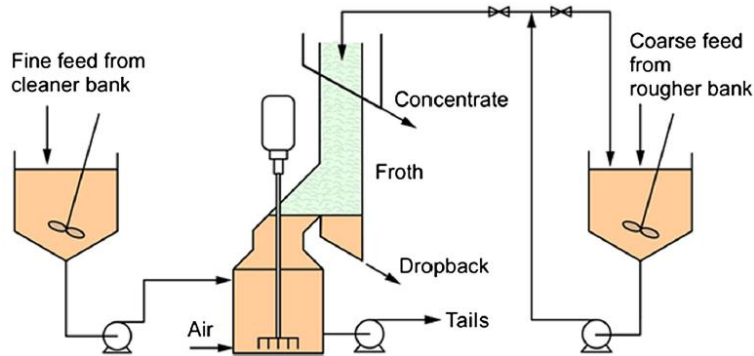
Figure 2.4: Test apparatus used for coarse particle flotation by Ata and Johnson (2013).

The results indicated that the superficial gas velocity plays an important role in the recovery of copper. At lower superficial gas velocities, the recovery of copper to the dropback lid was significantly higher, proving that the froth recovery for copper was poor. The size of coarse particles introduced into the froth did affect the copper recovery for this feed, although for 200 µm particles the recovery was still only 38%, versus a recovery of 50% for particles of 100 µm.

14

2.6 Water recovery and particle entrainment

The recovery of water is generally defined as the fraction of the water input to a flotation cell that is recovered in the concentrate (Zheng, Franzidis and Johnson, 2006). Water recovery is an important parameter in the design and operation of flotation plants, since it strongly affects recirculating loads and residence times. At the same time it affects entrainment of gangue minerals into the concentrate. The entrainment of unwanted minerals through the froth zone in flotation cells can be a problematic factor to reach a concentrate of a sufficient metal grade, while maintaining an acceptable recovery. The phenomenon is affected by many factors, of which the most important is particle size, besides the already mentioned water recovery (Savassi et al., 1998). Smaller particles are more easily caught in the upward flow of the quiescent zone due to their lower downward gravitational force, and end up in the froth zone. However, also the froth structure and froth residence time play an important role.

$$ENT_i = \frac{mass\ flow\ of\ entrainment\ to\ concentrate}{mass\ flow\ of\ water\ to\ concentrate}$$

in size class i
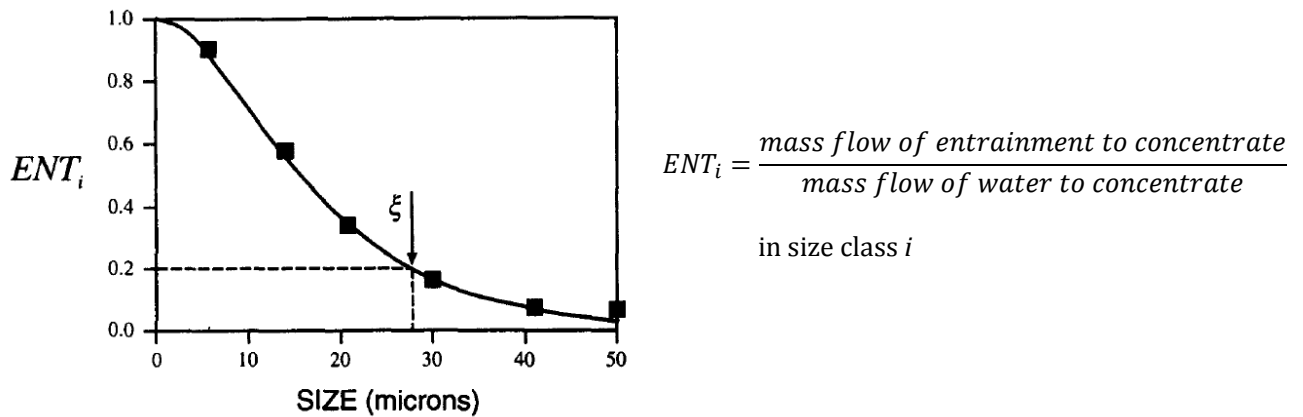
Figure 2.5: Empirical partition curve for entrainment (Savassi et al., 1998).

A stable froth enhances entrainment due to a lower degree of drainage back into the pulp zone, whereas a longer froth residence time allows more detachment of unwanted material before the froth flows into the launder (JKTech, 2007). Entrainment can be reduced by decreasing the water recovery, although froths need a certain degree of water recovery to retain stability and keep an acceptable froth recovery of the valuable minerals. Entrainment is known to be significant for particles under 50 μm (Wills, 2006). A typical entrainment curve as a function of particle size is shown in figure 2.5.

Yianatos et al. (2008a) showed that the contribution of valuable minerals recovered due to entrainment was negligible in comparison to the valuable minerals recovered by true flotation. For modelling purposes this implies that the assumption can be made that all of the valuable minerals are recovered by true flotation, and thus the remaining 'free' gangue minerals are recovered by entrainment (or entrapment for coarse gangue minerals in specific cases).

Yianatos and Contreras (2010a) created an empirical model to calculate the gangue mineral recovery by entrainment per size class. A dimensionless entrainment factor EF_i was defined as the ratio of the gangue mineral recovery of size class 'i' ($R_{G,i}$) and the water recovery (R_w), thus as $EF_i = R_{G,i}/R_w$. The empirical model for the dimensionless entrainment is given by:

$$EF_i = \frac{R_{G,i}}{R_w} = \exp\left(-0,693\left(\frac{d_{P,i}}{\delta}\right)^{\phi}\right) \tag{2.14}$$

In this model, the dimensionless entrainment is a function of the particle size class 'i' given by $d_{P,i}$, the mean particle size for $EF_i = 0,5$ given by δ, and a drainage parameter depending on mineral characteristics, cell design and operating conditions given by ϕ. The model was validated in a 130 m[3] flotation cell (type and make unknown) for different operating conditions. Calculation of the variables in this model only requires a number of operating parameters and metal grades of samples in different size classes, which makes it relatively easy to apply.

Gangue minerals can be recovered by entrapment, by slime coating on mineral surfaces, by entrainment, and attached to valuable minerals due to incomplete liberation. The first two causes are generally negligibly small, since entrapment is typical for coarse material at high gas holdup, and slime coating should only be taken into account for ultrafine particle flotation (Yianatos and Contreras, 2010a). In addition, recovery of gangue minerals due to incomplete liberation is effectively a form of true flotation. Therefore, when considering the total mass flow of concentrate from a flotation cell, the flow can be divided in the fraction recovered by true flotation and the fraction recovered by entrainment:

$$C \cdot w_{C,i} = T_{C,i} + E_{C,i} \qquad \qquad (2.15)$$

in which C is the concentrate mass flow rate, $w_{C,i}$ is the solids mass fraction of size class i in the concentrate, $T_{C,i}$ is the mass flow of minerals recovered by true flotation, and $E_{C,i}$ is the mass flow of minerals recovered by entrainment (Yianatos and Contreras, 2010a). When the assumption is made that the top of the froth contains the maximum grade of floatable material (i.e. no entrained or entrapped material), the flow rate of material recovered by true flotation is:

$$T_{C,i} = \frac{C \cdot w_{C,i} \cdot X_{C,i}}{X_{TOF,i}} \qquad \qquad (2.16)$$

in which $X_{C,i}$ is the concentrate grade of size class i, and the complete numerator term ($C \cdot w_{C,i} \cdot X_{C,i}$) comprises the concentrate mass flow rate of the valuable mineral in this size class. Combining equations 2.16 and 2.17 gives the mass flow rate of entrained material in the concentrate of size class i:

$$E_{C,i} = C \cdot w_{C,i} \cdot \left(1 - \frac{X_{C,i}}{X_{TOF,i}}\right) \qquad \qquad (2.17)$$

For each particle size class a feed balance can be created, consisting of the mass flow of non-perfectly liberated valuable minerals ($V_{F,i}$) and the mass flow of free gangue minerals ($G_{F,i}$):

$$F \cdot w_{F,i} = V_{F,i} + G_{F,i} \qquad \qquad (2.18)$$

When one assumes that the valuable mineral particles in the feed have the same grade as the valuable minerals in the concentrate, the gangue flow rate in the feed is given by:

$$G_{F,i} = F \cdot w_{F,i} \cdot \left(1 - \frac{X_{F,i}}{X_{TOF,i}}\right) \qquad \qquad (2.19)$$

Since the feed contains a non-floating valuable metal fraction (recovery is never 100%) the assumption is not strictly true, but this falsehood has the largest effect on the entrainment factor of coarse particles, while the finer particles are most relevant for entrainment. In addition, Yianatos and Contreras (2010a) use the grade of the bubble load instead of the concentrate grade since the top of the froth may contain a small fraction of entrainment, but this method requires more advanced measuring equipment. Subsequently, the recovery of gangue can be calculated by combining equations 2.17 and 2.19, giving the ratio of the flow rate of gangue in the concentrate and in the feed:

$$R_{G,i} = \frac{E_{C,i}}{G_{F,i}} = \frac{C \cdot w_{C,i} \cdot \left(1 - \frac{X_{C,i}}{X_{TOF,i}}\right)}{F \cdot w_{F,i} \cdot \left(1 - \frac{X_{F,i}}{X_{TOF,i}}\right)} \qquad \qquad (2.20)$$

Combining equations 2.14 and 2.20, the entrainment factor is the ratio of gangue and water recovery:

$$EF_i = \frac{R_{G,i}}{R_w} = \frac{C \cdot w_{C,i} \cdot \left(1 - \frac{X_{C,i}}{X_{TOF,i}}\right)}{R_w \cdot F \cdot w_{F,i} \cdot \left(1 - \frac{X_{F,i}}{X_{TOF,i}}\right)} \qquad \qquad (2.21)$$

These parameters are all easily measurable and can thus be used to calculate a range of entrainment factors for different particle sizes. The values are used to fit to the 2-parameter model of equation 2.14.

2.7 Flotation test work on different scales

Laboratory batch tests

The normal procedure for testing of the flotation process for a specific ore type starts with laboratory batch test in cells ranging from one to several litres of volume (Runge, 2010). The use of small-scale batch tests in the laboratory gives possibilities to explore different options in a relatively easy, fast and inexpensive way. Many designs are available when it comes to lab-scale flotation cells, but most designs have the impeller on a fixed depth in the bottom of the cell, of which the rotation speed and air flow rate can be adjusted. Figure 2.6 gives an example of a common laboratory flotation cell.

Figure 2.6: Eight litre batch flotation cell used by the Boliden mineralogical lab.

A typical test commences with grinding of the ore in a laboratory size rod mill. The rod mill is favoured above a ball mill, since it limits the amount of fines in the product and gives a less wide particle size distribution (Wills, 2006). However, true simulation is never really achieved, since a common feature of closed-circuit grinding is the overgrinding of high specific gravity minerals, although this is minimized by the use of a rod mill.

The pulp from the mill is washed into the flotation cell, and make-up water is added to reach the desired volume. The impeller speed is set to the desired value, and reagents are added. After a certain conditioning time, the air flow is started and the timing for the test commences. The froth is scraped off top of the cell by the operator into a tray, and at the chosen time intervals the trays are replaced by empty ones. This allows the calculation of the recovery as a function of time by creating a cumulative distribution, and modelling of these results to calculate a flotation rate constant. The obtained concentrates are dried, weighed and analyzed, for example by XRF, to determine the metal assays. If one also wants to determine water recovery, the samples should also be weighed before drying, and the volume of any flush water should be taken into account.

A more extensive overview of laboratory flotation testing is given by Runge (2010).

Pilot plant testing

Although laboratory flotation tests form the design basis for the commercial plants, pilot plant scale tests are often performed before industrial application (Runge, 2010). The main objectives are:

1. To provide data of continuous operation.
2. Preparation of larger concentrate samples that can be assessed by smelter for bonus of penalty elements.
3. Clarify the operational costs and compare these with alternatives.
4. Compare equipment of different producers.
5. Demonstrate the process feasibility to investors with a limited technical background.

The results of pilot plant tests also influence the design of up- and downstream equipment. The most prominent example is the design of the milling circuit, since the tests should provide an optimal grind size. The type of grinding media also influences flotation performance but its selection is mainly depending on the ore characteristics. Since the operational costs of grinding are by far the greatest of all unit operations in the concentration plant, the ore should not be ground finer than economically justifiable. Other operational factors based on pilot plant tests are the quantity of reagents, pulp density and pulp temperature.

Industrial flotation circuit testing

Obtaining information from an operational flotation circuit in order to identify potential improvements is, like mentioned earlier, a time consuming activity, and can therefore not be done too often since the required resources are not available on a day-to-day basis (Greet, 2010). In modern concentrators the process is monitored by a number of online analysis methods, and additional data are provided by daily samples of the most important streams, but optimization requires a more detailed look. Surveys in flotation plants are often divided into two types; the metallurgical survey, in which samples are taken to represent the metallurgical recovery and upgrading of the valuable minerals, and the survey for cell hydrodynamics, in which information of gas holdup, superficial gas velocity and bubble size data are collected and compared to other situations to identify potential improvements.

A survey starts with choosing the sampling points and the type of sample to be taken. Most often flotation circuits are only provided with sampling point at the most significant streams, such as feed, concentrate and tailings of a bank. The sampling method is important in order to provide a representative sample, for example by preventing segregation effects or dilution with wash water. Afterwards, a large number of samples needs to be weighed, filtered, dried, weighed again and prepared for metal assaying or other analysis methods. Depending on the purpose of the survey, for example locating badly operating sections of the plant or profiles within a bank or single flotation cells, the data can then be mass balanced or compared with results of a second line or a pilot plant.

2.8 Statistical analysis of flotation test results

After performing test work in either laboratory or pilot plant flotation tests, the results will be compared to give insight in the effect of the variable or variables that were changed, for example the collector type, or the weight percentage solids of the pulp. Common methods to compare results are the time-recovery curve and the grade-recovery curve, which give a quick and clear image of the metal recovery as a function of time and concentrate grade, respectively (Runge, 2010).

The grade values of a grade-recovery curve are often recalculated into the *enrichment ratio*, which is defined as the metal grade in the concentrate divided by the metal grade in the feed. This is especially useful for comparison of tests with variation in the composition of the feed. The left graph of figure 2.7 gives a grade-recovery curve for visual comparison of two tests, in which four concentrates were taken on fixed time intervals. The initial concentrate of test B (rightmost point) has both a higher grade and a higher recovery than test A, while the final cumulative concentrate of test B (leftmost point) has a higher grade but approximately the same recovery as test A. Very often this leads to the incorrect conclusion that the conditions in test B give better flotation performance than those in test A (Napier-Munn, 2012).
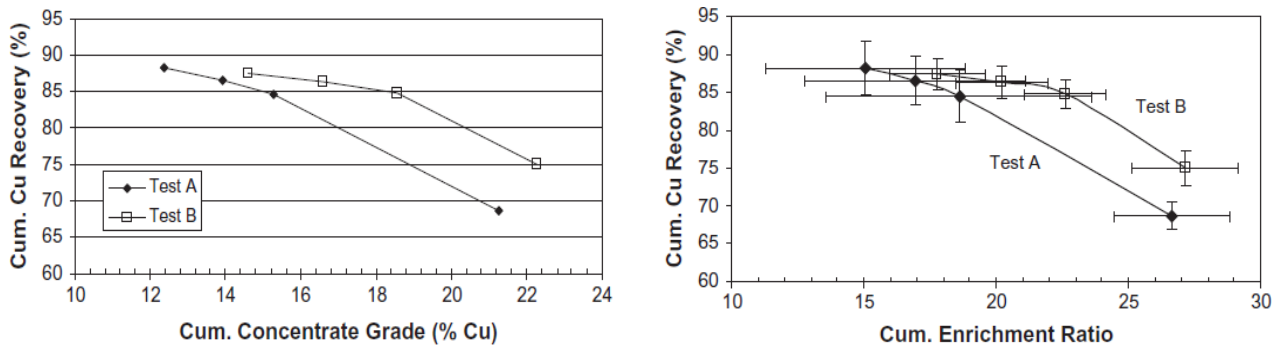
Figure 2.7: Grade-recovery (left) and enrichment ratio-recovery (right, including error bars)
curves to compare two batch tests (Napier-Munn, 2012).

The results of a single test under the same conditions ignore the existence of experimental error, which is always present in flotation testing and can arise from several sources (Napier-Munn, 2012), such as the sampling method, preparation of the feed, the method of performing flotation tests (this varies between people), or the assaying method. A single test gives no information on the error size, which is why batch flotation tests require replication in order to measure the experimental error. The confidence interval (CI) is given by:

$$CI = \pm \frac{t_\alpha s}{\sqrt{n}} \qquad\qquad (2.22)$$

in which t_α is the t-distribution value for a two sided confidence level of $100(1-\alpha)\%$, and s is the sample standard deviation with n replicates. The t-distribution value can be found with the MS Excel function =TINV(α, n-1). The tests of which the results are shown in figure(2.7 are in fact performed three times, and the average results are shown in the grade-recovery curve. The right graph of figure 2.7 gives the results including error bars for a 90% confidence level, i.e. there is 90% certainty that the results of a next test under the same conditions will be within these limits. From the graph it is clear that the validity of the results is relatively uncertain, mainly due to the low number of replicates.

3. Up-scaling of the flotation process

3.1 Influence of flotation cell design on up-scaling

The approach to flotation up-scaling that is traditionally applied makes use of batch and pilot plant testing, assuming that these cells work as a scale model of an industrial plant (Dobby and Savassi, 2005). From industrial experience it was observed that results from this approach are often not reliable, due to the difficulty of replicating variables in a batch or pilot cell, such as plant throughput and cell configuration. Other examples are the differences in geometrical aspects between laboratorial and industrial cells, which influence hydrodynamic effects such as the rising velocity of bubbles and transport distance of the floatable material.

According to Gorain (2007), previous up-scaling of flotation cell designs has mainly been based on geometrical similitude and dimensional analysis by using dimensionless numbers, in order to create similar solid suspension and pulp mixing conditions at different scales. During the process of up-scaling, understanding of the sub-processes that constantly take place in the flotation cells can help to clarify the dissimilarities between small scale laboratory or pilot plant tests and a full scale operation. In many researches and models it is assumed that flotation cells are ideally mixed, although from a logical point of view this is less and less applicable when the cell becomes larger. An illustrative example is the pulp density, which is rationally expected to be maximal at the bottom of the cell where feed comes in and tailings leave the cell, and at its minimum at the pulp-froth interface, where turbulence is lowest and ideally a low concentration of gangue minerals exists, to minimize gangue recovery to the froth. Clearly the equipment design has an important influence on cell fluid dynamics and sub-processes in the distinguishable zones of the flotation cell.

This section attempts to clarify some aspects of the design of flotation equipment, and how this influences the sub-processes within the distinct zones in flotation cells on different scales. The sub-processes on their own can behave in a variety of ways determined by equipment design, but also operational methods, and will therefore affect flotation performance.

3.1.1 Flotation cell types and sub-processes

Since experience has shown that flotation performance is reduced when the process is scaled up from a laboratory cell to an industrial circuit, it is clear that during scale-up a number of unidentified variables is changed and cause minerals to behave in another way in different cells. In order to characterize the possible effects in an industrial flotation cells that would not occur in a lab or pilot cell, it is vital to understand the basics of flotation cell design and identify these differences that arise during scale-up. The used types of flotation cells in the industry can be divided into two distinct groups: mechanical and pneumatic machines (Nelson et al., 2009).

Mechanical cells are the most common for base metal flotation, especially in rougher and scavenger flotation, and are driven by an impeller to agitate the suspension and introduce air bubbles in the cell. Pneumatic machines have air blown in through baffles or a permeable base within the cell, and the function of air is not only to aerate the cell and create froth, but also to keep the solids in suspension and circulate it. Since the flotation circuits of Boliden are exclusively operating with mechanical flotation cells, this research will also be limited to these types of cells. Nelson et al. (2009) divide mechanical flotation cells into three types:

1. Externally-aerated cells with the impeller near the cell bottom.
2. Externally-aerated cells with the impeller near the centre of the cell.
3. Self-aerating cells with the impeller near the top of the cell.

Of these machines, the first type is the most common in base metal flotation and is produced by all the main flotation cell producers, like FLSmidth Minerals (Dorr-Oliver and Agitair series), Metso Minerals (RSC and DR series) and Outotec (OK and TankCell series). An example of a centre-driven cell is the XCELL, produced by FLSmidth. Self-aerating cells are exclusively produced by FLSmidth as the Wemco-series. Considering that Boliden makes use of bottom-driven cells in the concentrator plants, and bottom driven cells are used for laboratorial batch testing, this research will mainly focus on this type of cell. However, since certain similarities exist with the other cell types, previous researches on other cell types are also consulted.
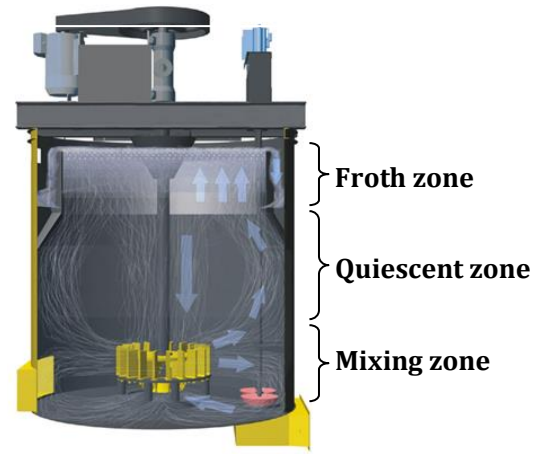
Figure 3.1: Subzones of a flotation cell (Outotec, 2014).

The bottom-driven mechanical flotation cell can be subdivided into three zones; the *mixing zone* with the impeller in the bottom of the cell, the *quiescent zone* above the impeller with relatively low turbulence, and the *froth zone* on top of the suspension. Figure 3.1 gives an overview of the mentioned subzones, although the thickness of the froth zone is not drawn to scale.

The mixing zone in the cell bottom is where the mineral particles and air bubbles are mixed, and where most collisions between particles and bubbles occur. The turbulence in this part of the cell is high enough to prevent particles from settling, but sufficiently low to prevent the detachment of particles and bubbles. The quiescent zone has a much lower turbulence and allows bubbles to rise freely within the cell due to buoyancy forces. During this process gangue minerals remain in suspension or detach from the bubbles, whereas valuable minerals stay attached, thus improving selectivity. Finally the rising bubbles reach the froth zone, where the separation of air bubbles with valuable minerals from water and gangue minerals continues. The froth overflows the cell and is collected in a launder as the concentrate.

Table 3.1 gives the dimensions of five Outotec TankCell-designs. Note that the given figures are external dimensions, and thus do not directly give dimensions for the calculation of effective flotation volumes of the cells. Since these are cylindrical cells, the cross-sectional area increases to the second power of the tank diameter, while the volume increases to the third power during a proportional scale-up.

Table 3.1: Dimensions of five Outotec TankCell® designs (Nelson et al., 2009; Boliden, 2008; Outotec, 2014).

Cell type	TankCell®-100	TankCell®-160	TankCell®-200	TankCell®-300	TankCell®-e500
Effective volume [m³]	100	160	200	300	500
Diameter [m]	6,0	6,8	6,8	8,0	10,0
Height [m]	4,3	5,2	5,8	7,0	10,0
Height/diameter [-]	**0,717**	**0,765**	**0,853**	**0,875**	**1,000**
Area/volume [m²/m³]	**0,283**	**0,227**	**0,182**	**0,168**	**0,157**

From table 3.1 it can be observed that the diameter/height ratio becomes higher for the larger designs, thus making the cell's shape higher and less wide in relation to smaller designs. As a result, the cross-sectional area decreases in proportion to the cell's volume for larger designs. The suspected reason for this is related to fluid dynamics; wider cells need a higher power input to create sufficient turbulence near the cell walls, and bubbles from the impeller will start to rise before reaching the cell wall of a wide cell, making particle-bubble collisions in the mixing zone less efficient. Designing wider cells has the potential problem of dead zones near the walls at the cell bottom, where turbulence is too low to keep solids in suspension and sedimentation occurs (Lelinski et al., 2005).

Ⓝ BOLIDEN

Since the bubble surface area flux is defined as the rate at which bubble surface area moves through the flotation cell per unit of cell horizontal cross-sectional area per unit of time, it will not grow proportionally to cell volume. This may impose a limit to the rate at which mineral float, according to the linear relationship between the flotation rate constant and bubble surface are flux given in equation 2.9.

A decreasing net cross-sectional surface area of the flotation cell during scale-up can accelerate reaching such a limitation of the rate at which minerals float. Meanwhile it enlarges the height of the quiescent zone, which reduces the volume fraction available as mixing zone, with possible consequences for the particle-bubble collision probability. In addition, an increased height/diameter ratio places the impeller and the mixing zone further away from the upper part of the cell and therefore lowers the turbulence in these regions, making the flotation cell behave less and less as a perfectly mixed system, an assumption made in many flotation models.

An additional advantage of up-scaling is that the installation of control systems becomes more cost-effective, since fewer systems are needed (Harcus, 2010). This simplifies the control of individual cells by adjusting factors like froth thickness and mass pull, and thereby controlling froth recovery and concentrates grades. Well working control systems are of increasing importance on large cells, since the performance of a single large cell will have greater effect on the total plant results.

3.1.2 Mixing zone characteristics

In the mixing zone of the flotation cell the mineral pulp is mixed with air bubbles in a highly turbulent regime in order to create collisions between particles and bubbles and facilitate the attachment of these particles to the air bubbles. As mentioned in the previous section on cell design, the mixer can be placed at different heights in the cell, thereby strongly affecting the mixing regime. In a mechanical cell the mixer provides the energy required for the breakup of bubbles, keeping the solids in suspension and facilitating the particle-bubble collisions (Evans et al., 2008). The energy input has a strong influence on the success of the flotation operation, as a too low input will reduce the particle-bubble collision probability and may cause particles to settle, whereas a too high input can cause detachment of particles and bubbles.

The mixing regime will also determine the mixing time of the pulp, before it either leaves the cell as tailing or reaches the quiescent zone. Yianatos et al. (2008b) was able to model the mixing zone residence time in a 130 m^3 Wemco cell with the use of radioactive tracers and measured an average mixing time of 100 seconds, along with a total pulp residence time of 340-360 seconds. The feed pulp circulated approximately 1,4 times through the mixing zone before reaching a well-mixed condition. Residence time measurements are useful to locate pulp short-circuiting (i.e. valuable minerals in the feed directly by-passing to the tailings), or loss of volume due to sedimentation (Govender et al., 2014).

Additionally, the hydrostatic pressure difference between the impeller and froth zones is minimal in batch flotation, while in full scale flotation it is significant at least. Hydrostatic pressure is calculated by:

$$p = p_0 + \rho_p \cdot g \cdot h \qquad\qquad\qquad (3.1)$$

in which p_0 is the atmospheric pressure (101,3 kPa). In a TankCell-160, the largest cell type at Boliden's Aitik mine, the impeller is placed at a depth of approximately 3,5 m, and with an average feed pulp density of 1469 kg/m^3 the ratio between the pressure at impeller depth and at the surface is:

$$\frac{101300 + 1469 \cdot 9,81 \cdot 3,5}{101300} = 1,498$$

This implies that pressure reduces with a factor of almost 1,5 between impeller and froth in industrial flotation. Apart from the possibility of bubbles merging, the product of volume and pressure is constant according to the ideal gas law, thus the volume of each bubble will increase with the same factor. A bubble that collects a mineral particle in the mixing zone will be significantly larger near the froth zone, and the bonding forces may not be as strong. Especially for the recovery of fine particles, this effect is believed to be detrimental. In a higher cell this effect would even be enhanced. Figure 3.2 gives the bubble volume expansion ratio for impeller depths up to 10 meter (the total cell height of a TankCell-e500 (Outotec, 2014)).
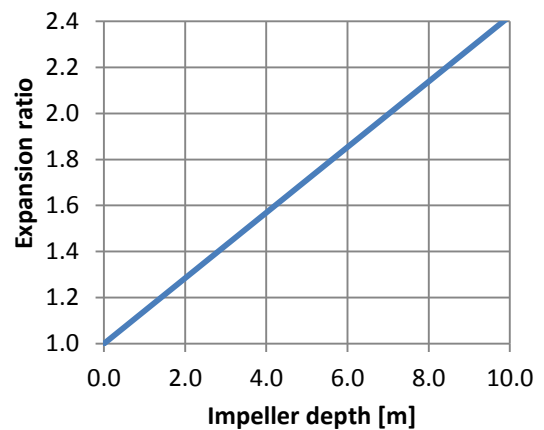
Figure 3.2: Bubble volume expansion ratio as a function of impeller depth.

3.1.3 Quiescent zone characteristics

The quiescent zone of the flotation cell has the main purpose of providing selectivity in the flotation process. After the air bubbles have been mixed with the pulp in the mixing zone and loaded with minerals, the buoyancy effect lets the bubbles rise into a zone with lower turbulence. This laminar flow field allows unwanted, hydrophilic particles to detach, while valuable, hydrophobic particles stay attached. Figure 3.3 shows an illustration of the fraction of bubble surface coverage in a batch flotation cell, which is highest directly above the impeller (red colours) and decreases at shallower depths.
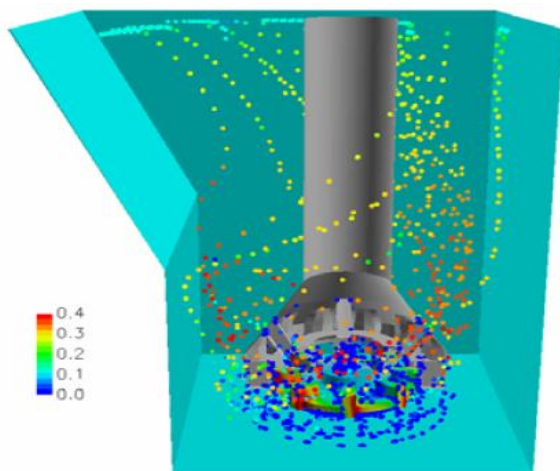
Figure 3.3: Fraction of bubble surface covered in 5 litre batch flotation cell (Koh and Schwarz, 2011).
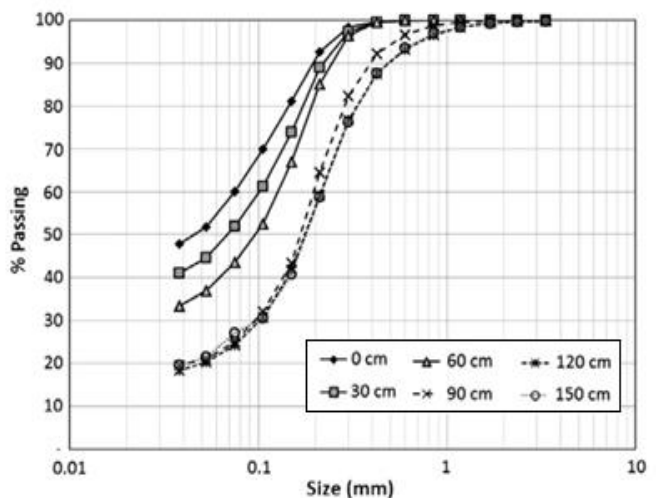
Figure 3.4: Particle size distribution curves at various cell depths in a flash flotation cell (Newcombe et al., 2012).

Although many models assume flotation cells to be perfectly mixed, segregation phenomena can occur, especially in the low turbulent quiescent zone. Grönstrand et al. (2006) reported accumulation areas of fine material in 38 m³ cells in the old Boliden Aitik processing plant, accompanied by a significantly lower pulp density of the slurry in these zones.

Newcombe et al. (2012) investigated hydrodynamic effects in a pyrite flash flotation cell in the concentration plant at Barrick Gold's Kanowna Belle mine in Australia. Flash flotation is a technique focussed on the recovery of the most liberated, high-grade particles, typically before rougher flotation or from the recirculating load in the grinding circuit. Gas dispersion measurements were taken with increasing depth in the cell. The superficial gas velocity ranged between 0,05 cm/s at a depth of 2,5 m,

and 0,35 cm/s directly under the froth, which is significantly lower than in previous researches (0,5-1,5 cm/s was found by Nesset et al. (2006)), which is attributed to the flash flotation operating conditions, which typically have a high weigth percentage solids in the pulp. Gas holdup was estimated by a linear relationship between the superficial gas velocity and the gas holdup reported by Finch et al. (2000) as $J_g \approx \varepsilon_g \cdot 5,5$ m/s. This resulted into gas holdup values between 1,0% in lower part of the cell and 6,3% in the upper part. Yianatos et al. (2010b) report typical gas holdup values of 10 to 15% in a bottom driven cell, decreasing with cell depth.

Profiles of particle size with depth made by Newcombe et al. (2012) showed coarser material near the bottom of the flash flotation cell, as shown in figure 3.4. However, since fines are pre-removed by hydrocyclones and coarse material is supposed to by-pass to the tailings in a flash flotation cell, this result will not be valid for conventional cells. The coarse material is generally insufficiently liberated and is recirculated to the grinding circuit. The percentage solids in the slurry showed to be strongly segregated between 80% in the feed and only 36% directly under the froth.

Yianatos et al. (2005a) showed that in conventional cells residence times are longer for coarser material, although mixing characteristics are generally assumed to be similar for all size classes. The longer residence times for coarse material become visible at the end of flotation banks when a majority of the fines has been removed. Yianatos et al. (2001) reported a slightly increasing weight percentage solids within a conventional cell, with several percentage points over the whole cell depth. The grade profiles with depth, measured as percentage sulphur and ppm gold, showed a consistency in grades for all depths.

3.1.4 Froth zone characteristics

The froth zone is known to play an important role in flotation processes, as it prevents direct transport of the pulp to the concentrate, and therefore defines the quality of the concentrate and the overall efficiency of the process (Yianatos et al., 2008b; Ata, 2012). It acts as an extra cleaning zone after minerals have been recovered from the pulp zone, as it further rejects unwanted particles and water, thus upgrading the concentrate purity.

Froth zone performance depends on a number of sub-processes that constantly interact and are complicated to directly measure and control in plant practice, such as particle-bubble detachment and attachment mechanisms. Therefore it can be useful to identify and understand the measureable and controllable factors in the froth phase, such as the froth residence times of the solid, liquid and gas phases. Froth characteristics are also known to play a role during up-scaling from batch to continuous processes, since froth recovery is approaching 100% in batch flotation and ranges between approximately 50 and 80% in industrial flotation, for example 66,2% found by Yianatos et al. (2008a). Froth recovery was defined by Finch and Dobby (1990) as the ratio between the overall flotation rate constant (k_G) and the collection zone flotation rate constant (k_C).

To control the froth performance several operational variables can be adjusted, of which the froth depth, and gas flow rate to the cell are directly controlled by operators. Figure 3.5 shows distinct zones within the froth phase according to Yianatos et al. (2008c). This figure suggests that the minimal froth residence time is achieved by transport near the cell wall, since material will first travel vertically from the pulp-froth interface until lip height, followed by a short distance until the concentrate overflows the cell into the launder. Furthermore there is a stagnant zone above the impeller, where an equilibrium of upward and downward transport exists, and thus no contribution to the concentration process occurs.
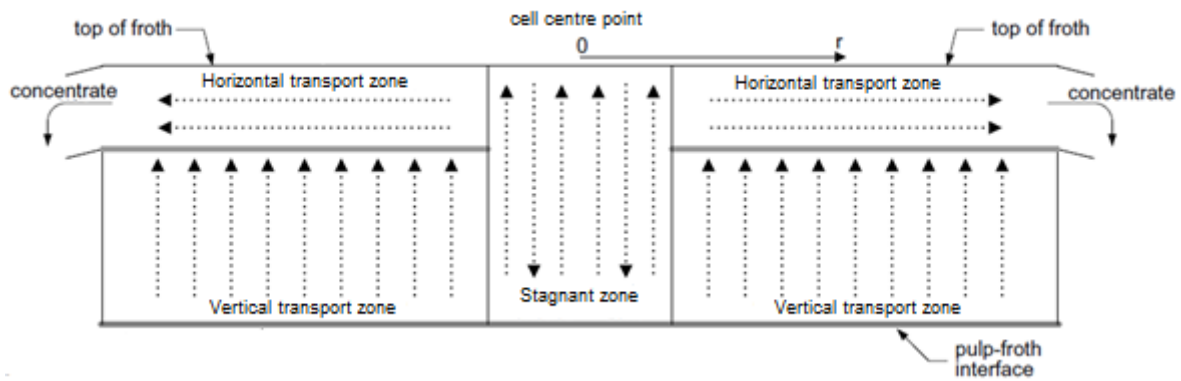
Figure 3.5: Transportation patterns in the froth zone of the flotation cell according to Yianatos et al. (2008c).

Many industrial flotation cells have an inverted cone dipping into the froth in the centre of the cell, also called a *froth crowder*, to accelerate the discharge of froth to the external launders and eliminate the stagnant zone. Additionally internal launders can be used to shorten the overall froth residence time, distribute the froth transport velocity more evenly, and eliminate a recovery restriction due to a limitation in lip length, which sometimes occurs in cleaning cells, where the fraction of the feed material recovered to the concentrate is large.

Yianatos et al. (2008c) used radioactive bromium-82 as a liquid tracer and three size classes of irradiated non-floatable and floatable material as solid tracers to measure the froth residence time in a 130 m³ flotation cell. The non-floatable material showed to have the shortest residence time, comparable with the mean time of gas transport. Since the non-floatable material is mainly recovered by entrainment, especially the particles in transportation paths near the launders will be recovered, whereas non-floatable material far from the launder can be washed out and sink back into the pulp. The floatable material and liquid had a significantly longer froth residence time, supposedly because of the longer average transportation paths and lower velocities in the various transportation zones.

Figure 3.6 shows an example of relative froth speeds according to King (2001) in a rectangular flotation cell with the concentrate overflow on the right side. The froth speed near the overflowing cell wall is distinctly higher, while the froth speed far away from the overflow is only a small fraction of the maximum froth speed.
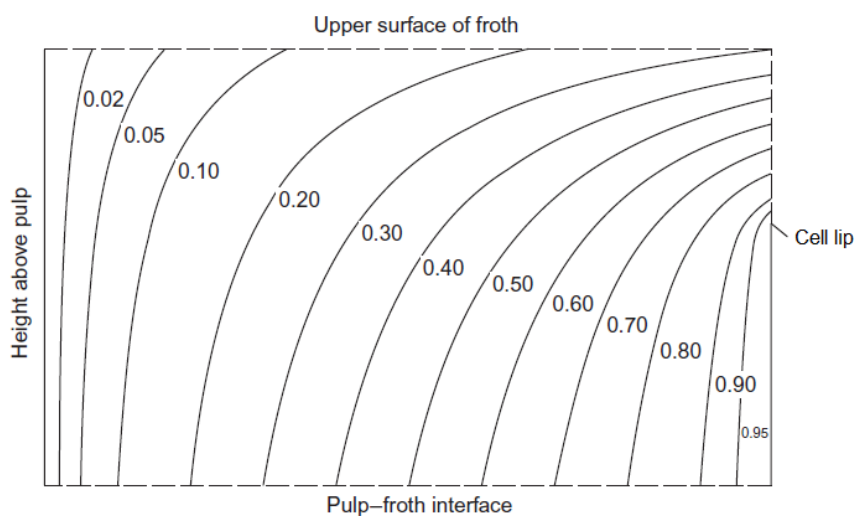
Figure 3.6: Relative froth speed in a rectangular flotation cell with concentrate overflow at the right wall according to King (2001), with unity froth speed near the overflowing cell wall.

25

3.2 Previous research on flotation up-scaling

This section covers prior researches on the up-scaling of flotation processes. Although literature on this subject is limited, most of the research that has been done was applied to copper mineral flotation, since this is one of the metals that typically deal with low grades and high throughputs in the flotation plant, therefore causing the use of large flotation cells to become more attractive. The most recent researches especially applied to operations in Chile, the world largest copper producing country. Although there is a certain amount of overlap, the flotation up-scaling methodologies are divided into four approaches:

1. Up-scaling based on gas dispersion in flotation cells.
2. Up-scaling based on flotation kinetics.
3. Up-scaling based on dimensional similitude and cell conditions.
4. Restrictions on carrying capacity during up-scaling.

Before the main aspects of these methodologies are described, firstly the economic aspects of flotation up-scaling are regarded.

3.2.1 Economics of up-scaling

As previously mentioned, two of the advantages of larger and fewer flotation cells are reduced capital and operational costs. Because of the high investment costs and low turnover in the start-up phase of mines, the capital investment costs for the flotation plant have often outweighed the lifetime costs of projects in the past. For expansion projects a company normally already has a cash flow and will have more capability to look into lifetime costs. Rinne and Peltola (2008) analysed that the initial investment comprises less than 10% of the costs in a 25-year lifetime of a flotation circuit, while energy accounts for roughly 60-80% of total costs, depending on local prices. Other major costs are reagent consumption and maintenance. Rinne and Peltola (2008) compared the lifetime costs of five possible flotation circuits with an effective volume of 1800 m^3. The five researched scenarios were:

- 18 cells of 100 m^3 in two lines of nine cells.
- 9 cells of 200 m^3 in a single line.
- 9 cells of 200 m^3 in a single line, fitted with variable speed drive mechanisms.
- 6 cells of 300 m^3 in a single line.
- 6 cells of 300 m^3 in a single line, fitted with variable speed drive mechanisms.

	100-m3 cells	200-m3 cells	200-m3 cells, optimized rotation speed	300-m3 cells	300-m3 cells, optimized rotation speed
■ Investment costs	11.9	7.4	8.2	7.0	7.7
▬ Reagents	18.7	17.0	17.0	15.4	15.4
▢ Maintenance	9.4	5.8	6.0	3.5	3.6
▥ Energy	60.0	55.9	45.4	41.5	35.6
LCC	100.0	86.1	76.6	67.5	62.3
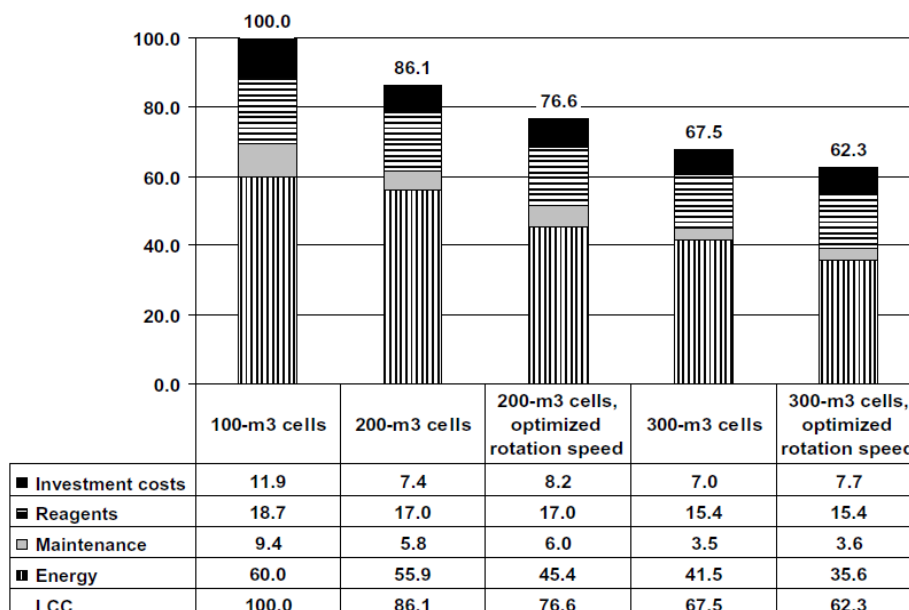
Figure 3.7: Relative lifetime costs of different flotation options (Rinne and Peltola, 2008).

The mechanism that allows a variable speed drive for the cell's impeller will results into a higher capital cost, but will lower the lifetime energy costs. A variable speed drive can be used to optimize power input for a specific material. The total lifetime costs for different scenarios are presented in figure 3.7. The circuit consisting of six 300 m³ cells fitted with variable speed drive mechanisms was calculated to have only 62,3% of the lifetime costs of the circuit with eighteen 100 m³ cells. However, the research does not cover metallurgical results, and the economics in terms of production losses are generally much more important than the lifetime costs of the flotation cell. The following sections will cover several previous flotation up-scaling researches and their performance during application on industrial flotation cells.

3.2.2 Gas dispersion approach towards up-scaling

Several scientific approaches have been attempted to obtain more reliable results in the scale-up process to larger flotation cells. One of the first methods was to make use of the relation between the rate at which valuable minerals float, and the gas dispersion effects within a flotation cell. Figure 3.8 gives a plot of the bubble surface area flux versus the first order rate constant in a 60 litre pilot cell and a 100 m³ industrial cell. It can be observed that there is a similar relation between these factors in the two cell sizes. This suggests that determination of the bubble surface area flux in industrial flotation cells can be used to predict its flotation kinetics, based on results from batch and pilot plants.
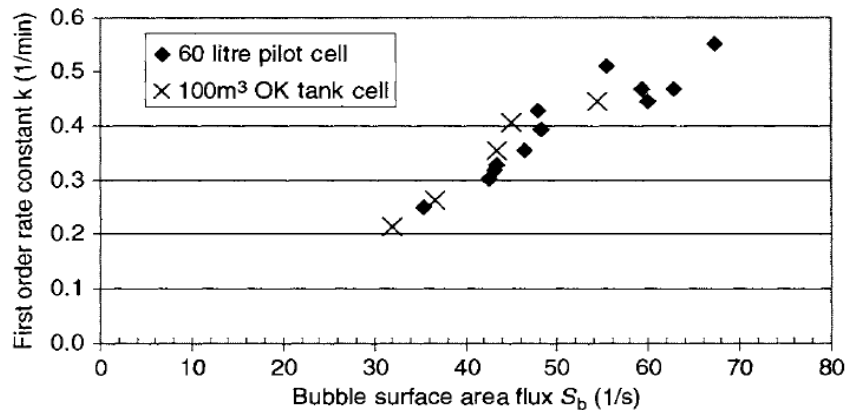
Figure 3.8: Relation between the first order rate constant and the bubble surface area flux in a 60 litre pilot cell and a 100 m³ industrial cell (Wills, 2006).

Gorain et al. (1997) observed the same relation between the flotation rate constant and the bubble surface area flux for different cell sizes for test work at the Mount Isa mine in Australia, and noted that this relationship was independent of the impeller type after performing the test with several types of impellers. The relation was valid as long as the ratio between froth height (h_{froth}) and superficial gas velocity (J_g) remained constant. This ratio is the *froth residence time* (τ_{fg}) of the gas. However, it was also recognized by Gorain et al. that turbulence is not included in the bubble surface area flux and may significantly change during up-scaling.

The relation between the flotation rate constant and froth residence time is known to change for different cell sizes (Gorain et al., 1998). One cause is the travelling distance of the solids to the froth, which is obviously longer for larger cells. Therefore the froth residence time can be divided by the distance between impeller and launder (L), to calculate the *specific froth residence time* (τ_{fs}) according to:

$$\tau_{fs} = \frac{\tau_{fg}}{L} = \frac{h_{froth}}{J_g \cdot L} \qquad (3.2)$$

Although this gave a much better fit with the rate constant for Gorain et al. (1998), a wide scatter of data points was observed for low froth residence time. This is caused by the fact that for a constant superficial

gas rate J_g, and thus a constant τ_{fs}, different values for S_b can arise due to variation in impeller speed causing varying mean bubble sizes.

A methodology for up-scaling was proposed by Gorain et al. (1998), using the obtained values of specific froth residence time and the corresponding flotation rate constants. This involves performing tests at different froth depths, impeller speeds and air flow rates. The proposed equation is given by:

$$k = \alpha \cdot e^{-(\beta \cdot \tau_{fs})}$$

(3.3)

The obtained relationship between τ_{fs} and k is used to determine the value of constant α in equation 3.3 for shallow froth depths, since $\alpha = k$ for $\tau_{fs} = 0$. Once α is determined, constant β can also be determined by fitting the data for different froth depths. Finally, k is determined for the value of τ_{fs} that corresponds with the specified S_b value.

Gorain et al. (1999) derived an empirical relation for the bubble surface area flux in bottom-driven externally-aerated flotation machines based on a regression model of different cell designs:

$$S_b = 123 \cdot N_S^{0,44} \cdot \left(\frac{Q_{air}}{A}\right)^{0,75} \cdot A_s^{-0,10} \cdot P_{80}^{-0,42}$$

(3.4)

in which N_S stands for the impeller peripheral speed, Q_{air}/A stands for the air flow rate per unit of cross-sectional area, A_s stands for the impeller aspect ratio (width/height), and P_{80} for the 80% passing size of the feed. N_S is calculated by multiplying the impeller's revolutions per minute with $\pi R/30$ to obtain the impeller peripheral speed in m/s. Based on 150 sets of experimental data from different cell designs, the standard deviation for S_b was found by Gorain et al. (1999) to be 0,151 s^{-1}.

Nelson et al. (2009) reported that during scale-up of flotation cells not the same results can be expected for larger cells due to the fact that when the volume of a cell is tripled in a proportional scale-up, the surface area only doubles. The residence time is directly related to volume, while the bubble surface area flux is related to the surface area of the cell. When a cell becomes larger, the production of concentrate will not increase in proportion to the residence time. However, for large low-grade ore bodies like most copper mining operations nowadays, the larger cells are expected to be better suited to treat the increased tonnage.

Lelinski et al. (2005) suggested that the use of the bubble surface area flux for up-scaling is questionable due to the problematic nature of the bubble size measurement. The measurement is difficult, especially in industrial scale cells, and has a subjective character depending on the mathematical approach. One approach is elaborated by Grau (2006). The measurement will also vary with location in the cell. Ideally, the measurement should be made directly outside the impeller where bubble-particle contact is the most intense, but where measurements are also the most difficult.

3.2.3 Kinetic approach towards up-scaling

The kinetics of flotation are one of the tools that are commonly used to design plants, in order to reach an end-product of a recovery and grade acceptable for a smelter after a certain flotation time and number of banks. Since the kinetics on industrial scale are generally not the same as on laboratory or pilot scale, this is a complex process for any unfamiliar ore and basically forms the basis for the whole up-scaling problem.

Additionally, an increased residence time in the flotation cell does not necessarily improve metallurgical results (Burstein and Filippov, 2010), for example when the concentrate in the last cells of a bank too strongly deteriorates the combined bank concentrate, even though it improves the metal recovery. The next section will cover a practical example of an up-scaling investigation based on flotation kinetics.

Kinetic up-scaling approach at Minera Escondida, Chile

Yianatos et al. (2005b) investigated the operating conditions of the rougher flotation circuit at Minera Escondida, one of the world's largest copper mines, located in the Chilean Atacama desert. The objective was to determine time scale-up factors by considering the hydrodynamic effects separately.

The rougher circuit at Minera Escondida consists of six banks with nine 160 m³ FLSmidth Wemco cells each. A plant survey was performed over a 7-hour period to evaluate the full flotation circuit performance. Meanwhile, samples were taken of the rougher feed to perform laboratorial batch tests. The data points were fitted to kinetic models under the assumption of a rectangular distribution of the kinetic distribution function $F(k)$ within the expression for the recovery of equation 2.2 on page 9, described by:

$$F(k) = \frac{1}{k_{max}} \quad for \ \ 0 < k < k_{max}, \qquad F(k) = 0 \ \ for \ \ k_{max} < k < \infty \tag{3.5}$$

The rectangular distribution accounts for different kinetic properties of complex minerals, while using a reduced number of fitting parameters (Yianatos and Henríquez, 2006). The parameter k_{max} is the maximal value of the first order flotation rate constant, which from a logical point of view is highest for a short residence time when more fast-floating material will be present. The residence time distribution function $E(t)$ for a continuous operation with N cells in series is given by (Yianatos et al., 2005a):

$$E(t) = \frac{t^{N-1} \cdot e^{-\left(\frac{t \cdot N}{\tau}\right)}}{(\tau/N)^N \cdot \Gamma(N)} \tag{3.6}$$

in which $\Gamma(N)$ represents the Gamma function, defined as $\Gamma(N) = (N-1)!$, to account for the non-integer values of N. By substituting equations 3.5 and 3.6 into equation 2.2, the recovery equation for N flotation cells in series becomes:

$$R(\tau) = R_\infty \cdot \left(1 - \frac{1 - \left(1 + k_{max}\tau_p\right)^{1-N}}{(N-1)k_{max}\tau_p}\right) \tag{3.7}$$

For the batch tests with undistributed residence time (i.e.: $E(t) = \delta(t)$) the model equation becomes:

$$R(t) = R_\infty \cdot \left(1 - \frac{1 - e^{-k_{max} t}}{k_{max} t}\right) \tag{3.8}$$

The models of formulae 3.7 and 3.8 were fitted to the test data of batch and continuous tests respectively, and showed a reasonably good fit. Figure 3.9 displays the copper recovery results of the plant survey and the prediction by the model of equation 3.7, and the model parameters are given in table 3.2. However, a number of factors proved to have a strong influence on the plant results and could not be implemented in the model, for example the introduction of a secondary collector in cell 4, which improved performance on the subsequent cells.
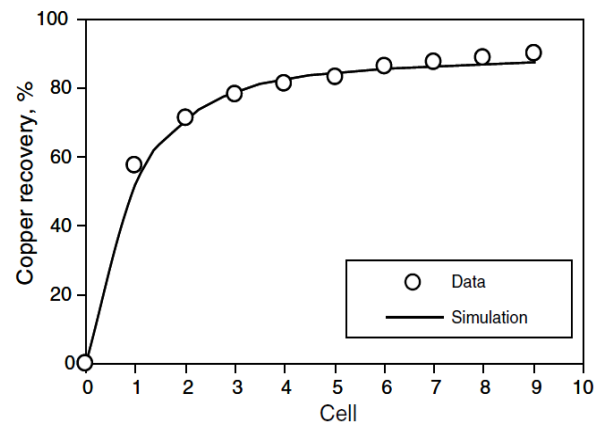
Table 3.2: Up-scaling model parameters from literature (Yianatos et al., 2005b).

	Batch	Plant
R_max	95,4%	91,0%
k_max	3,5 (1/min)	1,4 (1/min)

Figure 3.9: Plant survey recovery results and model prediction (Yianatos et al., 2005b).

Verification of (pilot) plant results is difficult in comparison to laboratory batch tests, since in lab tests the amount of representative samples is smaller and easier to handle. Yianatos et al. (2005b) report that the key consideration is the selection of recovery. Direct comparison of batch tests with a bank of flotation cells is complicated, because the recovery in the last cells of the bank is relatively small. A time scale-up factor was defined as a function of the maximum flotation constant and a dimensionless parameter φ to separate the effect of mixing and kinetic changes:

$$\frac{\tau_{plant}}{t_{batch}} = \varphi \cdot \frac{[k_{max}]_{batch}}{[k_{max}]_{plant}} \qquad\qquad (3.9)$$

In addition, a parameter η for the dimensionless recovery was defined as the ratio between the recovery reached in operation and the expected maximum recovery:

$$\eta = \frac{R}{R_{max}} \qquad\qquad (3.10)$$

The maximal recoveries given by the models were 91,0% and 95,4% for the plant and batch tests respectively. The recovery reached at the end of the rougher flotation bank was 88,5%, after a total residence time of 29 minutes. Thus in this case, the value of η for the rougher circuit was equal to 88,5/91,0 = 0,97. The obtained dimensionless recovery from the plant operation was used to calculate the required batch flotation time for which the recovery was equal, based on the maximal recoveries given by the models:

Figure 3.10: Mixing parameter φ versus the number of cells in a bank, at different dimensionless recoveries (Yianatos, 2005b).

$$R_{batch} = [R_{max}]_{batch} \cdot \eta = 95,4\% * 0,97 = 92,5\%$$

The required time to reach 92,5% recovery in batch tests was 9,2 minutes. The obtained time scale-up factor is:

$$\frac{\tau_{plant}}{t_{batch}} = \frac{29}{9,2} = 3,2$$

This scale-up factor is slightly higher than most scale-up factors of other investigated copper flotation operations, as shown in table 3.3.

Table 3.3: Time scale-up factors for flotation plants from literature.

Plant / mine	Cell size (m³)	Recovery (%)	Time scale-up factor	Reference
Kotalahti (Finland)	-	62	4,2	Kalapudas (1985)
Keretti (Finland)	16	86	2,7	Kalapudas (1985)
El Teniente (Chile)	28,3	86	2,2	Yianatos et al. (2005b)
El Teniente (Chile)	42,5	85	2,2	Yianatos et al. (2005b)
El Salvador (Chile)	42,5	81,4	2,3	Yianatos et al. (2003)
Escondida (Chile)	160	88,5	3,2	Yianatos et al. (2005b)

Finally, the empirical parameter φ for the mixing conditions was determined with the use of the scale-up factor and the maximum kinetic constants in table 3.2 according to equation 3.9:

$$\varphi = \frac{\tau_{plant}}{t_{batch}} \cdot \frac{[k_{max}]_{plant}}{[k_{max}]_{batch}}$$

$$= 3{,}2 \cdot \frac{1{,}4}{3{,}5} = 1{,}26$$

Comparison with the theoretical values of φ, as shown in figure 2.12, the obtained value of 1,26 only slightly differs from the theoretical value of 1,12 for 9 cells and $\eta = 0{,}97$. This implies that the differences in mixing conditions between batch test and continuous operation only have a minor impact on the required flotation time in a bank of 9 cells.

The main advantage of this method is that no time- and labour intensive plant surveys are required, since it is based on the results of the monthly average rougher bank results. However, application on greenfield projects is not possible since there will be no industrial data to determine the scale-up factors for the concerning ore type.

3.2.4 Up-scaling based on dimensional similitude and cell conditions

One method of creating similar conditions within flotation cells on different scales makes use of dimensionless numbers. Dimensionless numbers are widely used in engineering because they allow comparison of systems that are vastly different, since these numbers do not have any true physical dimensions. In the field of flotation research dimensionless numbers are applied in computational fluid dynamics (*CFD*) to model the fluid dynamics within cells and to better understand multiphase flow mechanisms between fluid, gas and particles (Xia et al., 2009). One of the most applied dimensionless numbers in fluid dynamics is the Reynolds number (*Re*), which describes the ratio between inertial and viscous forces in fluid dynamics. The Reynolds number and several other dimensionless numbers for flotation cells are given in table 3.4.

Furthermore, mixing can be characterized by the Froude (*Fr*) number, defined as the ratio of inertial and gravitational forces. The Froude number is generally around 0,6 for small industrial cells and 0,25-0,30 for large cells (Heiskanen, 2013), mainly resulting from a lower impeller speed for large cells. Rodrigues et al. (2001) found a plateau of optimal recovery in microflotation of coarse quartz at values of 3000<Re<8000 and 0,1<Fr<1,0, at which turbulence is sufficient to promote particle-bubble collision, and not too high to cause break up the contact between bubbles and particles.

The Reynolds number is in the order of 10^5 and 10^6 in the impeller zone (Heiskanen, 2013), but decreases further away from the impeller due to energy dissipation. For perfectly mixed systems, operating conditions with a Reynolds number below roughly 2000 is considered laminar flow, and above 3000 is considered turbulent, while 2000>Re>3000 is the transition zone (Truter, 2010). Figure 3.11 displays the CFD modelled turbulence intensity in a flotation cell, which is defined as the ratio of the root-mean-square turbulent velocity and the mean velocity.
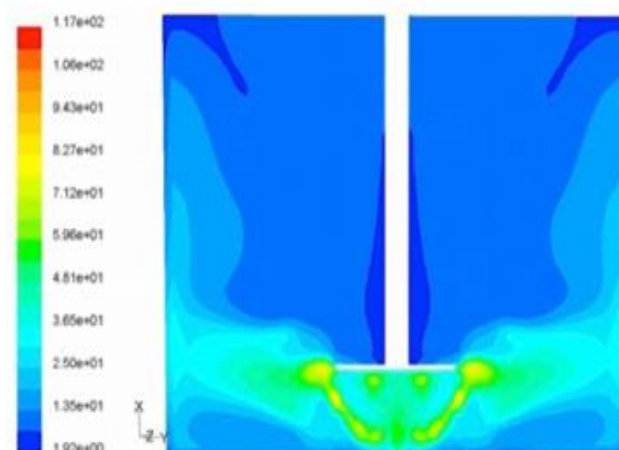
Figure 3.11: CFD modelled turbulent intensity in a mechanical flotation cell (Heiskanen, 2013).

Table 3.4: Dimensionless numbers for flotation cells.
(Nelson et al., 2002; Harris and Mensah-Biney, 1977; Truter, 2010).

Dimensionless number	Equation	Variables
Reynolds number (impeller zone)	$Re = \dfrac{ND^2\rho_p}{\mu_p}$	N = impeller rotational speed [1/s]
Froude number	$Fr = \dfrac{N^2D}{g}$	D = impeller diameter [m] ρ_p = pulp density [kg/m^3]
Aeration (air flow) number	$Ae = \dfrac{Q_{air}}{ND^3}$	μ_p = pulp viscosity [kg/m/s] g = gravitational acceleration constant (9,81 m/s^2)
Power number	$Po = \dfrac{P}{\rho_p N^3 D^5}$	Q_{air} = air flow rate [m^3/s] P = power draw [kg·m^2/s^3]
Weber number	$We = \dfrac{N^2D^3\rho_L}{\gamma}$	ρ_L = liquid density [kg/m^3] γ = surface tension of the air-liquid interface [kg/s^2]
Volumetric flow number	$Vo = \dfrac{Q_{pulp}}{ND^3}$	Q_{pulp} = pulp flow rate [m^3/s]

Other dimensionless numbers specified for flotation cells are the *aeration number* (the ratio of the air flow velocity and the impeller peripheral speed), the *power number* (the ratio of inertial and resistance forces), the *Weber number* (the ratio of inertia and surface tension forces) and the *Volumetric Flow number* (the ratio of pulp flow velocity and impeller peripheral speed).

A number of researchers (Rodrigues et al., 2001; Schulze, 1982; Harris and Mensah-Biney, 1977; Truter, 2010) claim that maintaining certain dimensionless numbers such as those in table 3.4 constant is an important consideration for successful up-scaling. The impeller diameter and rotation speed are known to directly influence turbulence and energy dissipation, thereby affecting recovery and grade results in flotation, and maintaining constant relations is advocated to minimize variations in results between different cells on different scales. The following case example applies dimensionless numbers to calculate a kinetic scale-up factor for flotation processes.

Furthermore up-scaling research has been done based on preserving constant energy characteristics to the cells per unit of volume or mass. Degner (Arbiter, 2000) estimated flotation cell hydrodynamics for 127 and 170 m^3 cells based on the operation of cells ranging from 8,5 to 85 m^3, while retaining a specific power input of 2,11 kW/m^3, and scaling the rotor dimensions to retain a constant power number, according to the formula in table 3.4. Schubert and Bischofberger (1998) proposed that maintaining a constant energy dissipation, specific power input and air flow number are useful up-scaling criteria, and that the impeller rotational speed and impeller diameter should be related according to:

$$N \propto D^{-\frac{2}{3}}$$
(3.11)

The main issue with these up-scaling methods is the difficulty of measurement of factors like the turbulence in industrial flotation cells, which makes it impractical to optimize the cells for a specific ore after they have been installed in the processing plant. The next section gives a practical example of the use of dimensionless parameters to describe distinct effects in the flotation cells, to be used for up-scaling.

Dimensionless parameter up-scaling approach at Codelco El Teniente, Chile

Yianatos et al. (2010c) developed a scale-up approach based on dimensionless parameters, and applied this method to evaluate the performance of new Outotec TankCell-300 rougher flotation cells in comparison with the old Outokumpu OK-160 rougher cells at Codelco's El Teniente copper mine in Chile. The first parameter ξ was defined as the ratio between the actual flotation rate in the collection zone of a single perfectly mixed industrial cell (k_{ac}) and the flotation rate in a laboratory batch cell (k_b):

$$\xi = \frac{k_{ac}}{k_b} \qquad\qquad (3.12)$$

Additionally, the apparent flotation rate constant (k_{app}) is based on the actual flotation rate constant, and three dimensionless parameters, named the *froth effect (α),* the *cell mixing effect (β),* and the *particle segregation effect (γ).* The froth effect is defined as the ratio of the apparent flotation rate and the collection zone rate constant k_c. The mixing effect is defined as the ratio of the mixing condition parameter φ, as explained in equation 3.9 on page 30, for a single cell and for the total number of cells in the bank at the same dimensionless recovery η, which was defined in equation 3.10 on page 30. Finally, the solids segregation effect is defined as the ratio between the effective solid residence time (τ_S) and the effective liquid residence time (τ_L). The apparent flotation rate constant is given by:

$$k_{app} = k_{ac} \cdot \alpha \cdot \beta \cdot \gamma \qquad\qquad (3.13)$$

with the individual dimensionless parameters given by:

$$\alpha = \frac{k_{app}}{k_c}, \qquad \beta = \left.\frac{\varphi(N=1)}{\varphi(N \neq 1)}\right|_\eta, \qquad \gamma = \frac{\tau_S}{\tau_L} \qquad\qquad (3.14)$$

Combining equations 3.12, 3.13 and 3.14 gives the ratio between the apparent flotation rate constant and the batch flotation rate constant as a function of dimensionless parameters, as given in equation 3.15. The results obtained by Yianatos et al. are shown in table 3.5.

$$\frac{k_{app}}{k_b} = \xi \cdot \alpha \cdot \beta \cdot \gamma = \xi \cdot \frac{k_{app}}{k_c} \cdot \left(\left.\frac{\varphi(N=1)}{\varphi(N \neq 1)}\right|_\eta\right) \cdot \frac{\tau_S}{\tau_L} \qquad\qquad (3.15)$$

Table 3.5: Dimensionless parameters and scale-up factors from literature (Yianatos, 2010a).

Cell type	k_{app} / k_b	α (froth)	β (mixing)	γ (segregation)	ξ (scale-up factor)	S_b [1/s]
TC-300	0,24	0,48	0,76	0,89	0,75	44,5
OK-160	0,21	0,44	0,79	0,89	0,68	41,7

The values for ξ can be used to determine the actual flotation rate constants for the tested cell types based on the flotation rate constant obtained in laboratorial batch tests with the same ore. However, application of the scale-up procedure in designing a greenfield flotation circuit requires a more extensive research, since no performance information is available for the optimal particle size distribution and chemical conditioning in that situation. Yianatos et al. (2010c) recommend a sequential calculation, in which the dimensionless parameters are estimated for each individual cell in the bank.

⧉BOLIDEN

3.2.5 Carrying capacity approach towards up-scaling

The *carrying rate* in a flotation cell has been defined as the mass transport of solids by bubbles per unit of time per unit of cell cross-sectional area (Yianatos and Contreras, 2010b), in kg/m²/s. The maximum carrying rate is defined as the *carrying capacity*, and may represent a limitation when a large fraction of solids needs to be recovered from the pulp. From a historical perspective, carrying capacity in flotation has mainly been associated with column flotation, because of the small horizontal cross-sectional surface area in comparison to mechanical cells, which limits the amount of material able of attachment to bubbles and being lifted to the froth.

Recently several researches have been conducted to determine the carrying capacity and bubble load in base metal flotation, but values strongly differ. Carrying capacity is calculated by multiplying the bubble load with the superficial gas velocity. Seaman et al. (2004) reported bubble loads of 141,9±2,8 kg/m³ in a 50 m³ zinc cleaning cell at Teck Cominco's Red Dog mine, whereas Yianatos et al. (2008a) reported a range of 26-51 kg/m³ in a 130 m³ copper rougher circuit at Codelco's El Teniente mine.

A classical method of evaluating the carrying capacity in column flotation was by measuring the total solids mass flow rate into the concentrate. This method is not valid for mechanical cells, since the recovery by solid entrainment is much higher, while in column flotation practically all material is recovered by true flotation. In order to achieve an actual limit on the carrying capacity, large amounts of materials need to be recovered in combination with a low bubble surface area flux (Yianatos et al., 2010b).

To determine carrying capacity in mechanical cells several attempts have been made in earlier times. Espinosa-Gomez et al. (1988a) derived an equation to relate carrying capacity to the particle density, superficial gas velocity, bubble size and particle size. However, at the time problems occurred in accurately determining bubble sizes and many assumptions had to be made, while currently many reliable methods exist to determine bubble size distributions and bubble loads with optical methods. Espinosa-Gomez et al. (1988b) were able to derive an empirical equation for the carrying capacity based only on the material's 80% passing size and particle density:

$$C_A = 0{,}068 \cdot P_{80} \cdot \rho_p \tag{3.16}$$

Yianatos and Contreras (2010b) proposed expressions, given in equations 3.17 and 3.18, for the carrying rate (C_R) and carrying capacity (C_A) in mechanical cells, as functions of the bubble surface coverage φ_S and maximal bubble surface coverage $\varphi_{S,max}$, the bubble surface area flux S_B, the Sauter mean particle diameter d_p, the solid density ρ_p and the froth recovery R_F. The froth recovery term accounts for the material recovery of entrained material in mechanical cells, as opposed to column flotation. The derivation of these equations is given in appendix A.

$$C_R = \varphi_S \cdot \frac{\pi}{6} \cdot S_B \cdot d_p \cdot \rho_p \tag{3.17}$$

$$C_A = \varphi_{S,max} \cdot \frac{\pi}{6} \cdot S_B \cdot d_p \cdot \rho_p \cdot R_F \tag{3.18}$$

Test work by Yianatos and Contreras (2010b) on rougher flotation cells resulted into a maximum bubble load of 363±26 kg/m³ for a fully covered bubble, for material with a solid density of 3,7 tonnes/m³. During tests the bubble surface coverage was in the range of 7 to 22%. The values were obtained by varying superficial gas velocity, Sauter mean bubble diameter and Sauter mean particle size. Table 3.6 gives carrying rates at the pulp-froth interface and for the concentrate for four different tests. For test 2 the bubble load was close to the maximum, resulting into a high value for the carrying rate. During test 4 problems with reagent dosing were encountered.

*Table 3.6: Carrying rate and froth recovery for rougher circuit test work
(Yianatos and Contreras, 2010b).*

Plant test	Interface true flotation carrying rate [tph/m³]	Concentrate true flotation carrying rate [tph/m³]	Froth recovery for true flotation [%]
1	1,42	0,67	47,1
2	3,10	0,91	29,2
3	1,76	0,66	37,6
4	0,73	0,52	71,2

As can be seen from table 3.6, it proved difficult to achieve the maximum carrying rates at the pulp-froth interface, due to the relatively large amount of entrained material in mechanical cells. This will also be the most important limiting factor during scale-up, since for a proportional scale up the volume will triple where the cross-sectional area doubles, and bubble load is roughly related to volume, whereas carrying rate and capacity are related to the cross-sectional area. Additionally, evaluation of the carrying capacity requires specialized equipment to measure the bubble surface coverage which is often not available, thus making this method less practical for up-scaling purposes.

A problem arises during modelling of flotation in the situation of a limitation in carrying capacity from the assumption of first order rate models that particles do not compete for space on the bubble surface (Burstein and Filippov, 2010), which would no longer be valid. This would significantly complicate the problem, since the well-tested kinetic models summed up in section 2.3 may no longer be applicable.

3.3 Mineral flotation and its up-scaling at Boliden Aitik

3.3.1 The new Aitik processing plant

The new processing plant of the Aitik mine has been taken into operation in August 2010, leading to an increase in annual processing capacity from 18 to 36 million tonnes of ore. By maximizing the throughput and elimination of bottlenecks the practical capacity limit of the processing plant is however estimated to be around 45 million tonnes per year. This limit may be tested in the future when the production capacity of the mine itself is planned to approach that figure.

The grinding stage consists of two lines of autogenous grinding, each with a primary and secondary mill. After the primary mill, screens separate particles with an intermediate size from the large and fine fractions, to return to primary grinding, or to serve as grinding media in flotation regrinding. The large fraction functions as grinding medium for secondary grinding. After secondary grinding the material is classified with screw classifiers, from where fine particles are separated for the flotation process, and coarse material returns to primary grinding. An overview of the grinding process is given in figure 3.12.
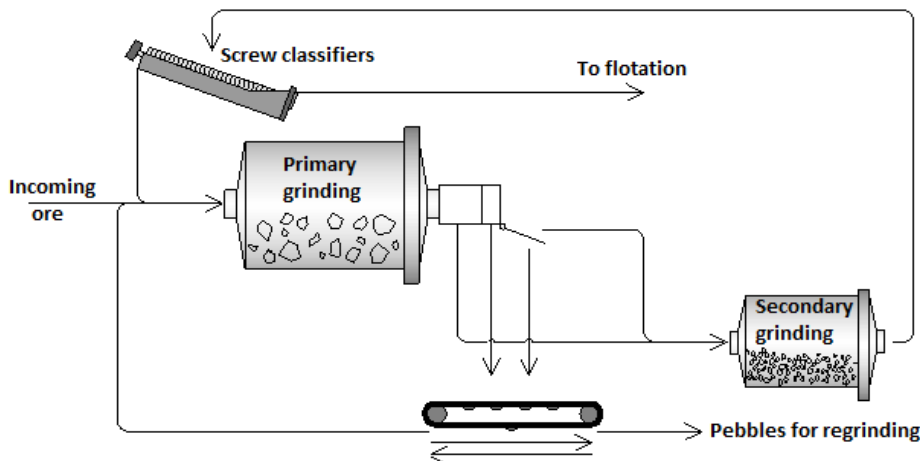

Figure 3.12: Overview of the grinding process at Boliden Aitik.

The ground material enters a conditioning tank together with recirculating material from the cleaner flotation, and reagents are added. The flotation plant is composed of cells from the Outotec TankCell-series. Like the grinding plant, the flotation plant has two separate lines. The conditioned material first enters the rougher stage, consisting of four TankCell-160 cells. The rougher tailings continue to the scavenger stage, consisting of five TankCell-160 cells. Scavenger tailings are refloated in a desulphurization step, consisting of four additional TankCell-160 cells, of which two cells can be used to prolong the scavenger banks. The desulphurization concentrate can be stored separately to prevent acid mine drainage problems in the tailings pond, although this is currently not done yet.

The rougher and scavenger concentrates are both reground in a separate pebble mill. The pebbles originate from the intermediate fraction of the screening step after primary grinding. The reground rougher concentrate enters the secondary cleaning stage, and after a tertiary and quaternary cleaning stage the final copper concentrate is obtained. Tailings from the secondary cleaning stage enter the primary cleaning stage, where also the reground scavenger concentrate is added. The primary cleaning's concentrate continues to the secondary cleaning, while tailings enter a cleaner scavenger bank. The tailings of this bank are relatively rich in sulphur and can be stored separately in the future with the desulphurization concentrate.

A flow sheet of the flotation plant is given in appendix B. Table 3.7 specifies the number of cells and effective flotation volumes for each stage of the flotation process at Aitik.

Table 3.7: Flotation stages, number of cells and effective cell volumes at the Aitik flotation plant.

Flotation stage	Number of cells (cells x lines)	Effective single cell volume [m^3]	Total effective stage volume [m^3]
Roughers	4 x 2	160	1280
Scavengers	5-7 x 2	160	1600-2240
Desulphurization	2-4 x 2	160	640-1280
Primary cleaner scavenger	4 x 2	50	400
Secondary cleaner scavengers	3 x 2	50	300
Primary cleaners	5 x 1	40	200
Secondary cleaners	4 x 1	40	160
Tertiary cleaners	3 x 1	40	120

3.3.2 Processing plant expansion research at Aitik

The research for the expansion of the flotation process at Boliden Aitik was mainly based on flotation performance in the old processing plant. For the rougher and scavenger sections calculations were made according to the restriction of retaining an equal residence time. In addition, four extra cells per line were added for desulphurization, of which two can be used to prolong the scavenger process.

For the cleaning section the calculations were made according to the known limitations of carrying capacity and lip length in the old concentrator plant. It was known that the re-cleaning stage was only able to treat roughly half of the primary cleaner concentrate at a standard throughput. Typical values of these limitations were 11 tonnes per hour per meter squared for the carrying capacity, and 6 tonnes per hour per meter for the cell lip length, which is equal to approximately 3,06 kg/m²/s and 1,67 kg/m/s in standard units, respectively.

Research in the new processing plant revealed that the flotation time in the rougher and scavenger sections does not restrict the performance of the flotation plant in terms of recovery (Bolin, 2014a). This implies that the current throughput of around 36 million tonnes per year can be increased (until an undefined limit) without affecting flotation performance. The realistic capacity limit of the flotation plant is estimated to be around 45 million tonnes per year. Beyond this value the ground ore will become too coarse to reach sufficient copper recovery, and a third grinding line would be needed for compensation. Currently the internal dart valves between individual cells limit the capacity to approximately 3200 t/h. The capacity of the cleaning stage is already higher than currently required.

4. Experimental procedure

4.1 Influence of the batch cell size

In order to answer the question why differences in flotation performance occur between cells on different scales, the issue is first explored in laboratory batch flotation cells of different sizes. If certain effects are already detectable in such a relatively small scale-up, this may point out up-scaling phenomena that are occurring on a larger scale in industrial flotation. These experiments are performed in order to answer the first partial research question, '*what causes the differences in results between laboratory and industrial flotation?*'.

The Boliden mineral research laboratory has the disposal over several sizes of Magotteaux batch flotation cells, with effective volumes of around 1,5, 2,5, 4,5 and 8,0 litres. It was observed that for previous research the 2,5 litre cell is the most commonly used for standard test work at Boliden. A reason for this might be that, at a constant weight percentage solids, a larger cell will require a larger ore sample, which might not always be available or reduces the total possible amount of tests.

Batch flotation tests were performed on several types of material to observe distinguishable effects between the cell volumes, and to see if the 2,5 litre cell is representative for future test work. The tests were performed only in the 2,5, 4,5 and 8,0 litre cells, since it is believed that the 1,5 litre cell will give a high degree of entrainment, and a minor amount of ore is used while the standardized input of the used rod mill is 5 kg of ore, thus wasting relatively much material.

To split the ground ore from the rod mill into the right amounts for flotation tests, a rotary pulp splitter is used, as shown in figure 4.1. The pulp splitter prevents effects of segregation and evenly distributes the material over eight funnels, allowing composition of the correct amount of ore for batch tests at different cells sizes and solid weight percentages. However, in practice it is difficult to attain the exact desired amount of ore, and small deviations in the weight percentage solids of the pulp occur.

A total of three test ores is used to perform the batch tests. Firstly, Aitik ore crushed in a laboratory jaw crusher to 80% passing 3 mm is ground in a laboratory rod mill for a period of 10 minutes before flotation. Secondly, a sample of the Aitik grinding circuit output is used for batch flotation. Thirdly, the feed to the rougher flotation circuit is used. The difference between the mill output and the rougher feed is the addition of reagents and the recycle stream from the cleaner circuits.

The test conditions are given in table 4.1. The aimed weight percentage solids for the test on the crushed ore is 45%, which is equal to the target in the Aitik flotation plant. The added reagents are identical to the industrial scale reagents, and no extra reagents are added to the batch test on rougher feed since this material already went through the conditioning tank. It is assumed that the industrial reagent dosing is already optimal, since this is no subject of investigation in this research.

Figure 4.1: Rotary pulp splitter.

Table 4.1: Test conditions for batch flotation tests.

Aimed weight % solids	45%
Collector type	Potassium amyl xanthate (PAX)
Collector dosage	5,0 g/tonne of ore
Frother	Nasfroth 240
Ore grinding time*	10 minutes
pH	10,5
Froth thickness	15 mm

*Grinding time only applies in the test with Aitik crushed ore.

Table 4.2 gives operational parameters of the batch flotation tests. The air flow rate has been scaled to the cross-sectional area of the cells to keep a constant superficial gas velocity according to equation 2.12, while preserving sufficient turbulence in the smallest cells, and also keeping a constant air flux over the surface, assuming the bubbles are of equal sizes at constant impeller speed. The cell cross-sectional area and air flow rate per unit of ore mass is almost equal for the 2,5 and 4,5 litre cells, but approximately half this value for the 8,0 litre cell. From a kinetic point of view this may result into a low recovery on the short-term, thus for the first and possibly second concentrate obtained during the batch test.

Table 4.2: Batch flotation cell operational parameters.

Cell size	Cell cross-sectional area [cm²]	Air flow rate [l·min⁻¹]	Ore mass [kg] (at 45 wt% solids)	Cell area per mass ore [cm²·kg⁻¹]	Air flow rate per mass ore [l·min⁻¹·kg⁻¹]
2,5 litre	222	7,50	1,58	140,5	4,75
4,5 litre	390	13,18	2,85	136,8	4,62
8,0 litre	346	11,69	5,07	68,2	2,31

4.2 Factorial design of batch testing operating parameters

The tests described in the previous section can be used to give insight in the influence of batch cell size during laboratory flotation tests. During an up-scaling procedure the test work will have to be performed on ore crushed and ground with laboratory equipment, since no representative samples of the new grinding circuit are available. Therefore, insight in other operational parameters of batch flotation tests can be valuable to improve the testing procedure. The factorial design also serves to answer the first partial research question '*what causes the differences in results between laboratory and industrial flotation?*', but especially focusses on the influence of operating conditions on the results.

With the use of the program MODDE by Umetrics (Eriksson et al., 2000), a 2^3 full factorial design is made to clarify the influence of a number of responses on batch flotation cell testing, and to apply several statistical tools on the results to determine the validity and reproducibility of the results. This program can also provide a predictive model for future tests under different conditions.

The design consists of three independent *factors,* i.e. the parameters that will be varied in the factorial design tests; the cell size, the weight percentage solids and the rod mill grinding time. In plant practice, a lower weight percentage solids is expected to improve flotation performance, since there is less interaction between solids and the slurry becomes less viscous, allowing bubbles to transport valuable minerals to the surface more rapidly, and with a lower throughput as the main disadvantage.

The grinding time for batch tests should result into a particle size distribution that is comparable to the full scale operation. The grinding should achieve sufficient mineral liberation and a suitable particle size range for sulphide flotation, while keeping in mind that grinding is the single largest processing cost for a mine. The expected result in batch tests can be an improved recovery due to better liberation, but a lower concentrate copper grade due to entrainment of gangue minerals.

For each variable an upper and lower limit are determined, which gives a total of 2^3 = 8 tests. Additionally four identical extra tests are performed with intermediate variable values to determine the repeatability of the tests. The limits and intermediate values are given in table 4.3. To quantify the results, a number of *responses* is chosen. These are the test results for which a predictive model will be fitted.

Table 4.3: Limiting values of factors for the 2^3 factorial design for batch flotation tests.

Values	Cell size [l]	Wt% solids	Grinding time [min]
Upper limit (+)	8,0	45%	12
Intermediate value (o)	4,5	35%	10
Lower limit (-)	2,5	25%	8

NEW BOLIDEN

4.3 Characterization of industrial flotation cells

Previous internal research by Boliden at the concentrator plant of the Aitik mine showed a certain degree of segregation in the desulphurization section of the flotation circuit. Such an effect may obstruct the recovery of the segregated minerals, or even negatively influence performance of the complete flotation cell. To obtain more information on possible segregation effects, the following sampling will be done as a profile of depth in the mixing zones, quiescent zones and froth zones of several industrial rougher and scavenger cells. Therefore, the following experiment will serve to answer both the second and third partial research question, '*what are the influences of the different sub-processes of the flotation cell on its performance?*', and '*what may happen during further up-scaling of industrial flotation cells?*'.

To characterize any effect of segregation in the largest cells of the flotation circuit, a sampling survey was performed on 04-12-2013 on the first and last cells of the rougher and scavenger section of the first line in the Aitik flotation plant (cell 9 is here the last scavenger). The complete rougher and scavenger sections consist of Outotec TankCell-160 cells. The main purpose is to identify effects within the different zones in the cells that would be of influence on flotation performance, and therefore on cell selection in future projects.

Samples from each cell were taken of the top of the froth, the complete froth overflow of the cells, directly under the froth, at every half meter under the top of the froth from 0,5 to 4,0 meters depth, and finally of the feed or tails of the cell where possible. Table 4.4 shows the sampling methods for the different sample types. Figure 4.2 shows the sampling points in an axial view of the flotation cell. Feed and tailing samples were taken at a by-pass stream for online XRF analysis.

Table 4.4: Sample points and sampling types for Aitik flotation plant survey on 04-12-2013.

Sample	Sampling method
Top of froth	Scraping
Complete froth	Cell overflow
0,1 m – under froth	Gas holdup probe
0,5 m – 4,0 m	Gas holdup probe
Feed	By-pass stream
Tails	By-pass stream
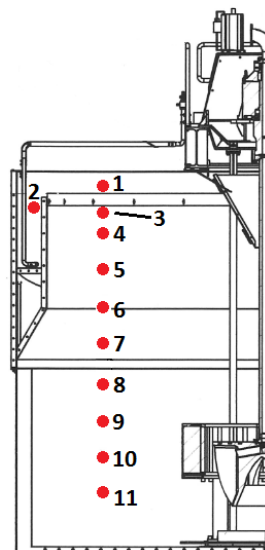
Sample locations:
1: Top of froth
2: Complete froth (sampled at cell overflow)
3: Under froth (approximate depth of 0,1 m)
4: 0,5 m depth
5: 1,0 m depth
6: 1,5 m depth
7: 2,0 m depth
8: 2,5 m depth
9: 3,0 m depth
10: 3,5 m depth
11: 4,0 m depth

Figure 4.2: Sample locations in the rougher and scavenger flotation cells.

The slurry sampling is done with an in-house constructed sampling probe, primarily consisting of a tube with valves at both ends, which is shown in figure 4.3. The system operates on pressurized air and while keeping the device in the slurry, both valves can be shut simultaneously. Since the internal volume of the

tube is known, the local gas holdup can be calculated based on a density measurement of the slurry sample. The slurry samples are filtered and dried to determine the weight percentage solids and analyse the dry material. Because of the difficulty to directly determine the slurry volume while sampling in the plant, the local gas holdup ε_g is calculated with the use of the solids density according to equation 4.1.

$$\varepsilon_g = 1 - \frac{\left(\frac{M_s}{\rho_s} + \frac{M_w}{\rho_w}\right)}{V_{tube}} \qquad (4.1)$$

In equation 4.1, M_s and M_w stand for the mass of solids and water, ρ_s and ρ_w stand for the densities of solids and water, and V_{tube} stands for the volume of the sampling tube. The density of the dry solid samples is determined with a helium gas pycnometer.

Figure 4.3: Sampling probe used in flotation cell characterization test work.

All samples undergo sieve analysis to examine the particle size distributions, and five fractions are analyzed by XRF for their metal assays to look into the distribution of the metals in the different fractions. The used fractions are displayed in table 4.5. It is expected that recovery is optimal in the 45-90 μm fraction, which is part of what is generally seen as the optimal flotation particle size range of 10-100 μm (Rahman et al., 2012). Furthermore it is expected that hardly any copper minerals are recovered in the +180 μm fraction, since these minerals are generally too large (i.e. badly liberated and too heavy) to float. In the -45 μm fraction copper recovery is expected to be good, although this particle size is also known to typically have a high degree of gangue mineral entrainment (Wills, 2006)., thus reducing the concentrate grade.

Table 4.5: Expected recoveries for different fractions.

Fraction (μm)	Expected result
-45	Reasonable recovery
45-90	Optimal recovery
90-125	Good recovery
125 – 180	Moderate recovery
+180	Minor recovery

4.4 Direct comparison of laboratorial, pilot plant and full scale flotation

After obtaining a clearer image of the various phenomena in both laboratory batch flotation and full scale flotation, as described in the previous sections, a pilot plant set-up is constructed to allow better comparison of flotation results on different scales. The main advantage of the pilot plant is that it provides data of a continuous operation on a smaller scale, and is able to give a direct comparison to the full scale operation, since its feed material can be taken directly from the industrial scale conditioning tank. Meanwhile, the same feed material can be sampled to perform batch tests and relate these results to the continuous flotation results, which is important since batch tests will remain the most important method to quickly and cheaply evaluate flotation performance. This test work serves to answer both the first and third partial research question, '*what causes the differences in results between laboratory and industrial flotation?*', and '*what may happen during further up-scaling of industrial flotation cells?*'.

The used pilot cells are shown in figures 4.4 and 4.5. The pilot plant consists of four cells in series, with two launders to collect the combined concentrate of the first and last two cells. The feed material is taken from the material by-pass leading to the online analyzing system. The cell characteristics of the various flotation cells on different scales are given in table 4.6.

Table 4.6: Flotation cell dimensions for all used size scales.

	8,0 litre batch	Pilot	Full scale
Height	240 mm	55 cm	~488 cm
Horizontal area	346 cm²	0,360 m²	31,85 m²
Impeller height	3,3 cm	11,5 cm	86,3 cm
Impeller diameter	10,1 cm	37,4 cm	1,40 m

Figure 4.4: Pilot cells used for test work.

Afterwards, the obtained samples were weighted before and after drying to calculate water recovery figures. Furthermore the samples were sieved and analyzed in three different size classes, namely -45 µm, 45-125 µm and +125 µm. The expectation is that recovery in the +125 µm size class is considerably lower due to decreasing mineral liberation and increased downward gravitational forces. For the -45 µm size class a relatively high degree of entrainment is expected. In addition to the sampling, flow rate measurements of concentrate and tailing flows were done to estimate their values, in order to have a reasonable estimation as a mass balancing starting value.

Figure 4.5: Location of pilot cells (lower left corner) next to industrial flotation cells.

5. Experimental results

5.1 Batch flotation: The influence of batch cell size on laboratorial tests

5.1.1 Comparison of time-recovery curves

The batch cell flotation tests on Aitik ore sampled on different stages of the enrichment process were performed under the conditions given previously in table 4.1 on page 37. The main objective of these tests is to determine differences in performance between the various batch cell sizes, and not between the individual test materials of lab crushed ore, mill output and rougher flotation feed. It is important to consider that the test materials will also differ in composition, size distribution and mineral structure, although the mill output and rougher feed were sampled on the same day in the Aitik processing plant. The crushed ore was taken from the Aitik mine in an earlier stage.

Figure 5.1 shows the time-recovery curves of copper for all batch tests; the final recovery values are given in table 5.1. From the graphs it can be observed that the initial recovery (after 0,5 min) is highest in the 2,5 litre cell in all cases; this may be caused by the relatively small amount of total copper in the cell. The available bubble surface and flotation cell cross-sectional area per unit weight of copper is larger in this cell, thus giving better possibilities for flotation of chalcopyrite. However, the final recovery is highest in the 8,0 litre cell in all cases. In general, the curves do not differ significantly.

Table 5.1: Final recoveries of copper in laboratory tests.

Cell size	Crushed ore	Mill output	Rougher feed
2,5 L	88.68%	91.81%	85.11%
4,5 L	86.75%	92.19%	91.47%
8,0 L	90.51%	94.46%	92.08%
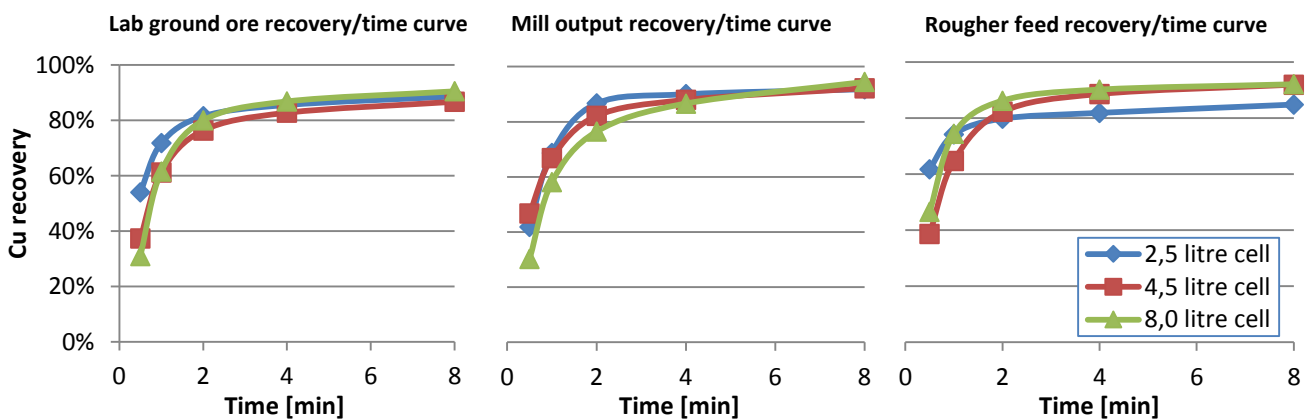
Figure 5.1: Cu recovery as a function of time for batch tests on different materials.

As was explained in section 2.8, the results of a single test under equal conditions neglects the existence of experimental error. However, performing every test twice or even more often, to reduce the standard error, strongly increases the time required for test work, and is often not even possible due to limited amounts of ore or changing properties of ore pulp sampled from a continuous system during the time the test work is performed.

The test work on ore pulp samples from the Aitik processing plant were not replicated because this feed material is not constant in properties. Performing these tests in triplicates would give a total of 6 x 3 = 18 tests, which cannot be performed on a single day, and ore properties are known to change over such longer time intervals, while sampling all the pulp at once will give gradually oxidized ore and altered chemical conditions (breakdown of reagents, changing pH/Eh due to oxidation, etc.) for the latest tests. For these reasons, only the tests on Aitik crushed ore were performed in triplicates to give insight in the experimental error and determine the confidence levels.

The time-recovery curve can be described by the first order recovery equation as given in equation 2.3 on page 9, which is most commonly used for batch flotation. The experimental results are firstly fitted to this equation by using the Solver option in Microsoft Excel, by minimizing the sum of squares (*SS*) between the copper recovery from the test data and from the model equation. Table 5.2 gives the standard error (σ) and the coefficient of determination (R^2) of the model fits. The coefficient of determination describes how well data points fit to a statistical model.

Table 5.2: Time-recovery model fitting standard error and coefficients of determination.

Cell size:	2,5 litre	4,5 litre	8,0 litre
Standard error of fit (σ):	4,91%	2,28%	4,43%
Coefficient of determination (R^2):	0,887	0,986	0,961

The results of flotation tests on crushed Aitik ore in different sizes of batch cells were analysed with a bootstrap method as described by Napier-Munn (2012). After obtaining the fitted model curve, a normally distributed random number with a zero mean and a standard deviation equal to the standard error of the model fit (see table 5.2) is added to the modelled recovery values. The Excel Solver add-in is set up to minimize the sum of squares between the original model and the model summed with normalized random numbers.

Subsequently, the add-in MCSimSolver (Barreto and Howland, 2006) is used to run 1000 simulations of the Solver, while new normalized random numbers are generated for every turn. The user can select which parameters are to be recorded during simulation; in this case these will be the model parameters (R_∞ and k), and copper recovery every 10 seconds until 480 seconds (8 minutes).

One of the main advantages of this method is that a direct comparison can be made between two modelled curves as a whole, even if these curves are not parallel or cross each other. In addition, no assumptions are made on linearity or the distribution of the test data (only the random errors are assumed to be normally distributed). The bootstrapped data have the same statistical uncertainties as the test data, since the randomized numbers have the same standard deviation. After obtaining 1000 simulated values of the model parameters and the recovery after different time intervals, a number of questions can be asked (Napier-Munn, 2014):

1. Are the model parameters different?
2. Is the predicted recovery after specific time intervals different?
3. Are the fitted models as a whole different from each other?

Firstly, the model parameters are compared. By calculating 1000 differences in the model parameters between two cell sizes, the significance of the differences is calculated. For abbreviation, the 2,5 litre cell is named test A, the 4,5 litre cell is named test B and the 8,0 litre cell is named test C. As a criterion on the significance of the result, a confidence level of 95% is used for all results.

Table 5.3: Time-recovery model parameter comparison and confidence levels
(red values indicate insufficient confidence in the results).

	Comparison 2,5 and 4,5 litre cells (B-A)		Comparison 2,5 and 8,0 litre cells (C-A)		Comparison 4,5 and 8,0 litre cells (C-B)	
Parameter	R_∞ [%]	k [s^{-1}]	R_∞ [%]	k [s^{-1}]	R_∞ [%]	k [s^{-1}]
Mean (μ)	-0,870	-0,0117	4,282	-0,0146	5,152	-0,0029
Standard dev. (σ)	1,932	0,0029	2,586	0,0030	2,160	0,0014
z-test value (=$|\mu/\sigma|$)	0,450	4,083	1,656	4,856	2,385	2,096
1-sided *P(z)*	0,326	0,000	0,049	0,000	0,009	0,018
1-sided conf. level	67,4%	100%	95,1%	100%	99,1%	98,2%
Conclusion	-	$k_A > k_B$	$R_{\infty, A} < R_{\infty, C}$	$k_A > k_C$	$R_{\infty, B} < R_{\infty, C}$	$k_B > k_C$

ΝΞW BOLIDEN

Table 5.3 gives a comparison of the model parameters of the different cell sizes. A *z*-hypothesis test is used to judge the significance of the data. The z-test is applicable in this situation because it deals with a large amount of samples (i.e. 1000), and thus approximates a normal distribution according to the central limit theorem (Barreto and Howland, 2006). This can also been seen in figure 5.2, which shows a histogram of the differences between the 1000 bootstrapped sample values of the maximum recovery R_∞ of tests C and A, and the shape approximates that of a normal distribution. Note that the major amount of the data is positive; this represents a fraction of 0,951 of the total data, and corresponds with the 95,1% confidence level for the comparison of R_∞ for tests A and C given in table 5.3.

The z-value is calculated as the absolute value of the mean divided by the standard deviation. The one-sided probability value can be found in a z-test table or calculated in Excel as =1-NORMSDIST(z). Only the result for the R_∞-comparison between the 2,5 and 4,5 litre cells is not reliable, according to its confidence level of 67,4% shown in table 5.3. The other results indicate that R_∞ is largest in the 8,0 litre cell, and that the flotation rate constant *k* is larger for the smaller cells ($k_A > k_B > k_C$). This statistically justified result supports the theory that copper minerals float faster in the smaller cells, as was suggested from the graphs in figure 5.1.
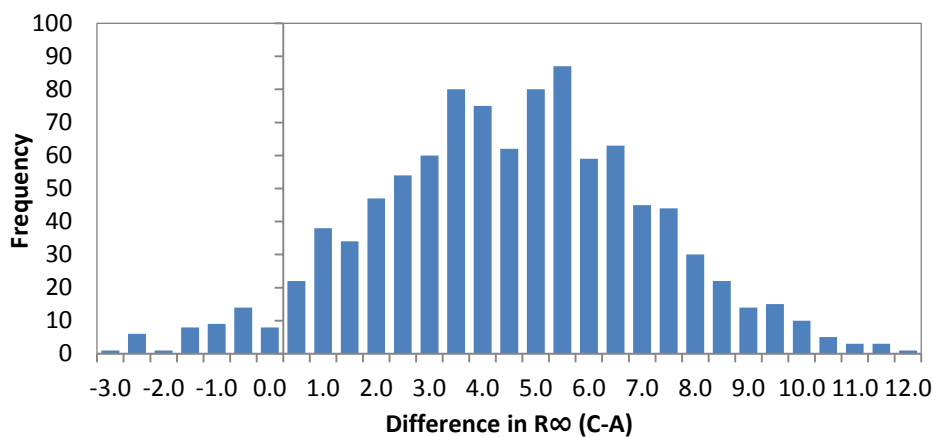

Figure 5.2: Histogram of bootstrapped differences in R_∞ between the 2,5 (A) and 8,0 (C) litre cells.

The same method can be applied to the recovery at the individual sampling times. Table 5.4 gives a summary of the recovery comparisons, with confidence levels between parentheses. The results shows that the recovery for the short time intervals (30-120 s) is highest in the 2,5 litre cell (test A), while for the long time intervals the recovery is highest in the 8,0 litre cell (test C).

Table 5.4: Summarized results of recovery comparisons at sampling times
(confidence levels between parentheses, red values indicate insufficient confidence in the results).

Time interval (s)	$\Delta\mu_{rec}$ 2,5 and 4,5 litre cells (B-A)	$\Delta\mu_{rec}$ 2,5 and 8,0 litre cells (C-A)	$\Delta\mu_{rec}$ 4,5 and 8,0 litre cells (C-B)	Conclusions
30	-14,19 (100%)	-16,44 (100%)	-2,25 (90,5%)	$R_A > R_B$ and $R_A > R_C$
60	-13,44 (100%)	-15,11 (100%)	-1,67 (80,7%)	$R_A > R_B$ and $R_A > R_C$
120	-6,54 (100%)	-5,38 (99,7%)	1,17 (77,9%)	$R_A > R_B$ and $R_A > R_C$
240	-1,52 (79,0%)	2,80 (88,1%)	4,31 (98,9%)	$R_C > R_B$
480	0,88 (67,5%)	4,25 (95,1%)	5,13 (99,1%)	$R_C > R_A$ and $R_C > R_B$

Since the bootstrapped data are assumed to have a normal distribution, they are also assumed to be symmetrical. This means that the upper and lower 2,5% of the 1000 samples will fall outside the 95% confidence interval, and these data can be used to plot the confidence intervals of each test. Figure 5.3 displays the modelled curves fitted to the data in the left graph of figure 5.1, and includes the 95% confidence intervals. Although the short-time recovery in the 2,5 litre cell is clearly higher, after approximately 150 seconds the confidence intervals start to overlap. This raises the question if the fitted models are actually different from each other. To investigate this, a null-hypothesis (H_0) is formulated which agrees that there is no relationship between the data, and thus the alternative hypothesis (H_1) agrees that there is a relationship.
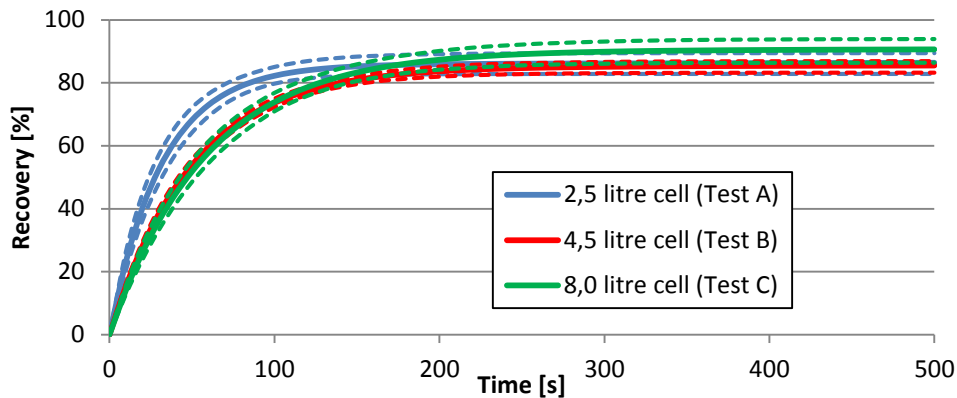
Figure 5.3: Model curves for Aitik crushed ore batch flotation tests with 95% confidence intervals.

The original data were already fitted to a model, and can now be compared to a fit of the total combined data of all tests. For example, when comparing the 2,5 and 4,5 litre cells, a model is fitted to the total time-recovery data of these two cells, and fitting coefficients like in table 5.2 are obtained. The comparison of the separate models with a model of the combined data will demonstrate if both data sets are statistically different from each other.

Table 5.5 is the Analysis of Variation (ANOVA) table for the comparison of shared and separate data. The meaning and construction of the ANOVA table is more thoroughly explained in appendix C. As a result, there is 100% confidence that models of A and B, and the models of A and C are different. However, for the comparison of models B and C a confidence of 94,8% is obtained, and thus its null hypothesis is rejected and the models are not proven to be significantly different.

Table 5.5: ANOVA tables for comparison of shared and separate models
(the ANOVA table is explained in appendix C).

Comparison A and B	N	SS	DF	MS	F	P	Confidence
H0 (shared data AB)	30	1009,8	28	36,1			
H1 (separate data A and B)	30	381,0	26	14,7			
Difference	0	628,8	2	314,4	21,5	$3,1 \cdot 10^{-6}$	100%
Comparison A and C	**N**	**SS**	**DF**	**MS**	**F**	**P**	**Confidence**
H0 (shared data AC)	30	1396,6	28	49,9			
H1 (separate data A and C)	30	568,5	26	21,9			
Difference	0	828,1	2	414,1	18,9	$8,4 \cdot 10^{-6}$	100%
Comparison B and C	**N**	**SS**	**DF**	**MS**	**F**	**P**	**Confidence**
H0 (shared data BC)	30	405,9	28	14,5			
H1 (separate data B and C)	30	323,1	26	12,4			
Difference	0	82,8	2	41,4	3,3	0,052	94,8%

5.1.2 Comparison of grade-recovery curves

Figure 5.4 displays the curves of copper recovery versus the enrichment ratio. Use of the enrichment ratio is preferred in graphs above use of the copper grade to prevent a distorted image as a result of different feed grades, but the graphs are otherwise analogous to the grade-recovery curves. As could be seen in table 5.1, the final copper recovery is between 85% and 95% in all cases. However, there is no information on the recovery of gangue minerals or the concentrate grades.

From figure 5.4 it can be observed that the enrichment ratio is highest for the 8,0 litre cell and smallest for the 2,5 litre cell for all materials at their maximum recovery. This is likely caused by a higher degree of entrainment in the smaller cell; the higher air flow rate per unit of ore mass (as shown in table 4.2) and the smaller cell dimensions enhance transport of fine particles into the froth and concentrate.
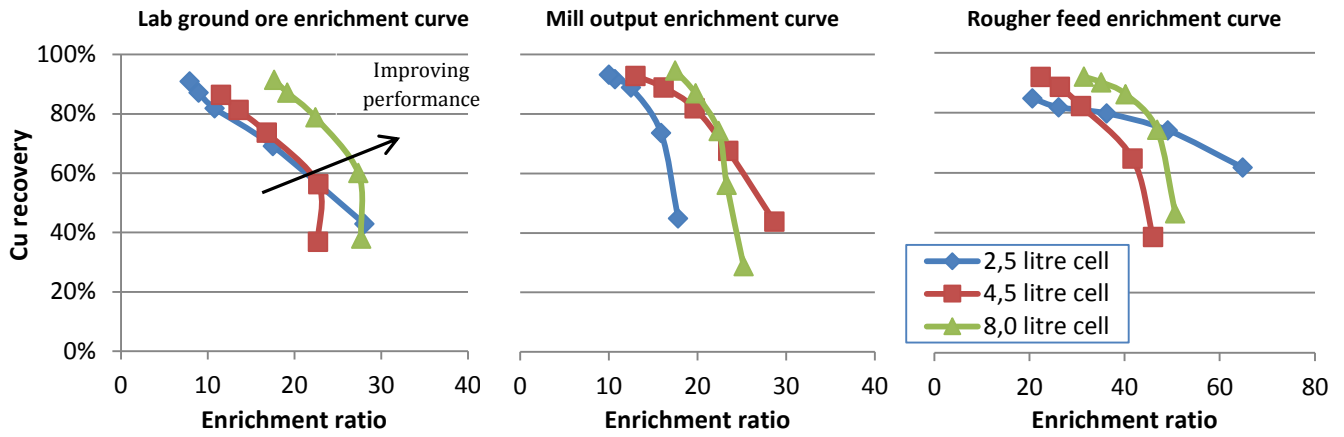
BOLIDEN

Figure 5.4: Cu recovery vs. enrichment ratio for batch tests on different materials.

Additionally, the residence time of particles in the froth can affect the recovery by entrainment. Froth residence time can be calculated according to:

$$\tau_F = \frac{H_F \cdot \varepsilon_{G,F}}{J_g} \tag{5.1}$$

in which H_F is the froth height, $\varepsilon_{G,F}$ is the gas holdup in the froth, and J_g is the superficial gas velocity (Yianatos et al., 2012). Combining equation 5.1 with equation 2.12 for the superficial gas velocity on page 12 gives:

$$\tau_F = \frac{H_F \cdot \varepsilon_{G,F} \cdot A}{Q_A} \tag{5.2}$$

in which Q_A is the air flow to the cell and A the cell cross-sectional area. Since the chemical conditions, feed material and weight percentage solids is equal in all tests, the froth gas holdup should be constant by approximation. As starting criteria, the froth thickness and air flow rate per unit of surface area were kept constant between tests, and thus the froth residence time is also constant according to equation 5.2. This eliminates any froth effects on entrainment and attributes it entirely to the cell dimensions and hydrodynamic conditions in the pulp zone.

Like the time-recovery curves, the data can be modelled to make a more statistically supported conclusion. A model for cumulative recovery as a function of the enrichment ratio was proposed by Bruey (Napier-Munn, 2012) as:

$$R = R_\infty - \exp(10 - c) \sinh\left(\left\{\frac{ER}{ER_{50}}\right\} \cdot \sinh^{-1}\left\{\frac{R_\infty - 50}{\exp(10 - c)}\right\}\right) \tag{5.3}$$

in which c describes the curvature of the curve ($c = 0$ gives a straight line), and ER_{50} is the enrichment ratio value for which the cumulative recovery is 50%. The model was fitted to the test data with the same bootstrap method as for the time-recovery curves. Figure 5.5 gives the modelled curves including the 95% confidence intervals, whereas tables 5.6 and 5.7 give comparisons between the cells at low and high enrichment ratio, respectively, similar to what was done for time-recovery model parameters in table 5.3. Although no confident conclusions can be drawn on the comparison of the 2,5 and 4,5 litre cells (tests A and B), the recovery of the 8,0 litre cell is the highest of all cell sizes at both a low and high enrichment ratio. This suggests a lower recovery of gangue minerals, since a higher recovery is reached for a fixed concentrate copper grade.

Table 5.6: Cell recovery comparisons at ER = 10.

ER = 10	(B-A)	(C-A)	(C-B)
Mean [%]	-3,32	5,89	9,22
Confidence	79,1%	95,6%	97,2%
Conclusion	-	$R_C > R_A$	$R_C > R_B$

Table 5.7: Cell recovery comparisons at ER = 25.

ER = 25	(B-A)	(C-A)	(C-B)
Mean [%]	-8,23	8,25	16,48
Confidence	84,2%	95,9%	98,1%
Conclusion	-	$R_C > R_A$	$R_C > R_B$
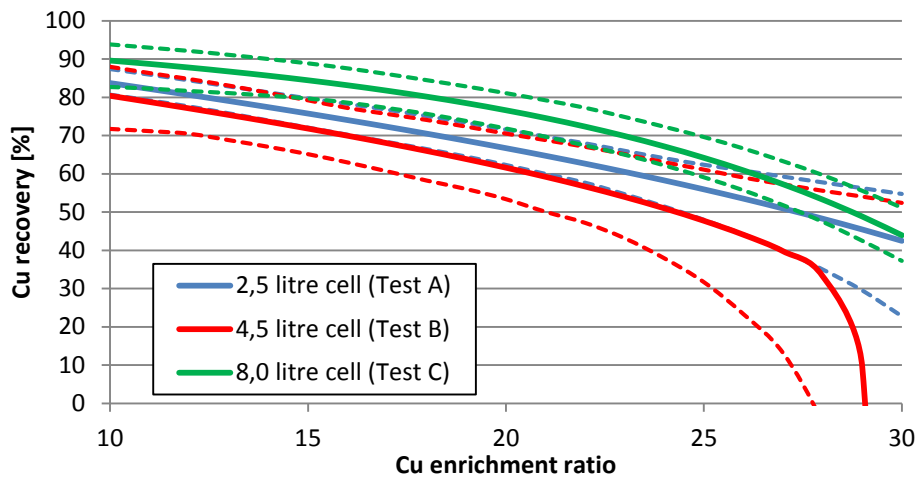
Figure 5.5: Modelled ER-recovery curves of copper with the corresponding upper and lower confidence intervals (dotted lines).

5.1.3 Comparison of particle size distributions

To illustrate the theory of particle entrainment leading to dilution of the concentrate with gangue mineral fines, size distributions are made of the concentrates and tailings of each test, and the average results per cell size are shown in figure 5.6. It can be seen that the size distribution curves for the tailings are approximately equal, while the curves for the concentrates are distinctly finer, especially under the 100 μm particle size range. Since flotation is optimal in the 10-100 μm size range (Rahman et al., 2012), this is more likely to be a result of the flotation process itself.

However, the concentrates seem to become finer with decreasing cell size, indicating that entrainment may play a role. Another possibility would be a better recovery of fine copper minerals in the smaller cell, but the time-recovery graph of figure 5.3 already showed that the final recovery is better in the largest cell. In the case of equal flotation performance the concentrates should also have the same size distributions, since the feed material is the same and was ground for the same time period.
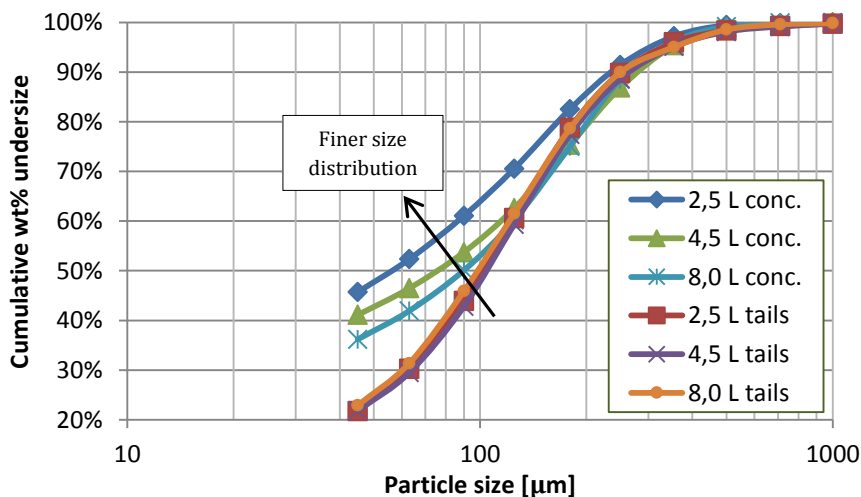
Figure 5.6: Averaged particle size distributions of concentrates and tailings per cell size for batch tests on different materials.

To statistically support the theory of enhanced recovery of fine particles by entrainment in the smaller batch flotation cells, the previously explained bootstrap method was used to model the particle size distribution data of the flotation concentrates according to a Rosin-Rammler distribution (Rosin and Rammler, 1933), given by:

$$F(x) = 1 - \exp\left(-\left(\frac{x}{x_r}\right)^n\right) \qquad (5.4)$$

in which $F(x)$ is the percentage particles smaller than particle size x, and x_r and n are fitting parameters. An advantage of this equation is that the parameter x_r has a physical meaning, which can be evaluated for $x_r = x$:

$$F(x) = 1 - \exp(-(1)^n) = 1 - \exp(-1) = 0{,}632 \qquad (5.5)$$

Thus, x_r is the particle size for which 63,2% of the particles is smaller than x_r. The left graph of figure 5.7 gives the combined modelled Rosin-Rammler curves with 95% confidence intervals for tailings and concentrates. It can be observed that the concentrates have a distinctly finer size distribution; a logical result of the flotation process. The right graph of figure 5.7 gives the separate Rosin-Rammler curves of the concentrates per cell size including confidence intervals. Although the curves for the 2,5 and 4,5 litre cells mostly overlap, the size distribution of the 8,0 litre cell concentrate is distinctly coarser.
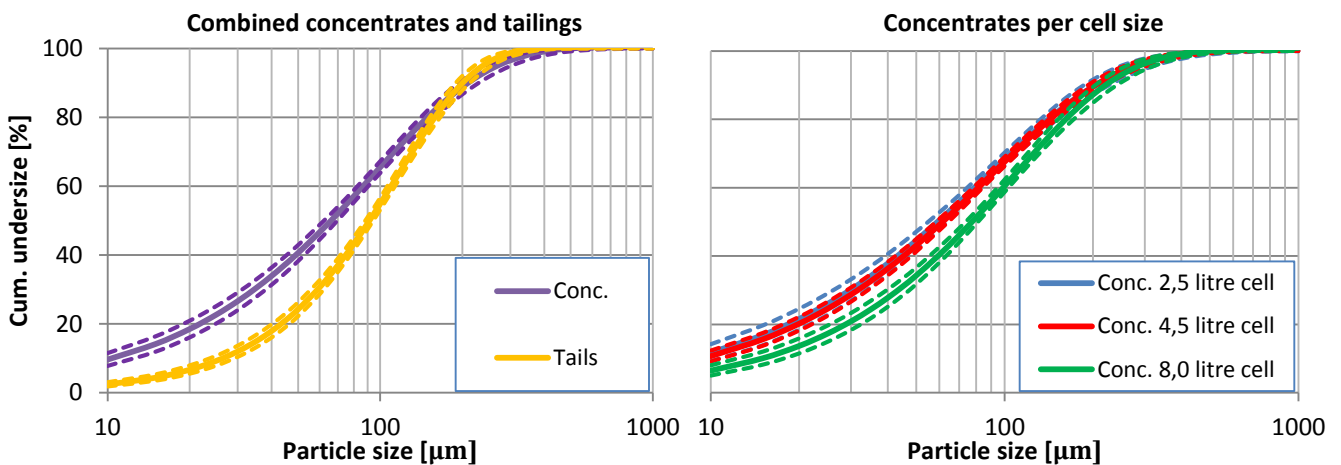

Figure 5.7: Modelled size distribution curves with upper and lower confidence intervals (dotted lines) for batch flotation.

5.2 Batch flotation: Factorial design of batch test parameters

A total of 12 tests batch flotation tests were performed according to a 2^3 factorial design in order to give additional information on the influence of the conditions at which lab flotation tests are carried out. The test conditions are named *factors*, whereas the test results that are used for modelling are named *responses*. An illustration of the cubical factorial design is given in figure 5.8. The upper and lower limits of the factors are shown as the eight corners of the cube, and the additional repeatability test is given in the centre. This centre point test was performed four times to determine the reliability of all tests.

The test responses used for modelling are given in table 5.8. An additional response is the product of the Cu recovery and the Cu grade ($R^{Cu} * X^{Cu}$), since ultimately these are both desired to be maximized during the flotation process. The used sampling times for batch flotation are ½, 1, 2, 4 and 8 minutes.
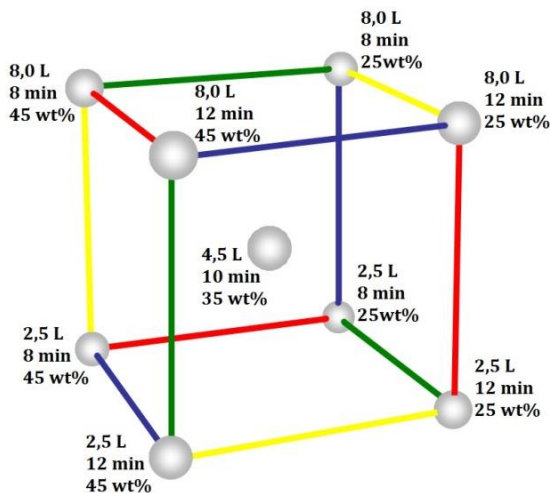

Figure 5.8: Cubical 2^3 factorial design.

Table 5.8: Factorial design responses.

Responses (number of responses)
• **Cu recovery[1]**
• **Cu grade[1]**
• **Mass pull[1]**
• **Cu enrichment ratio[1]**
• **Recovery of other sulphides[1]**
• **Flotation rate constant (k)**
• **Maximum recovery (R_∞)**
• **Cu recovery * grade**
[1] *Responses calculated at all 5 sampling times.*

The order at which the tests were carried out was randomized to prevent bias, and five of the final responses (i.e. after 8 minutes of batch flotation) are given in table 5.9. It should be noted that, while the cell size and grinding time are always constant, the weight percentage solids deviates from its target value, since it is difficult to attain the exact desired amount of solids with the use of the pulp splitter.

Table 5.9: Batch flotation tests according to factorial design, including five responses.

Test	Testing order (test #)	Grinding time [min]	Cell size [l]	Aimed wt% solids	Real wt% solids	*Final Cu recovery [%]*	*Final Cu grade [%]*	*Final mass pull [%]*	*Final Enrich- ment ratio [-]*	*Final recovery of other sulphides [%]*
a	7th	8	2,5	25%	20,5%	89,89%	7,67%	8,27%	10,9	56,55%
b	12th	12	2,5	25%	26,2%	90,74%	7,53%	8,91%	10,2	68,51%
c	5th	8	8,0	25%	26,9%	89,82%	9,97%	7,18%	12,5	65,39%
d	10th	12	8,0	25%	23,3%	89,43%	10,09%	6,60%	13,6	67,90%
e	6th	8	2,5	45%	37,6%	91,32%	6,56%	8,94%	10,2	67,64%
f	11th	12	2,5	45%	41,1%	91,42%	5,60%	11,43%	8,0	60,02%
g	1st	8	8,0	45%	46,7%	89,73%	8,58%	6,76%	13,3	57,12%
h	2nd	12	8,0	45%	46,6%	87,27%	7,10%	8,89%	9,8	54,06%
i	9th	10	4,5	35%	35,8%	92,62%	7,38%	8,26%	11,2	64,39%
j	4th	10	4,5	35%	34,7%	91,40%	8,30%	7,76%	11,8	63,89%
k	8th	10	4,5	35%	34,2%	90,94%	7,26%	7,51%	12,1	57,00%
l	3rd	10	4,5	35%	34,8%	94,40%	7,09%	9,11%	10,4	56,23%

The results were analysed with the program MODDE by Umetrics. The data were fitted with an MLR model (*Multivariate Linear Regression* model) with least squares fit. Figure 5.9 displays a summary of the regression fit for the same final responses that were given in table 5.10. The R^2 and Q^2 values give the *goodness of fit* and *goodness of prediction*, respectively. The methods of calculation are given in appendix C. Both need to be sufficiently high, and not separated too much, preferably less than 0,3 (Eriksson et al., 2000).

Unfortunately the responses shown in figure 5.9 all have a negative Q^2 value, and thus the corresponding regression models are considered not confident enough. In fact this was the case for every single response, making this factorial design unsuitable for model predictions depending on all three factors.
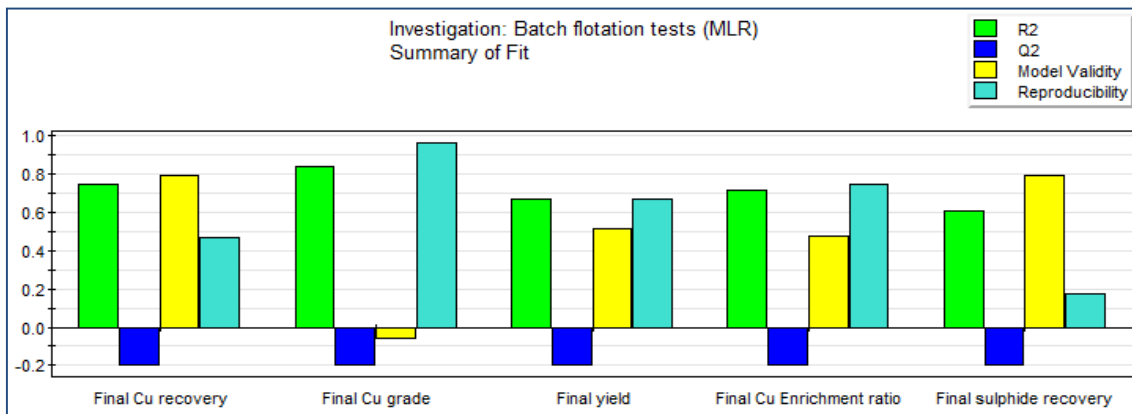

Figure 5.9: Summary plot of the factorial design analysis with MODDE.

The effectiveness of the model is quantified by the *model validity* parameter. If the model validity is smaller than 0,25 there is a *lack of fit*, meaning that the model variance is significantly larger than the data variance. Additionally the reproducibility of the test results is determined by the centre point tests performed under the same conditions, and is calculated by:

$$Reproducibility = 1 - \frac{\sigma^2_{rep.\ tests}}{\sigma^2_{total}}$$ (5.6)

in which $\sigma^2_{rep.\ tests}$ is the variance of the centre point tests, and σ^2_{total} is the variance of all experiments. The reproducibility is poor for values below 0,5 (Eriksson et al., 2000). It can be observed from figure 5.9 that in the case of final copper and sulphide recovery, the reproducibility is insufficient; this suggests that these responses are not strongly dependent on the chosen factors.

In addition to the R^2 and Q^2 values, the *Analysis of Variation* (ANOVA) provides a diagnostic tool for the estimation of different types of variability in the response data. Construction of the ANOVA table is explained in appendix C. In other words, it can be used to determine if data sets are significantly different or not. The ANOVA table from MODDE for the final copper recovery is given in figure 5.10. The most important value in this table is the *probability* value p, which indicates the confidence in the modelling of this response. For the regression model, a p-value of 0,05 or lower corresponds with a model confidence of 95% or higher, and thus p-value of 0,338 shown in red in figure 5.10 indicates insufficient confidence. The responses for which a model confidence higher than 95% was calculated are:

- Cu grade after ½, 1, 2 and 4 minutes (confidences of 95,9%, 99,3%, 99,1% and 97,2%, respectively).
- Cu recovery * grade after 1, 2 and 4 minutes (confidences of 97,5%, 99,4% and 98,3% respectively).

The models for these responses can be considered sufficiently confident, and can thus be used to predict the effect of varying factors. Figure 5.11 depicts contour plots of the weight percentage solids versus the cell size at grinding times of 8, 10 and 12 minutes for the copper grade after 1 minute. It can be observed that at low grinding time the copper grade mainly depends on the cell size, while for a long grinding time the wt% solids has the greatest influence. Furthermore, the copper grade decreases for longer grinding times at the same cell size and wt% solids, indicating that the ore may have been ground too fine.

Figure 5.10: Analysis of Variation (ANOVA) table from MODDE for the final copper recovery model fit.

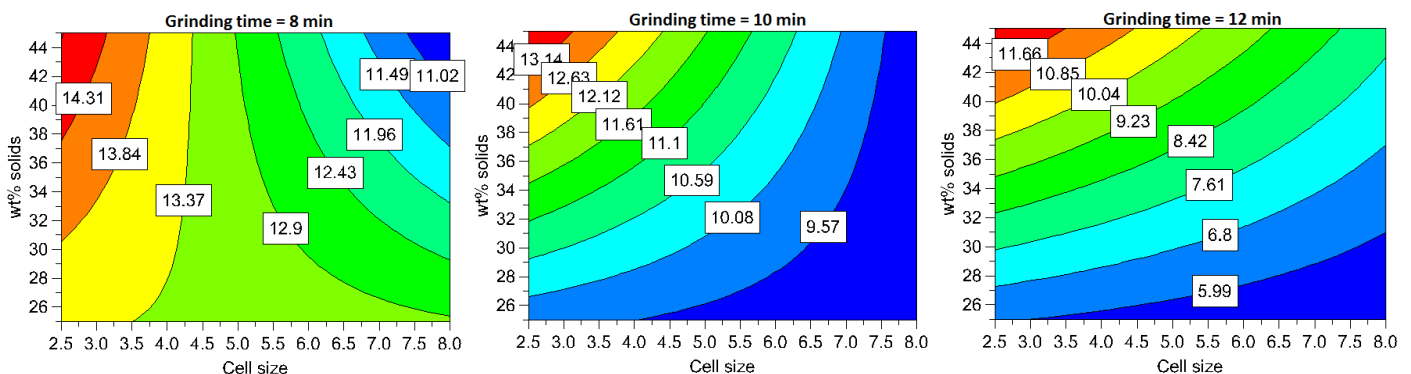| Final recovery	DF	SS	MS (variance)	F	p	SD
Total	12	98857,7	8238,14			
Constant	1	98823,1	98823,1			
Total Corrected	11	34,5469	3,14063			1,77218
Regression	6	22,1776	3,69626	1,49413	0,338	1,92257
Residual	5	12,3693	2,47386			1,57285
Lack of Fit	2	5,11314	2,55657	1,05699	0,449	1,59893
(Model Error)						
Pure Error	3	7,25617	2,41872			1,55522
(Replicate Error)						
	N = 12	Q2 = 0,241		Cond. no. = 9,217		
	DF = 5	R2 = 0,642		Y-miss = 0		
	Comp. = 5	R2 Adj. = 0,212		RSD = 1,573		

Figure 5.11: Model contour plots from MODDE for the copper grade after 1 minute.

Apart from modelling of the responses as a function of all factors, varying a single factor while keeping the other factors constant can be shown to have an effect on the outcome of a response. Table 5.10 gives the positive and negative effects of the factors on each of the responses with sufficient confidence (>95%), when the two other factors are kept constant. For example, a negative effect on the copper grade in concentrates obtained between 0,5 and 4 minutes is observed for an increasing cell size. For the 8 minute concentrate this effect is no longer observed, likely due to increasing entrainment in the smaller cells for long flotation times, as was shown in section 5.1. The mass pull after 0,5 and 1 minutes is increased for a longer grinding time, due to the larger fraction of fine particles. Furthermore, in order to maximize both copper recovery and grade, the smaller cell gives better results for a short flotation time, since the copper recovery is relatively high for short flotation times in this cell. This indicates that entrainment in the small cell is especially significant for flotation times longer than 4 minutes.

These results statistically prove that especially the concentrate copper grade, and not copper recovery, is affected by the operating conditions of the lab flotation tests. Entrainment is suspected to be the most important cause. Since metal grades are an important result of flotation test work, the operating conditions for lab tests should be well considered in order to confidently and representatively scale-up lab results to an industrial operation. Also the point of time at which a comparison between test results is made is of great importance, as entrainment increases when less floatable minerals are left in the pulp.

Table 5.10: Positive (+) and negative (-) effects of factors on responses at specific time intervals.
Only results with a sufficient confidence level are shown.

Factor	Cu grade				Mass pull		Enrichment ratio (ER)				Rec * grade			Rec * ER	
Conc. time (min)	½	1	2	4	½	1	½	1	2	4	1	2	4	2	4
Cell size	-	-	-	-				-	-	-	-	-	-	-	-
wt% solids	+				-		+								
Grinding time	-				+	+									

51

5.3 Industrial flotation cell characterization

The characterization study of industrial size flotation cells was performed on the first and last rougher, and first and last scavenger of line 1 of the Aitik mine processing plant, on 04-12-2013. All cells of the Aitik rougher, scavenger and desulphurization banks consist of Outotec TankCell-160 cells. The main factors considered were:

- Gas holdup.
- Weight percentage solids in the pulp.
- P80 values and mass distributions for different size classes.
- Solids density and sulphide content.
- Mineral distributions and enrichment for different size classes.

Since the pulp-froth interface cannot be seen physically, the samples were taken at fixed distances under the top of the froth. In addition, samples were taken of the top of the froth, the complete froth, directly under the froth and when possible of the feed and tailing streams. The froth thickness measurement varied between 20 and 30 cm, and thus the depth at which the sample directly under the froth was taken also varied per cell. Sampling of the top of the froth was not possible for the last scavenger. It should also be noted that the tailings of the last rougher are equal to the feed for the first scavenger, and thus the data for both streams are identical.

According to the construction drawings, the lip height of the TankCell-160 is at a height of 488 cm from the cell bottom, with the impeller mechanism between the cell bottom and roughly 150 cm above the cell floor (Boliden, 2008). For simplification, the lip height is assumed to be equal to the top of the froth layer. A representation of the flotation cells is given in figure 5.12.
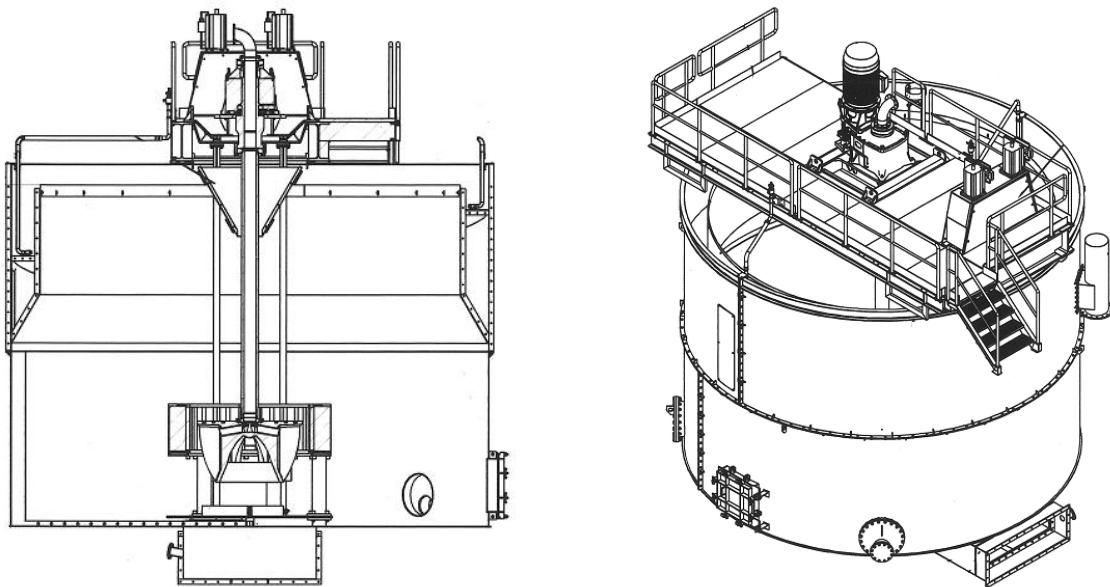

Figure 5.12: Representation of the Outotec TankCell-160 as used by Boliden Aitik (Boliden, 2008).

5.3.1 Gas holdup

The gas holdup was calculated with the use of equation 4.1 on page 40. Results per cell and on average are shown in figures 5.13 and 5.14. The values directly under the froth and at 0,5 m depth for the rougher cells were out of proportion, likely due to accidental partial sampling of the froth zone, and are therefore not included.

From figure 5.13 it can be observed that the gas holdup is significantly higher in the first cells of both banks, in comparison to the last cells. The most likely reason for this is the high availability of floatable minerals and thus a high load of material on the bubble surfaces, causing bubbles to rise slower.

The gas holdup seems to increase slightly toward the top of the cell, from an average of 3,5% at 4,0 m depth to 4,1% at 1,5 m. The gas holdup is expected to increase with a factor of 1,5 between the cell bottom and pulp-froth interface due to the hydrostatic pressure effect, as explained in section 3.1.2. Between 1,0 m depth and the pulp-froth interface the gas holdup significantly increases, which may indicate the build-up of material in this zone. The gas holdup and its intermediate range within the tank are considerably lower than reported in literature on bottom-driven mechanical cells, which typically lies between 8 and 15% (Yianatos et al., 2010c; Finch et al., 2000; Schwarz and Alexander, 2006, Nelson et al., 2000).

However, Harbort and Schwarz (2007) report values from 5 to 13% in the old concentrator plant at Boliden Aitik, which was taken out of operation in 2010. The high value for 1,0 m depth can be the result of material build-up under the froth and it is therefore unfortunate that the data for 0,5 m depth are incomplete and no good comparison is possible.
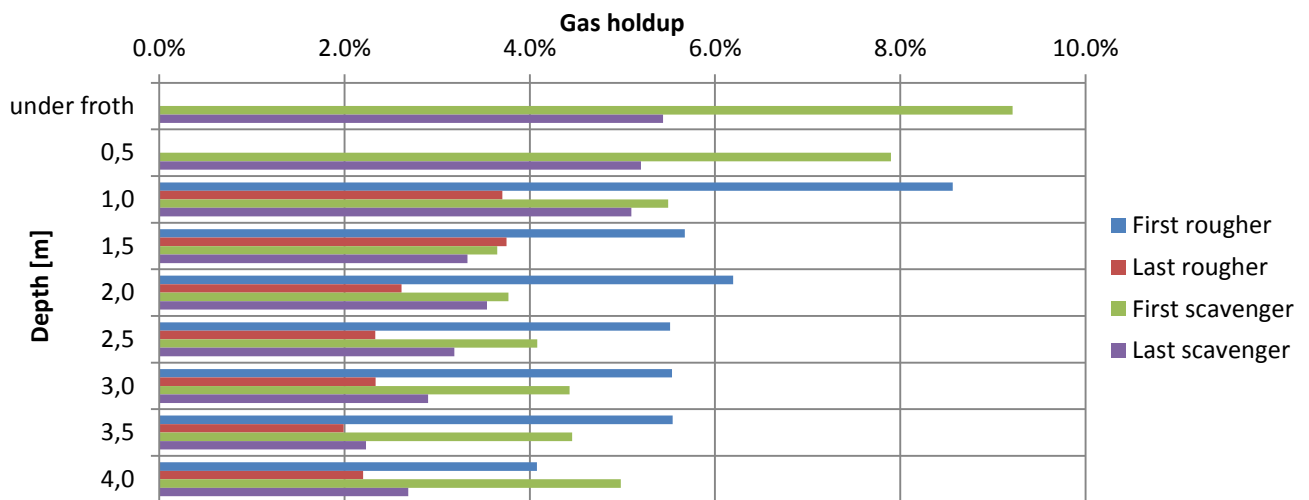

Figure 5.13: Gas holdup per cell for Aitik survey on 04-11-2013.
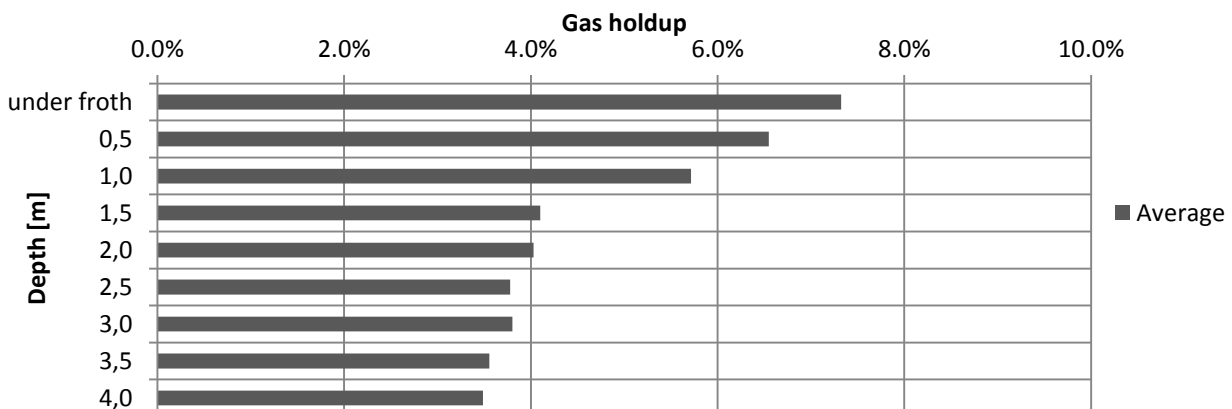*No reliable data for first and last rougher under froth and at 0,5 m depth.*

Figure 5.14: Average gas holdup for Aitik survey on 04-11-2013.

5.3.2 Weight percentage solids in the pulp

The weight percentage (wt%) solids for the different flotation cells as a profile of depth is given in figure 5.15. The profile is reasonably constant in the zone around and above the impeller, between 4,0 and 3,0 m depth, but starts to decrease at higher levels. This is an expected effect, due to lower turbulence in the upper part of the cell and since ideally gangue minerals are not supposed to float and can only rise in the cell due to the mixing effect in the impeller zone (apart from a small degree of mechanical entrapment between bubbles, typical for coarse particles at high gas holdup (Yianatos and Contreras, 2010a)). The weight percentage solids for the first scavenger under the froth could not be calculated accurately due to accidental material loss during filtering.
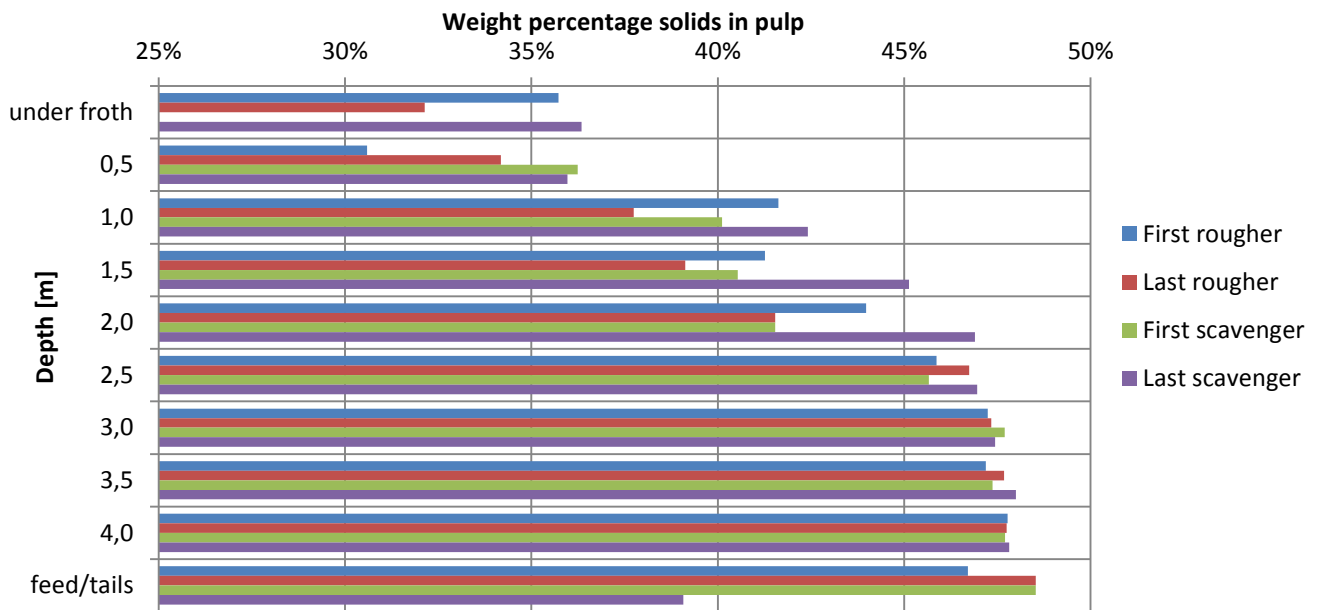
Figure 5.15: Weight percentage solids in pulp per cell for Aitik survey on 04-11-2013.

Figure 5.16 displays the wt% solids of samples from the first rougher during the current research, and the wt% solids of samples taken during a previous research held roughly one month earlier on 05-11-2013. These samples were taken by peristaltic pump on five levels within the cell. It can be seen that the wt% solids is lower in the previous research, most likely the result of different operating conditions, but a comparable profile of an increasing wt% solids with depth exist. In both researches a lower value for the wt% solids between the froth and 1,0 m depth is measured. This does not necessarily reject the theory of material build-up under the froth, since accumulation of fine particles can represent a low weight amount of solids.

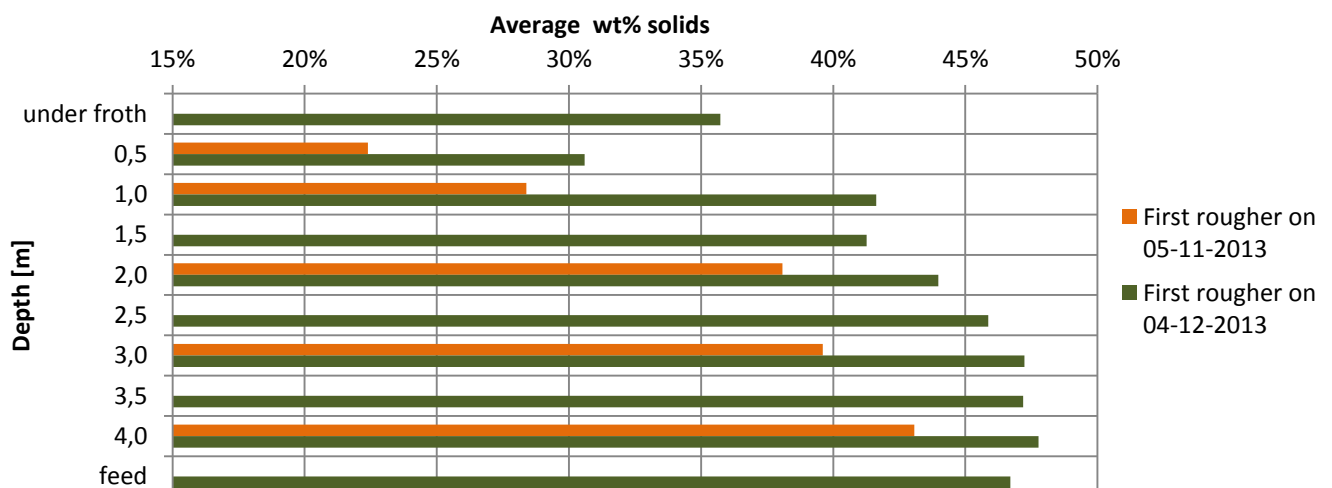*Figure 5.16: Average weight percentage solids in pulp per cell for Aitik survey on 04-11-2013.*

54

5.3.3 P_{80} values and mass distributions for different size classes

All samples were sieved to create size distributions and to determine the 80% passing size (P_{80}). Figure 5.17 represents a profile of the particle P_{80} values with depth within the sampled flotation cells. The P_{80} can be used to give a quick overview of the size distribution in a single parameter, but lacks information especially on the distribution of smaller particles. However, due to large contributions of the -45 µm fraction in certain samples it was not possible to determine a 20% or even a 50% passing size for all samples. The P_{80} values show to be relatively uniform in the bottom of the cell and between the feed and tailings, with values between approximately 185 and 200 µm. Towards the top of the cell the material clearly becomes finer, with P_{80} values of 100-130 µm at a depth of 0,5 m and directly under the froth. The coarsest particles do not seem to be able to rise above the impeller zone due to lack of turbulence.
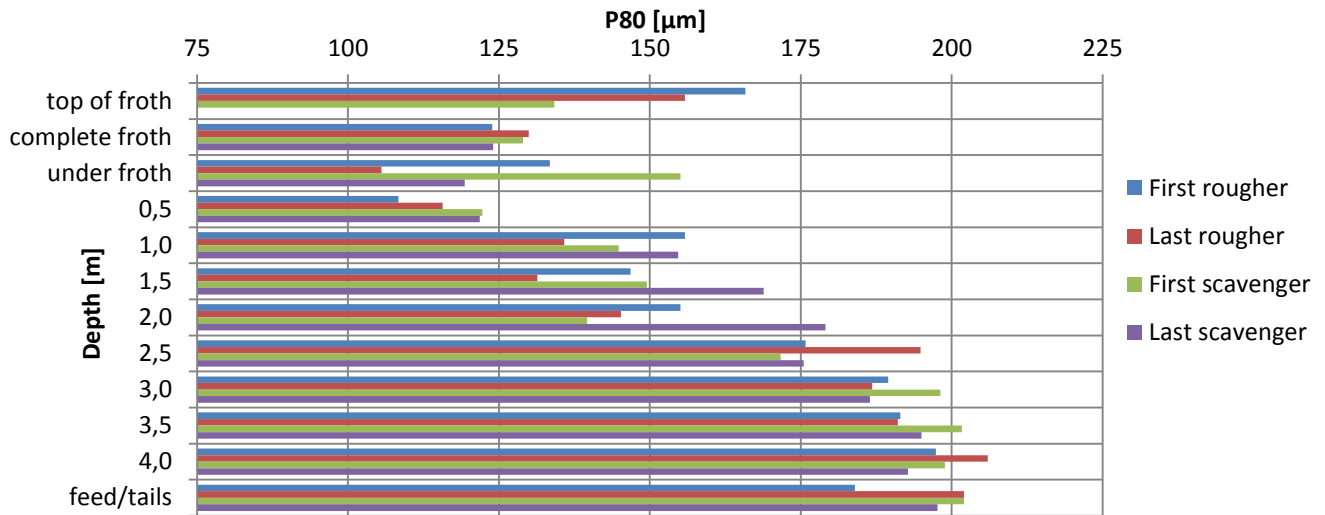
Figure 5.17: P80 values per cell as a profile of depth for Aitik survey on 04-11-2013.

Figure 5.18 gives the contribution of five size classes to the total weights of the samples taken in the first rougher and first scavenger. The graphs shows that especially the -45 µm size class has an increasing weight percentage in the froth zone, and thus in the concentrates. For both cells the contribution of this size class even strongly increases above the impeller zone, starting at around 2,5 m depth. The particle size classes coarser than 90 µm have a decreasing contribution in these zones, while the +45 -90 µm class stays approximately constant. The top of the froth of the first rougher has a distinctly coarser distribution than the complete froth; most likely the complete froth partially exists of entrained fine gangue minerals, while the top only contains the most hydrophobic particles. The mass distribution profiles were comparable for the other sampled cells.

Figure 5.18: Mass distribution curves per size class for the first rougher and first scavenger.

5.3.4 Solids density and sulphide selectivity

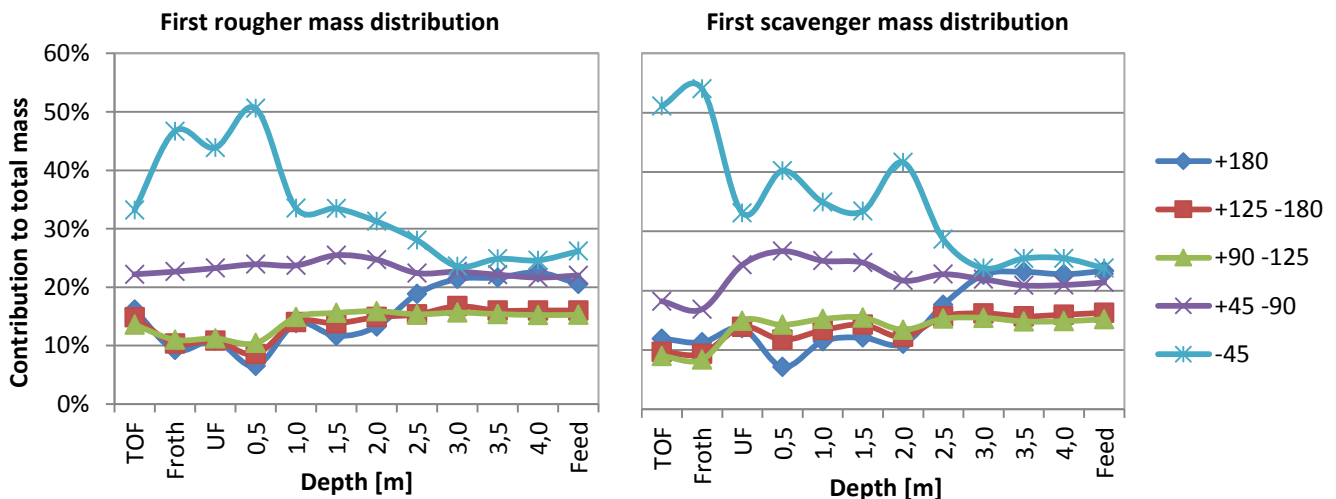The density of solids in the flotation cells is closely related to the sulphide content. The main gangue minerals are silicates with solid densities of around 2,75 kg/dm³, while sulphides have a considerably higher solid density, such as 4,10-4,30 kg/dm³ for chalcopyrite and 4,95-5,10 kg/dm³ for pyrite. Since silicates and sulphides are the two main mineral classes in the Aitik ore body, a higher solid density can be explained as a higher sulphide content, apart from some traces of heavy minerals like barite.

Amongst the sulphides in the ore, the two main minerals are pyrite and chalcopyrite, with minor amounts of for example molybdenite (MoS_2), sphalerite (ZnS) and galena (PbS) and pyrrhotite ($Fe_{1-x}S$). Although the flotation is optimized for chalcopyrite flotation, these other sulphides will also float to a certain degree. For the flotation process it is of great importance that the recovery of other sulphides to the concentrate is limited to preserve a certain copper grade, and since zinc and lead are penalty elements in copper concentrate smelting.

Figure 5.19 represents the solid density and percentage of copper in the sulphides for the sampled cells as a profile of cell depth. Since the weight of copper and sulphur in chalcopyrite are approximately equal, a value of 100% Cu in the sulphides can be interpreted as a sample with chalcopyrite as the only sulphide mineral. The solid density is constant under the 1,0 m level, but starts to increase directly under the froth and in the froth itself as a logical result of the enrichment of sulphide minerals. The percentage copper in the sulphides is high for the first rougher, but becomes distinctly lower for the other cells. In the case of the last scavenger the tailings even have a larger Cu/S value than the froth, indicating that the process is no longer selective and recovers other sulphide minerals better than chalcopyrite itself.
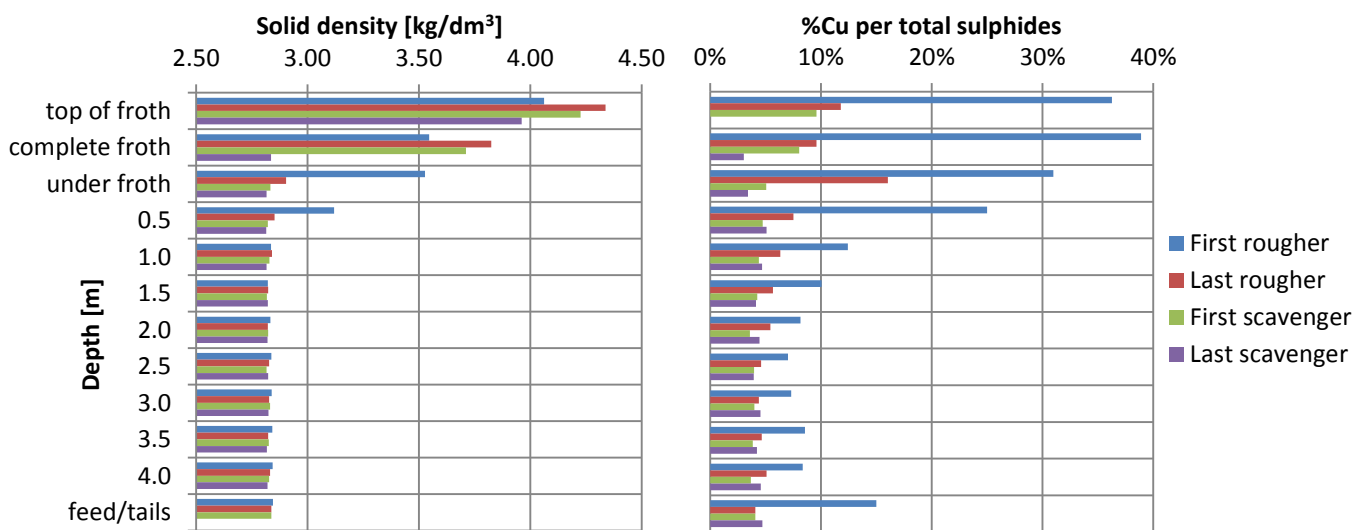
Figure 5.19: Solid density and Cu-percentage in sulphides per cell for Aitik survey on 04-11-2013.

Five different size fractions were analysed to determine their copper and sulphur contents. Figures 5.20 and 5.21 represent the copper content in the total sulphide minerals, i.e. the Cu/S factor, for the rougher and scavenger cells, respectively, as a profile of depth.

For the first rougher a clear profile is visible; the selectivity of copper versus other sulphides increases in the upper part of the cell, and is optimal in the froth. Furthermore the copper content in the sulphide minerals increases especially for smaller size classes. This corresponds with a good floatability of the 10-100 μm size range as proposed by Rahman et al. (2012), although there is no information on the contribution of particles smaller than 10 μm, since the smallest sieve size is 45 μm. Furthermore, figure 5.18 already showed an increasing share of -90 μm particles in the froth zone. Part of this could be contributed to entrainment, but figure 5.20 confirms that the recovery of copper minerals in this size class is also selective.

For the last rougher cell a comparable profile is visible, although the copper content of the total sulphides in the froth zone is significantly lower than for the first rougher (5-12% vs. 20-55%). The Cu/S value under the froth is higher than in the froth itself, which may be contributed to unliberated copper minerals able to rise in the quiescent zone of the cell, but not hydrophobic enough to enter the froth zone.
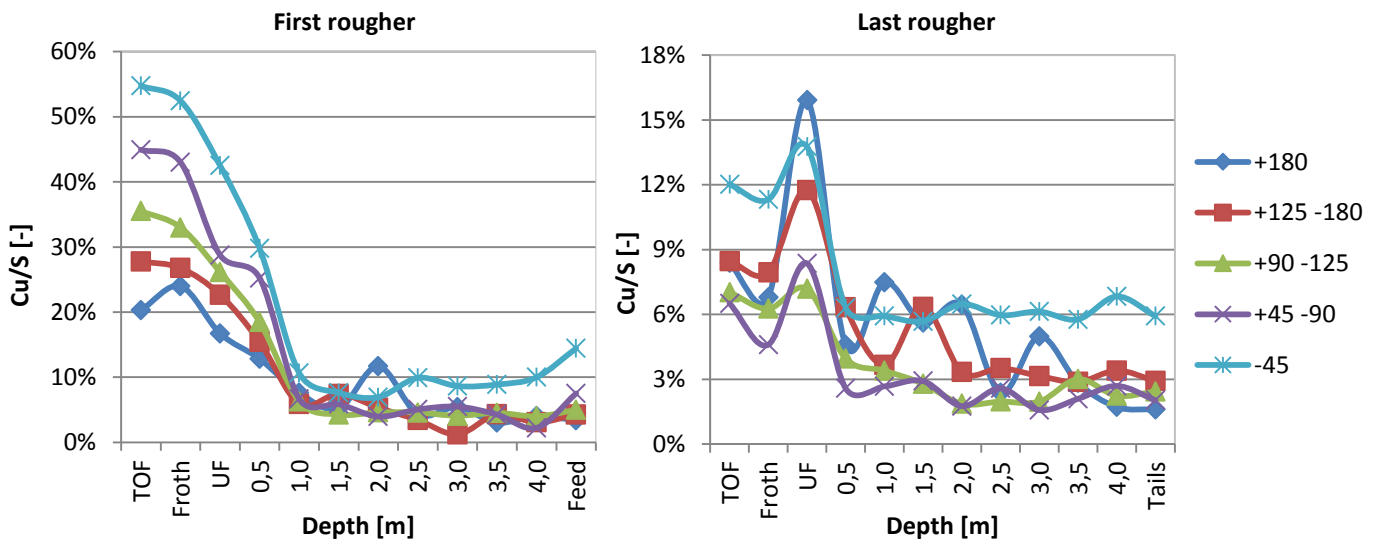
Figure 5.20: Copper content in the total sulphides (Cu/S) vs. cell depth for the first and last rougher cell.

The profile of the copper content in the total sulphides in the scavenger cells, as shown in figure 5.21, is clearly different than in the rougher cells. The increasing profile in the froth zone is not as present as in the roughers, or even almost absent for the last scavenger. Also, the +180 µm size class in and under the froth zone has a higher Cu/S value in comparison to the other size classes than in the roughers, which likely are too heavy to enter the froth zone. The froth of the last scavenger even has lower Cu/S values (1-3%) than most of the other locations in the cell, indicating bad selectivity and a high recovery of other sulphides compared to the copper minerals.
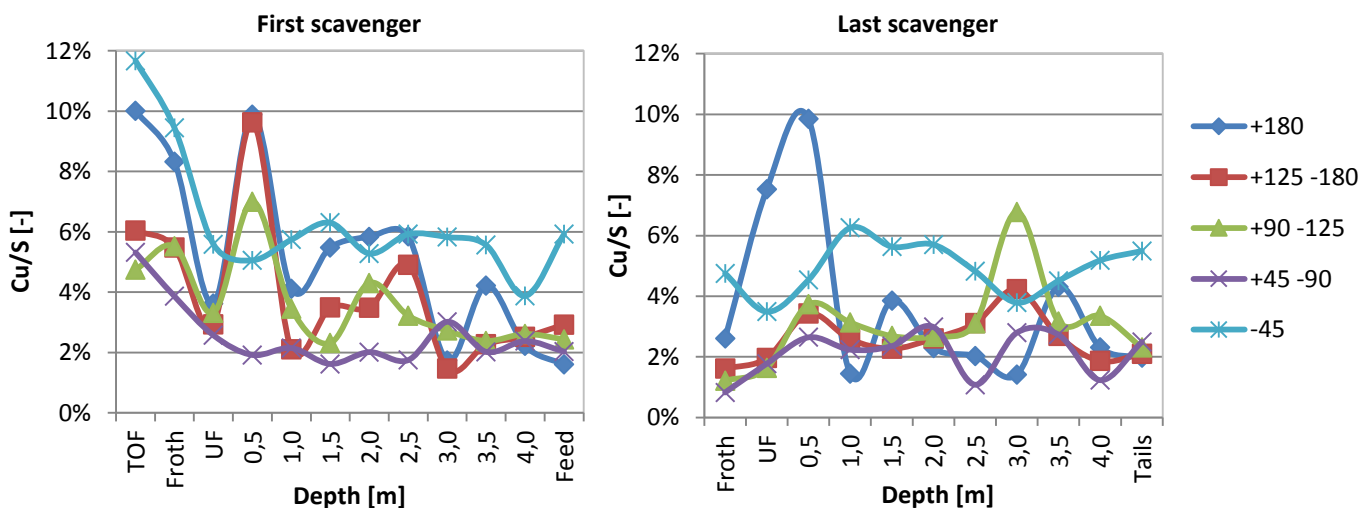

Figure 5.21: Copper content in the total sulphides (Cu/S) vs. cell depth for the first and last scavenger cell.

5.3.5 Mineral distributions and enrichment

Sulphide minerals

The analysis of different particle size classes also allows investigation of the distribution of minerals over the chosen particle size ranges, and comparison of their performance in the flotation process, as the optimal size range for flotation is commonly regarded as 10-100 μm (Rahman et al., 2012). Since the Aitik ore contains relatively coarse grained minerals and the limiting factors for coarse particle flotation are insufficient liberation of mineral surface and decreasing attractive forces, the particle size upper limit may well be higher than for other cases.

The enrichment of copper and non-Cu sulphides per size class for the first rougher, first scavenger and total rougher bank concentrates is shown in figure 5.22. Enrichment calculations were made for all cells where feed sampling was possible, plus the complete rougher bank.
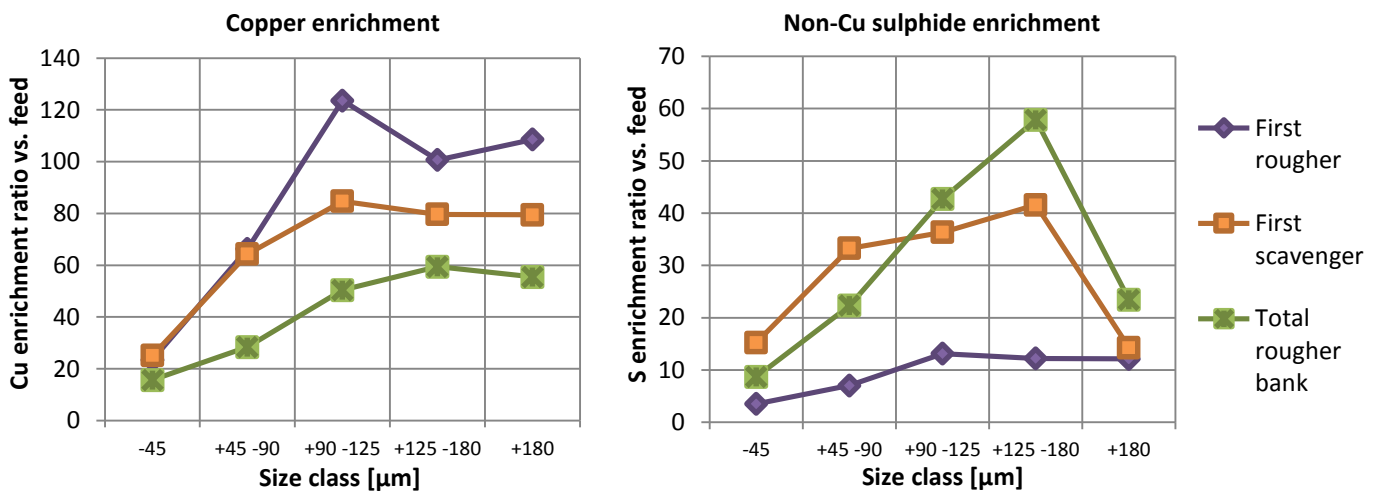

Figure 5.22: Copper and non-Cu sulphide enrichment per size class.

The enrichment of the -45 μm class is the lowest in all cases for both copper minerals and non-Cu sulphides, and is also approximately equal for the different cells and total rougher bank. This would suggest that recovery of this size class is not - or less - dependable on operating conditions and/or presence of other minerals. Likely the recovery of fine particles partially occurs due to entrainment; this can be clarified later by comparison to silica recovery in the -45 μm size class.

Based on literature, flotation should be optimal for the +45 -90 μm size class of copper minerals. However, the enrichment of the coarser size classes is distinctly higher. Also, the enrichment of copper minerals larger than 90 μm is especially high in the first rougher. Copper enrichment over the complete rougher bank is relatively low, while non-Cu sulphide enrichment is high, especially for particles between 90 and 180 μm. Comparison to the profile of the first rougher alone suggests that the rougher bank recovers a high amount of non-Cu sulphides within this size class after the first cell. On the other hand, copper enrichment in the total rougher bank is relatively high for the +180 μm size class, and only slightly lower than for the +90 -180 μm size class, while non-Cu sulphide enrichment is significantly lower in the +180 μm size class. This indicates that coarse copper minerals (+180 μm) are recovered surprisingly well, in combination with good selectivity.

Figure 5.23 gives the copper and non-Cu sulphide distributions per size class for the concentrates of the four sampled cells. A large part of the recovered copper is shown to be present in the -45 μm class, and this increases downstream the banks, from approximately 45% in the first rougher to 65% in the last scavenger. Also, the contribution of copper in the 'optimal' floatable +45 -125 μm size class decreases for concentrates down the bank, as is expected, since this material will generally float the fastest. A similar profile is observed for non-Cu sulphides, although the contribution of the -45 μm size class is lower in all stages (25-40% for non-Cu sulphides versus 45-65% for copper sulphides).
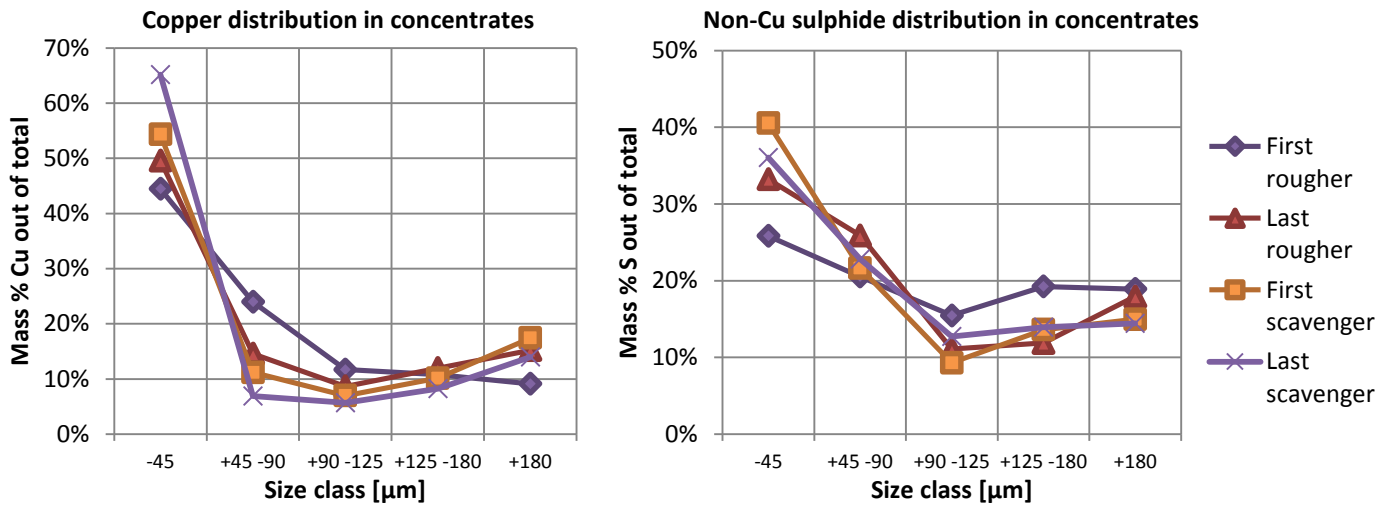
Figure 5.23: Copper and non-Cu sulphide distribution in the concentrates per size class.

To compare the mineral distributions in feed and concentrate streams, an imaginary parameter is used to express if the contribution of a metal or mineral increases or decreases between two material streams within a fixed particle size class, for example a cell's feed and concentrate flow. By comparing the values, it can be deduced which mineral size classes have a better floatability. This parameter is named the *dimensionless metal (or: mineral) distribution ($\psi_{s,x}$):*

$$\psi_{s,x} = \frac{\%\ of\ metal\ or\ mineral\ X\ in\ downstream\ flow}{\%\ of\ metal\ or\ mineral\ X\ in\ upstream\ flow}\Bigg|_{particle\ size\ class} \qquad (5.7)$$

The value of ψ_s will be larger than 1 when the contribution of metal X increased within the chosen size class, and smaller than 1 when its contribution decreases. For example, when the feed and concentrate of a flotation cell respectively have 40% and 20% of their total copper content in the -45 μm size class, the dimensionless metal distribution will be:

$$\psi_{-45,Cu} = \frac{20\%}{40\%} = 0,5$$

Figure 5.24 gives the dimensionless chalcopyrite and pyrite distributions between feed and concentrate of the first rougher, first scavenger and total rougher bank for the five investigated size classes. The y-axis is plotted on a logarithmic scale to give a representative image of increasing or decreasing metal content per size class in the graph. The red lines represent $\psi = 1$, when no change in the mineral distribution occurs during the flotation process.
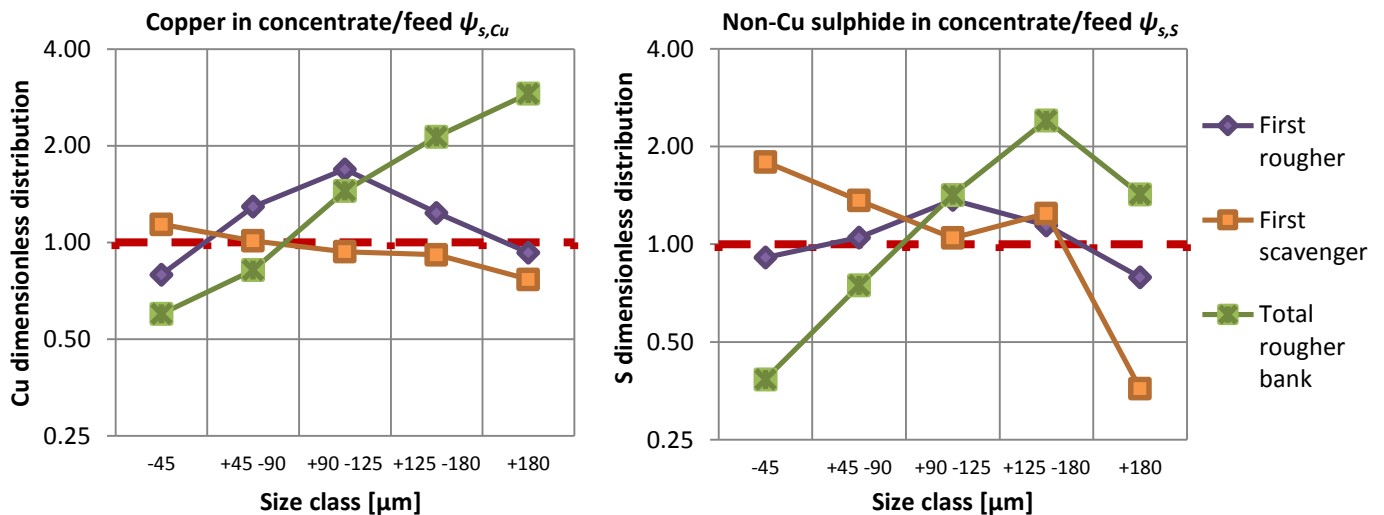

Figure 5.24: Copper and non-Cu sulphide dimensionless distributions of feed vs. concentrate per size class.

59

For the first rougher, both for copper minerals and non-Cu minerals the +90 -125 μm size class is enriched well, judging by the dimensionless distribution values larger than 1. However, over the total rougher bank the +125 -180 μm and especially the +180 μm size classes are well recovered. This statement is also valid for non-Cu sulphides, although in a lesser degree for the +180 μm size class. A possible explanation is that the first rougher has a surplus of copper minerals in the optimal size range, which hinder the flotation of coarser particles. These particles will then float further downstream in the bank. In the first scavenger cell the particle size does not seem to have a large influence on copper mineral flotation, while for non-Cu sulphides the recovery in this cell is especially high in the -45 μm fraction, and low in the +180 μm fraction.

Silicate minerals

The enrichment ratio for silica for the first rougher, first scavenger and total rougher bank is displayed in figure 5.25. Since the percentage silica decreases from the feed to the concentrate the term enrichment is less applicable, but is used anyhow to give a good comparison with the previously shown enrichment profile per size class for sulphide minerals. The mechanism behind silica recovery to the concentrate can be hydraulic entrainment of fine particles by liquid convection, mechanical entrapment between bubbles (typical for coarse particles at high gas holdup), or silica attached to the sulphide mineral due to incomplete liberation (Yianatos and Contreras, 2010a). Since gas holdup was shown to be low, it will be of negligible impact in this situation. Slime coating can also recover silica, but generally has a minor, negligible impact, and should only be considered in the case of ultrafine particle flotation.
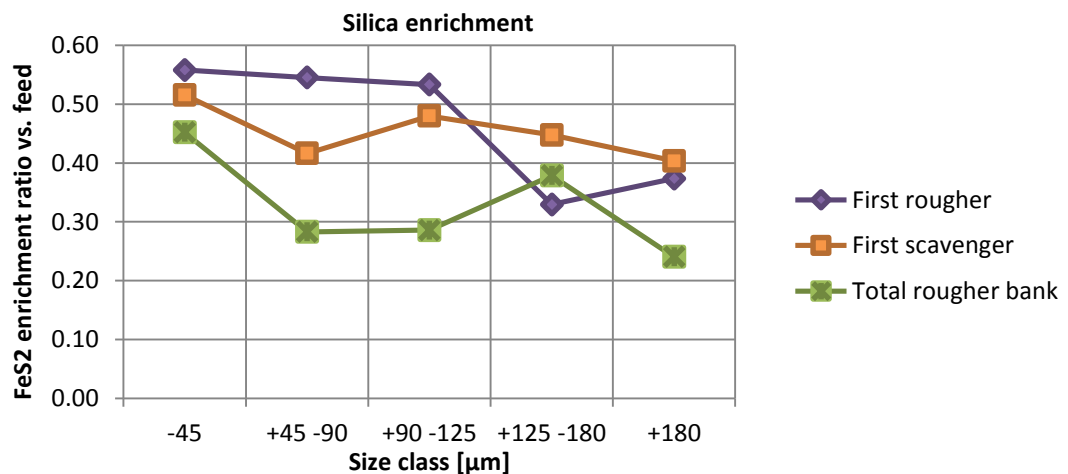
Figure 5.25: Silica enrichment per size class.

The enrichment of silica is largest in the -45 μm size class, likely the result of entrainment of fine silica particles. The concentrate of the first rougher will consist of the best liberated and most easily floatable particles, which explains its lower enrichment of silica in the coarser fractions. In general it is not possible to draw conclusions from this graph, since the silica recovery mechanism per each sample is not identified.

The silica distribution in concentrates, feed and tailing streams per size class is shown in figure 5.26. The silica distribution in the concentrates is similar along the rougher and scavenger banks, although the last scavenger contains more silica in the +180 μm size class, most likely due to badly liberated minerals that are only recovered under scavenger conditions. The -45 μm fraction of the feed and tailings stream is decreasing in silica along the bank, which corresponds with the theory of particle entrainment in the rougher cells. For the intermediate size classes (45-180 μm) the silica distribution is relatively constant along the bank, indicating that the flotation process conditions in all stages hardly affects these minerals and their recovery is caused by incomplete liberation.
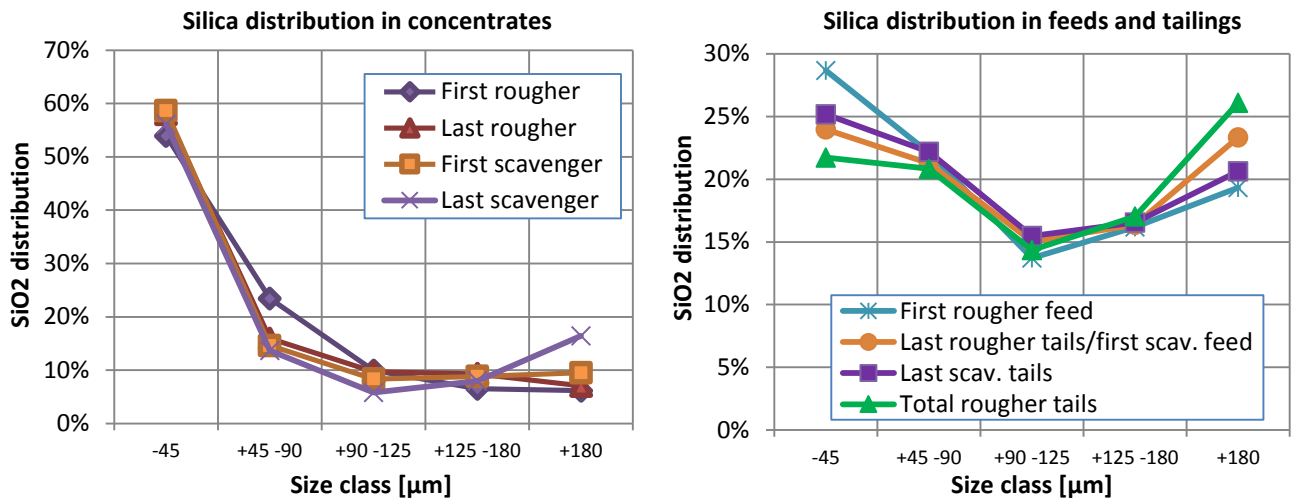
Figure 5.26: Silica distributions in concentrates, feeds and tailings of various cells.

Figure 5.27 displays the dimensionless distribution for silica between the feeds and concentrates for the first rougher, first scavenger and total rougher bank. The graph clearly shows that silica is most strongly recovered in the -45 μm fraction, and that silica recovery decreases with increasing particle size. An exception to this are the +125 μm particles for the roughers beyond the first cell; this can indicate recovery of badly liberated particles in these cells, which bring silica into the concentrate.

If it is assumed that complete liberation of minerals is reached for particles smaller than -45 μm, the silica in this size class is entirely recovered by entrainment. Based on the recovery of silica, this would indicate that a larger fraction of copper minerals within this size class are recovered by entrainment instead of true flotation. Electron microscopy techniques such as Qemscan or MLA can be used to analyse the liberation of the -45 μm size class and test this hypothesis. Unfortunately, due to time restrictions no Qemscan analyses were possible.
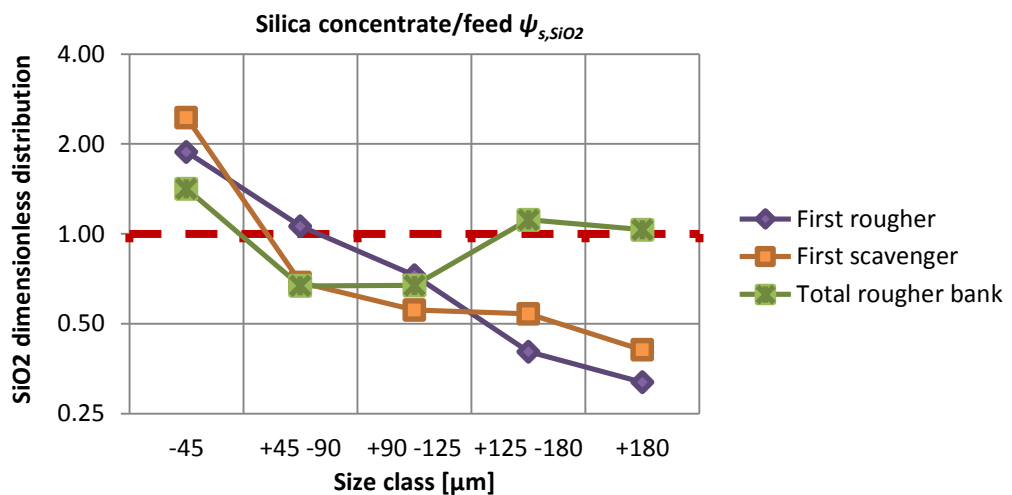
Figure 5.27: Silica dimensionless distribution between feed and concentrate per size class.

61

5.4 Direct comparison of laboratorial, pilot plant and full scale flotation

The tests for comparison of laboratory, pilot plant and full scale operation were performed on the 12th and 13th, and 19th and 20th of March 2014. The pilot and full scale cells were sampled every 10 minutes for one hour, resulting into combined samples of 6 individual samples, in order to sufficiently reduce the statistical error according to Gy's sampling theorem (Gy, 1979). This process was repeated four times for both the rougher and scavenger cells, giving a total of eight sampling rounds. Approximately 8 litres of feed pulp to the industrial cells was sampled and used for batch flotation. No additional reagents were added during the batch tests.

The data were mass balanced with the measurements of sample weights, density and metal assays of all samples, according to methods described by Morrison (2010). Although the incoming flow rate to the rougher cells itself is not measured by the plant instrumentation, this flow rate was calculated by the combined flows of the corresponding milling line and the recirculating flow from the cleaner line. This recirculating flow to the rougher flotation is shown as the concentrate of the secondary cleaner scavengers on the plant flow sheet in appendix B. On average, the cleaner line recirculation comprised 1,013% (σ = 0,008%) of the rougher flotation input during the first 3 months of 2014 (Aitik iPAK, 2014).

5.4.1 Flotation kinetics

Rougher flotation
The kinetics of the full scale and pilot cell tests in both the rougher and scavenger circuits were modelled for the three chosen size classes (-45 μm, 45-125 μm and +125 μm) and the complete size range. However, the concentrate quantities of the batch tests were too small to create and analyse separate size classes. The batch test concentrates sampled after fixed time intervals were therefore combined and analysed for different size intervals to give an indication for their comparison to pilot and full scale flotation. Note that in this case of batch flotation no error estimation can be made.

The calculation of kinetic models was done according to the rectangular kinetic distribution model, as given in equations 3.7 and 3.8 for continuous and batch processes, respectively. This model showed to have the best fit to the test data from all models mentioned in chapter 2. Comparison of the plug flow and fully mixed models (equations 2.3 and 2.5) equals comparison of two models with different basic assumptions, whereas the Kelsall model (equation 2.7) assumes all material is recovered for infinite time, and gives extra fitting inaccuracy due to a third fitting parameter. Additionally, the plug flow model converges to its maximum recovery far more rapidly, which basically means the model reaches its maximum recovery at the last sampling time of the batch test (8 minutes). Curves of each of the mentioned models are shown in figure 5.28.
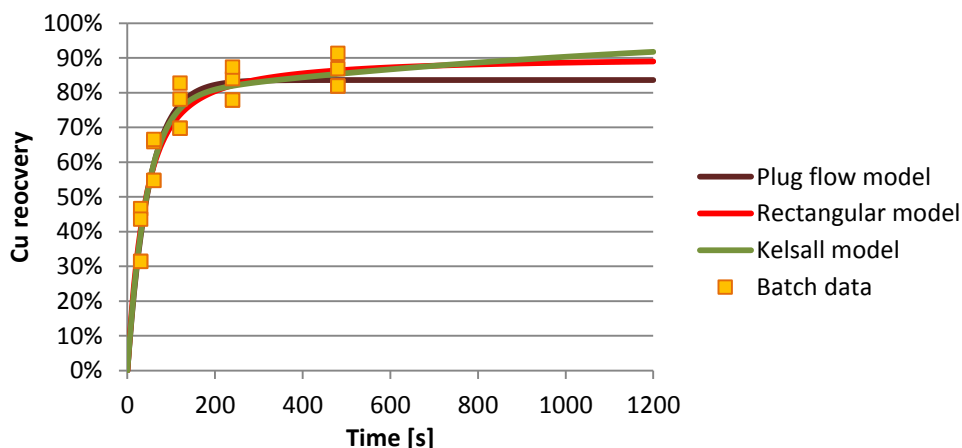

Figure 5.28: Rougher batch test results modelled according to three different methods.

Figure 5.29: Time-recovery test data points and model curves of batch, pilot and full scale rougher tests for three different size classes.

Figure 5.29 shows time-recovery model curves for the three different size classes of the rougher tests on all scales. The left graph represents the finest fraction (-45 μm), which is clearly recovered least well in the full scale cells. This can be an important influence on the difference in flotation results between laboratory and full scale. For the intermediate size class of 45 to 125 μm, the recovery is also less rapid in the full scale cells, but for long residence times the recovery approaches that of the batch and pilot cells. The coarsest material of +125 μm even seems to be recovered better in the full scale cells, although the test data points are more scattered and thus the model has a relatively large error. Table 5.11 gives the standard errors of the models fits.

Table 5.11: Standard errors of rougher test time-recovery model fits.

Test	-45 μm	+45 -125 μm	+125 μm
Batch	1,15%	2,75%	1,65%
Pilot	9,75%	4,46%	6,03%
Full scale	2,83%	8,29%	8,85%

Figure 5.30 presents the distribution of copper in the feed and tailings over the three size classes for flotation tests on different scales for rougher flotation. Approximately 57% of the copper in the feed is contained in particles in the -45 μm size class. Since the majority of copper will end up in the concentrate, the copper distribution graph for the concentrates will not look very different from the feed copper distribution. The copper distribution of the tailings shows that a large part (~72%) of the copper lost through rougher tailings is contained in the -45 μm size class, whereas this is only 38% in batch flotation. This confirms the poor recovery of this size class in industrial flotation.
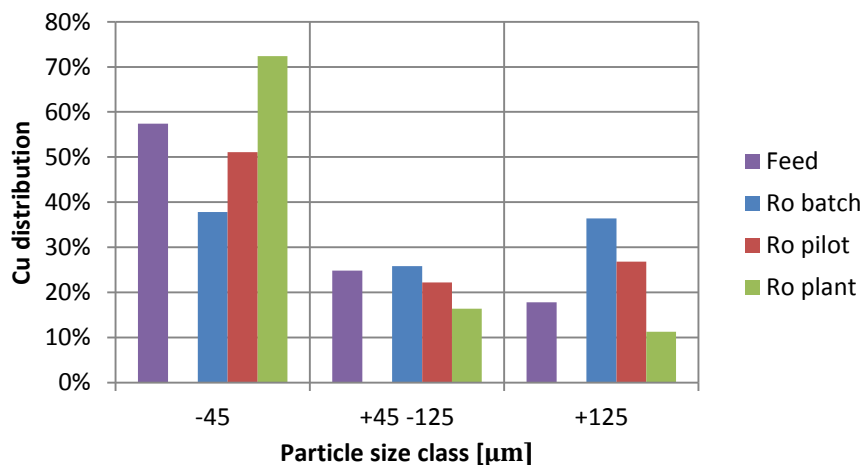
Figure 5.30: Copper distribution in feed and tailings over the different size classes in rougher flotation.

63

Scavenger flotation

Since the test work on the rougher flotation revealed a lower recovery of copper in the rougher flotation, the performance of the scavenger flotation will be of importance on the final plant results. The tailings of the scavenger flotation comprised 98,54±0,02% of the total tailings of the flotation plant during the first three months of 2014 (Aitik iPAK, 2014).

Figure 5.31 shows time-recovery model curves for three different size classes in the scavenger flotation. Like in the rougher flotation, the -45 μm size class is poorly recovered in the full scale cells, in comparison to batch flotation. As could be expected, the recoveries on all scales are considerably lower than in the rougher flotation. For the +45 μm particles the low recovery is expected to be a result of poor liberation, since well liberated copper minerals in this size class are mostly recovered in rougher flotation. It must however be noted that especially for the pilot cells the test data points are widely spread, thus resulting in a relatively high uncertainty of these results.
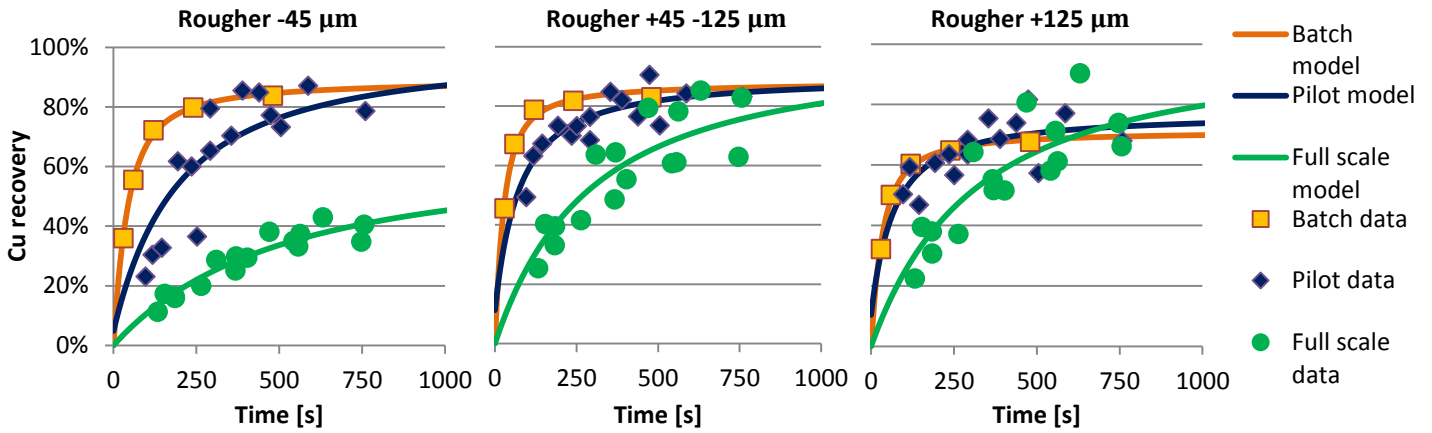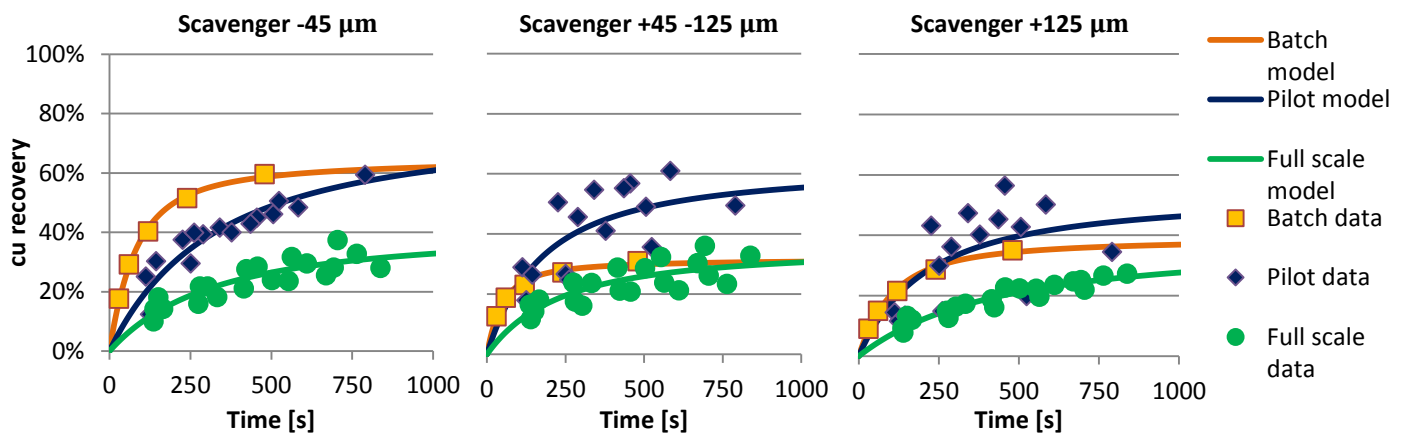

Figure 5.31: Time-recovery test data points and model curves of batch, pilot and full scale scavenger tests for three different size classes.

Figure 5.32 displays the distribution of copper over the three size classes for the flotation tests on different scales for the scavenger flotation. It is notable that the copper contained in the -45 μm size class in the feed is considerably lower than in the rougher tailings shown in figure 5.30 (40% versus 72%). Most likely this is a result of different feed materials and operating conditions, since the test work on rougher and scavenger lines were not performed simultaneously.

A similar profile as for rougher flotation is visible, in which the copper contained in tailings in the -45 μm size class is higher for industrial flotation. The differences are however not as large as in rougher flotation, and a considerable amount of copper is lost through the +125 fraction. The copper loss through the +45 μm particle classes of industrial scale tailings is slightly lower than the feed contains, meaning that the -45 μm copper minerals are also that well recovered in industrial scavenger flotation.
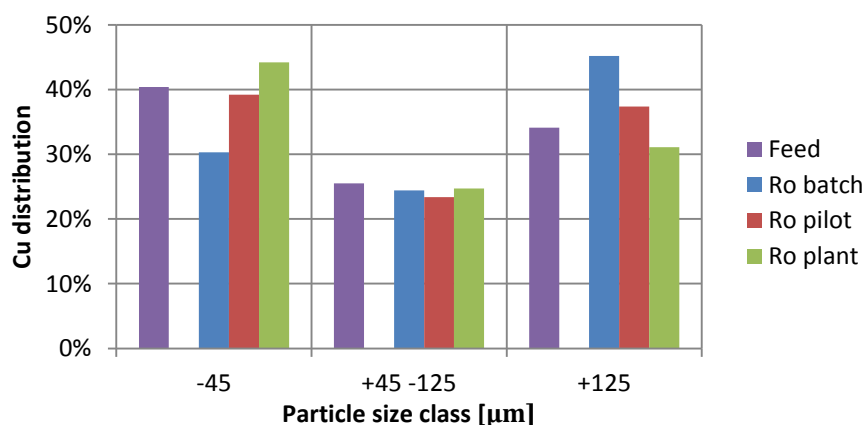
Figure 5.32: Copper distribution in feed and tailings over the different size classes in scavenger flotation.

Time up-scaling factor

Section 3.2.3 covered the calculation of a time up-scaling factor based on a rectangular distribution of the flotation rate constant, as described by Yianatos et al. (2005b). The same method was applied on the test work in this research.

Table 5.12: Maximum recovery (R_∞), maximum flotation rate constant (k_{max}), final test recovery (R), final residence time (τ) and dimensionless recovery (η) of rougher and scavenger test work on all scales.

|		Batch	Pilot	Full scale
Rougher	R_∞	92,3%	99,5%	89,4%
	k_{max} [1/s]	0,0465	0,0030	0,0011
	Test R	88,1%	83,0%	55,0%
	Res. time [s]	480	616 (4 cells)	669 (4 cells)
	η [-]	0,954	0,834	0,622
Scavenger	R_∞	46,0%	84,6%	42,2%
	k_{max} [1/s]	0,0224	0,0012	0,0012
	Test R	41,7%	50,7%	28,1%
	Res. time [s]	480	651 (4 cells)	750 (5 cells)
	η [-]	0,907	0,609	0,674

Table 5.12 shows the model maximum recovery and maximum flotation rate constant of the test work, together with the final recoveries and corresponding dimensionless recovery η, which was defined in equation 3.10 as the ratio of the recovery and the maximal recovery. The dimensionless recoveries of the full scale rougher and scavenger banks were 0,622 and 0,674, respectively. Thus, the corresponding recoveries in batch and pilot plant flotation are:

	Batch (R)	Pilot (R)
η = 0,622 (rougher)	92,3% * 0,622 = 57,6%	99,5% * 0,622 = 61,9%
η = 0,674 (scavenger)	46,0% * 0,674 = 30,7%	84,6% * 0,674 = 57,5%

By using the rectangular model equations and the model parameters that given in table 5.13, the corresponding residence times to reach these recoveries were calculated as:

	Batch (t_{batch})	Pilot (τ_{pilot})
τ = 669 s (rougher)	53,8 s	819 s
τ = 750 s (scavenger)	137 s	2880 s

From these values, a time up-scaling factor can be determined, which was defined in equation 3.9 as the ratio of the full scale and batch (or pilot) residence times. The up-scaling factors for rougher and scavenger flotation with corresponding standard deviations are:

	Batch (τ_{plant}/t_{batch})	Pilot ($\tau_{plant}/\tau_{pilot}$)
Rougher:	12,5 (σ = 0,89)	0,82 (σ = 0,12)
Scavenger:	5,76 (σ = 1,29)	0,30 (σ = 0,11)

The up-scaling factors between batch and full scale flotation are considerably larger than those mentioned in literature, which were shown in table 3.3. The origin of these values can be further evaluated by considering the individual particle size classes, since differences in the kinetics between different cell sizes were already observed, especially for the finest material. The same calculation to determine the up-scaling factor was repeated for the three size classes individually, resulting into the following up-scaling factors:

BOLIDEN

		Batch (τ_{plant}/t_{batch})	Pilot ($\tau_{plant}/\tau_{pilot}$)
Rougher:	-45 µm	12,4	0,89 ($\sigma = 0,14$)
	+45 -125 µm	5,79	1,07 ($\sigma = 0,44$)
	+125 µm	2,98	1,02 ($\sigma = 0,59$)
Scavenger:	-45 µm	3,90	0,71 ($\sigma = 0,52$)
	+45 -125 µm	5,09	0,27 ($\sigma = 0,13$)
	+125 µm	3,98	0,23 ($\sigma = 0,08$)

The up-scaling factors between batch and full scale flotation are derived from the combined concentrates of the batch tests, and thus no standard deviation could be calculated. Therefore these results cannot be considered too reliable, and are only meant as an indication. For the rougher flotation, the very high up-scaling factor seems to be caused by the large difference in fine particle flotation between batch and industrial scale. Figures 5.29 and 5.30 already showed that fine particles float very rapidly in batch flotation, and take a much longer residence time to reach the same dimensionless recovery in industrial flotation.

On the other hand, the factors between pilot and full scale flotation are less varied between size classes, although the standard deviations are large. Strange enough most of the up-scaling factors from pilot to full scale flotation are smaller than 1, thus in fact down-scaling factors. This is caused by higher values of R_∞ in the pilot cell models, which are suspected to be a result of spread data in the pilot cell test results.

The empirical parameter φ, as given in equation 3.9 on page 30, is determined to account for the non-ideal mixing conditions in the (pilot) plant. Since this research does not separately consider the effect of the froth zone, this is automatically included in the φ parameter.

$$\varphi = \frac{[k_{max}]_{plant}}{[k_{max}]_{batch}} \cdot \frac{\tau_{plant}}{t_{batch}} \qquad\qquad (5.8)$$

	Batch φ	Pilot φ
Rougher:	0,305 ($\sigma = 0,019$)	0,307 ($\sigma = 0,018$)
Scavenger:	0,303 ($\sigma = 0,015$)	0,304 ($\sigma = 0,015$)

These results show a very consistent value of φ between the test results of around 0,305, although this value does suggest that the mixing conditions and froth zone have a considerable impact on the flotation kinetics. Yianatos et al. (2005b) already showed that for longer flotation banks the mixing conditions hardly influence differences in the test results between batch and industrial application.

5.4.2 Relating enrichment ratio and mineral recovery

Since it is generally accepted that an increased residence time in the flotation cell does not necessarily improve metallurgical results (Burstein and Filippov, 2010) and this has been shown to apply to the Aitik deposit (Bolin, 2014a), an attempt was also made to model the recovery of copper as a function of the enrichment ratio, according to equation 5.3. However, several of the models, especially for the pilot plant and in a lesser degree for full scale test work, showed to have a poor fit to the models.

Figure 5.33 shows a scatter plot of the copper recovery versus the enrichment ratio in rougher flotation. For the pilot and full scale results the data spread is wide, which also caused the poor model fits. As was shown before, copper recovery in the full scale cells remained low (maximally around 60%). A more detailed look revealed that especially the -45 µm size class had poor copper enrichment in the industrial cells, while the larger fractions had a comparable copper recovery and enrichment ratio. Since no confident conclusions can be drawn based on these data, no further calculations can be done at this point. It is suspected that the relation between recovery and enrichment is strongly dependent on the feed grades and ore type.
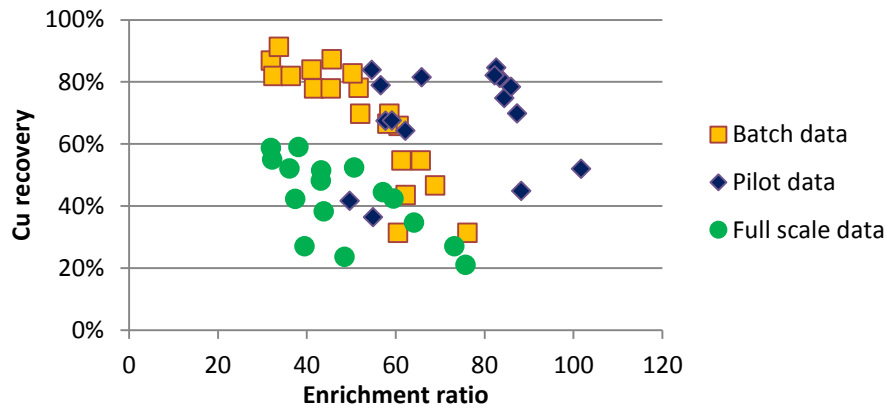
BOLIDEN

Figure 5.33: Copper recovery vs. enrichment ratio in rougher flotation.

5.4.3 Sulphide mineral selectivity

Apart from the copper sulphide minerals that are recovered by true flotation, there are other minerals recovered by the flotation system, which negatively affect the concentrate copper grade. Part of the unwanted material is recovered by entrainment, entrapment or incomplete mineral liberation, which will be covered in the next section. Another important part consists of sulphide minerals that are similarly recovered by true flotation, but are a result of the imperfect selectivity of the flotation system. Since these sulphide minerals are still recovered by true flotation, their recovery can be at the expense of the floating capabilities of the cell for valuable copper sulphide minerals.

Figure 5.34 displays the Cu/S values of feed, concentrate and tailing streams of the three particle size classes on different flotation scales. As one would expect, the selectivity decreases with the concentrate number and residence time, since the system is optimized for copper sulphide flotation. In batch flotation the Cu/S values are high in the concentrates and low in the tailings, showing good selectivity, especially for particles under 125 μm. For particles smaller than 45 μm the selectivity on pilot scale is comparable, while the full scale tailings under 45 μm have a Cu/S value only slightly lower than in the feed material. The selectivity for particles larger than 125 μm is poor on the pilot scale.

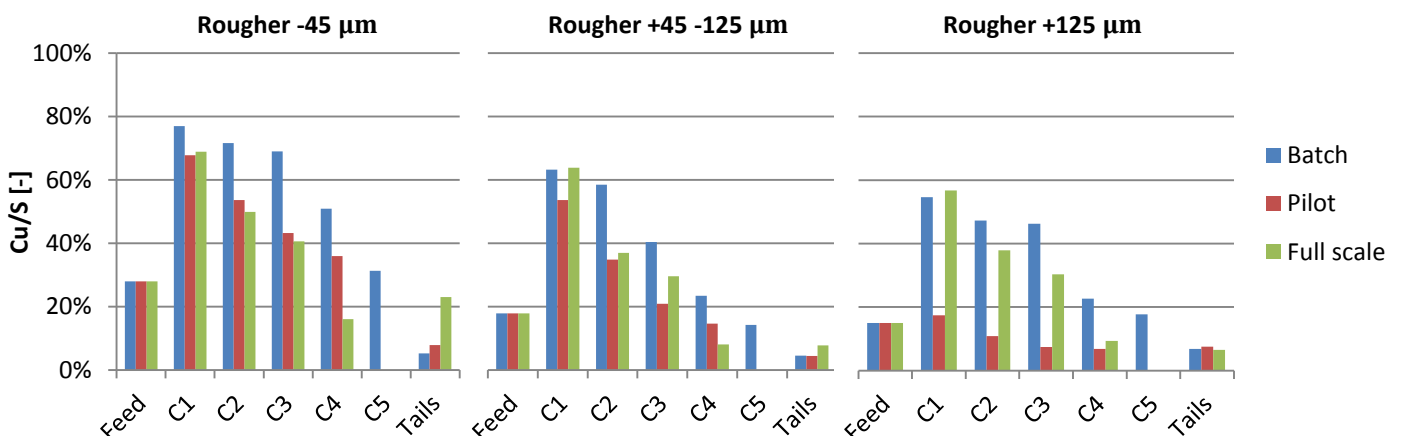*Figure 5.34: Cu/S values for three particle size classes on different rougher flotation scales.*

Figure 5.35 displays the Cu/S values of the process streams on different scavenger flotation scales. In comparison to the pilot and full scale tests, the selectivity in batch flotation shows to be even better than in rougher flotation. Furthermore the same effect of low selectivity for +125 μm particles on pilot scale is visible.
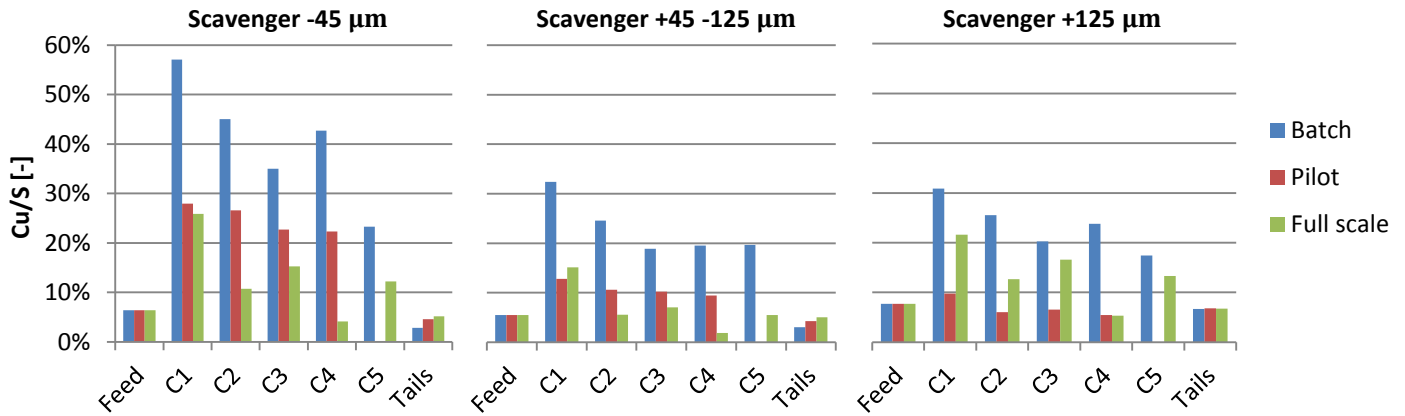
Figure 5.35: Cu/S values for three particle size classes on different scavenger flotation scales.

5.4.4 Relations between water recovery, gangue recovery by entrainment and mass pull

The water recovery for the batch tests was calculated as the fraction of recovered water out of the initial water quantity, while for the continuous tests the water recovery is defined as the fraction of the water feed flow to a flotation cell that is recovered in the concentrate (Zheng, Franzidis and Johnson, 2006).

Figure 5.36 represents a scatter plot of the cumulative water recovery versus the cumulative mass pull of the batch, pilot and full scale test work, with linear trendlines. The relationship between the two parameters is clear for all flotation scales, although the batch test has a distinctly higher water recovery for equal mass pull. The trendlines indicate that on average 0,272% of mass pull is generated for every percent of water recovery in batch tests, while this is 0,464% and 0,942% of mass pull for pilot and full scale cells, respectively. Since several researches mention water recovery as one of the main causes for entrainment (Savassi et al., 1998; Zheng, Franzidis and Johnson, 2006), the superior recovery of -45 μm particles in batch flotation over pilot and full scale flotation may therefore be partially caused by entrainment phenomena instead of 'true' flotation.
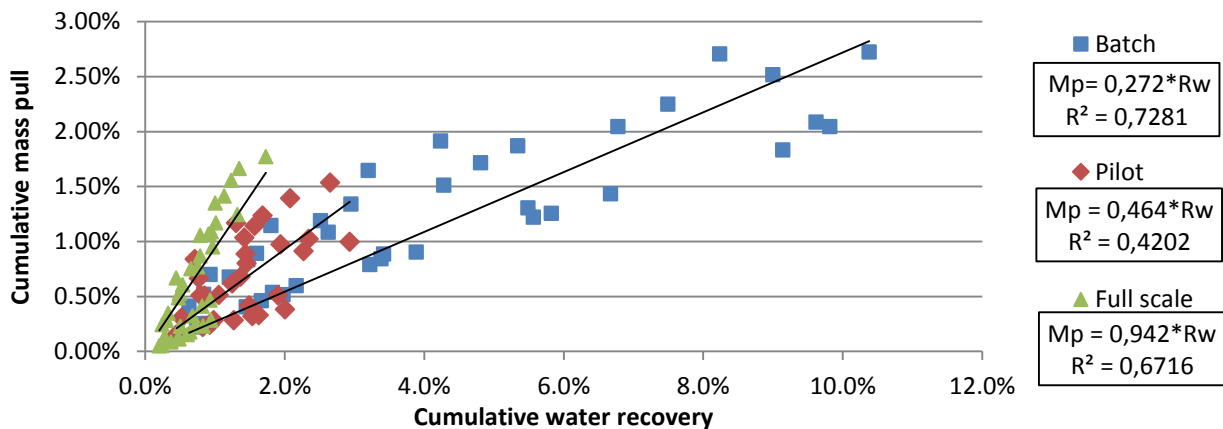
Figure 5.36: Scatter plot with trendlines for the cumulative mass pull vs. the cumulative water recovery.

The entrainment of gangue minerals was estimated with the method described by Yianatos and Contreras (2010a) as presented in section 2.6. This comprises the calculation of the dimensionless entrainment factor EF_i for different particle size classes, and fitting of these data to the model of equation 2.15. The entrainment factor was defined as:

$$EF_i = \frac{R_{G,i}}{R_w} \qquad\qquad (5.9)$$

in which R_w is the water recovery and $R_{G,i}$ is the gangue recovery in particle size class i. Since the batch test has no actual feed flow, an imaginary feed flow was approximated by dividing the concentrate mass flow rate by the mass pull, which would give the mass feed flow in a continuous process.
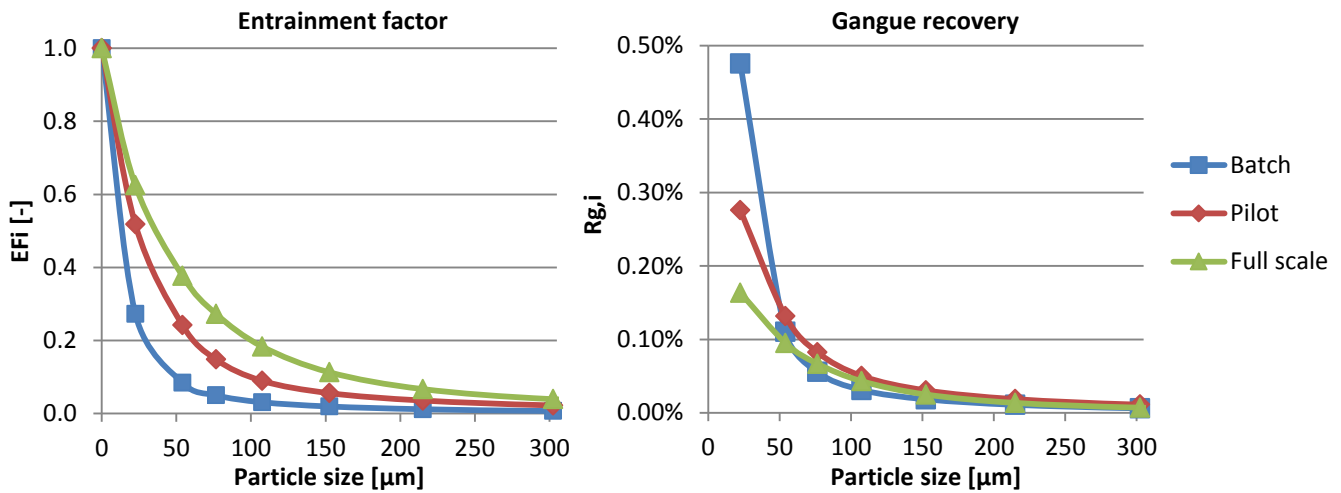
Figure 5.37: Entrainment factor (left) and corresponding gangue mineral recovery (right) versus particle size.

The left graph of figure 5.37 gives the modelled entrainment factors in batch, pilot and full scale flotation cells, averaged from all tests. The entrainment factor is smallest in batch flotation and largest in full scale flotation for all particle sizes, which means that for a fixed water recovery the batch cell will recover the least gangue minerals, while the full scale cells will recover the most gangue minerals.

However, figure 5.36 showed that the water recovery in the batch cells is much higher for a fixed mass pull. According to equation 5.9, multiplication of the entrainment factors with the water recovery will give the gangue recovery for individual size classes, as shown in the right graph of figure 5.37. Note that this method is not able to make a distinction between the mechanisms of gangue recovery, which in this case will mainly be entrainment, and attachment of gangue to incompletely liberated sulphide minerals recovered by true flotation.

The gangue recovery in the right graph of figure 5.37 is shown to be relatively constant between the different scales for particles larger than approximately 50 μm. This can be contributed to recovery by incomplete liberation, as the degree of liberation ideally should be equal for all scales, since the same feed material is used. For particles smaller than 50 μm, the gangue recovery in batch flotation is strongly enhanced, while this is limited for full scale flotation. Since the smallest sieve size used in this research was 45 μm, the relation between entrainment and particle size under 45 μm is not clear, but detailed analysis by microsieving or cyclosizer can provide extra information if required.
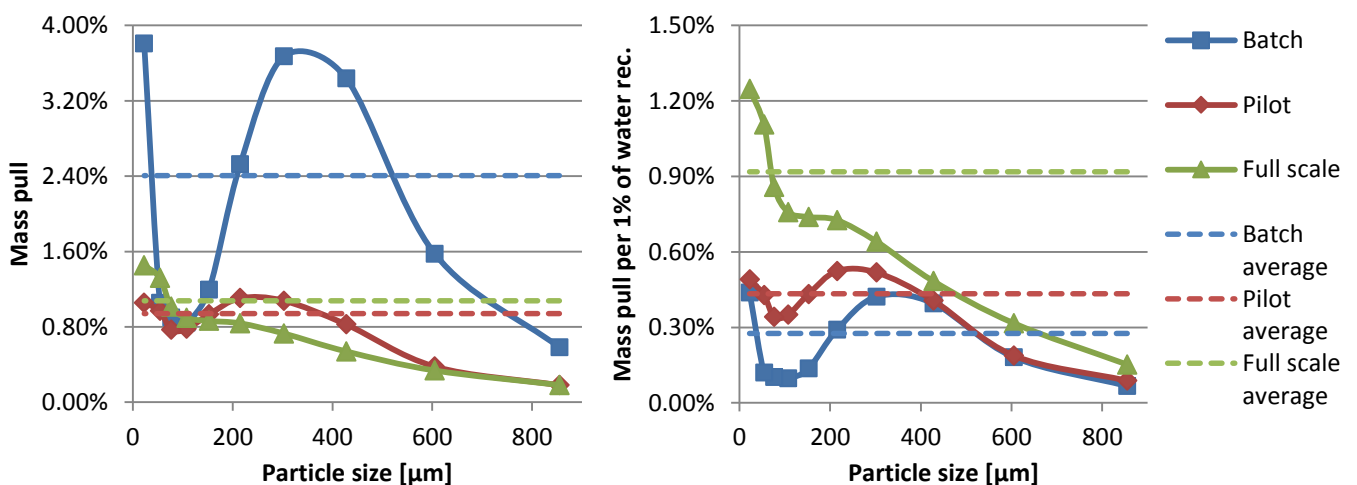

Figure 5.38: Mass pull (left) and mass pull normalized per 1% water recovery (right) vs. particle size.

The left graph of figure 5.38 displays the mass pull for different particle sizes. Apart from the higher values for the finest particles due to entrainment, the mass pull in pilot and especially batch flotation has a peak between approximately 200 and 500 μm. Only in the 'optimal' particle size range for flotation between around 100 μm is the mass pull approximately equal for all scales. The right graph of figure 5.38 shows the same mass pull, but normalized for 1% of water recovery, since it was shown in figure 5.36 that the relations between water recovery and mass pull differ between flotation scales. The mass pull for full scale flotation shows a distinctly higher mass pull at constant water recovery, presumably caused by the low water recovery compared to pilot and batch flotation. For the larger particle sizes (+400 μm) the graphs mostly overlap, indicating that recovery of these particles is not dependent on flotation scale, even though particles of this size are only a small fraction of the total recovered material.

5.4.5 Comparison of cell conditions

The previous sections have revealed some essential differences in operational results for flotation on batch, pilot and industrial scale. The analysis of dimensionless numbers may help to explain such results, and possibly suggest new areas of research for the future. Since no computational fluid dynamics were possible in this research, the use of this method for up-scaling purposes was not possible, and only some global cell values could be compared. Table 5.13 gives the values of several dimensionless parameters for the flotation cells on different scales.

Table 5.13: Dimensionless parameters for batch, pilot and industrial flotation cells
(no deviation where none is mentioned).

Dimensionless number	Batch (8,0 litre cell)	Pilot	Full scale
Reynolds number	$9,6 \cdot 10^4$	$5,3 \cdot 10^5$	$2,3 \cdot 10^6$
Froude number	1,401	2,264	0,252
Aeration number	0,014 (σ = 0)	0,012 (σ = 0,002)	0,049 (σ = 0,004)

The Reynolds number increases with scale as a result of the increasing impeller dimensions, thus causing a more turbulent system in the impeller zone. The pulp viscosity was calculated with an empirical relation given by Rodrigues et al. (2001):

$$\mu_p = \mu_w \, (1 - \phi)^{-2,5} \hspace{4cm} (5.10)$$

in which μ_w is the water viscosity and ϕ is the volume fraction of solids in the pulp. Newell and Grano (2007) showed that in an industrial flotation cell the highest energy dissipation occurs in the area near the impeller, with a strong decrease of energy dissipation with increasing height and radial position. It is suspected that efficient particle-bubble collisions will need to occur in a much smaller volume fraction of the cell than in laboratory scale.

The Froude number is clearly higher in both batch and pilot cell flotation, as a result of higher impeller rotational speed in these cells. The higher Froude number indicates a higher resistance by inertial forces, and thus a greater energy dissipation by the impeller's movement.

The influence of the aeration number was described by Gupta and Yan (2006), who reported an optimal range of 0,02>Ae>0,05. For smaller values the size and number of bubbles is too small, while for larger values the gaps between the blades are occupied by air and very large bubbles are formed, an effect which is known as *flooding*. These bubbles also unnecessarily occupy volume in the cell. Generally an increasing air flow leads to lower power consumption, due to an increasing proportion of the space within the impeller that is occupied by air instead of pulp. This can lead to a lower circulation rate and the danger of particle settling. When flooding occurs (at Ae > 0,05), the power consumption strongly decreases, and thus optimal operation is reached well below this point (Gupta and Yan, 2006). The aeration number for the industrial flotation cell still falls within the limits given by Gupta and Yan, but is lower for laboratory and pilot scale flotation.

NEW BOLIDEN

5.4.6 Other up-scaling methods

In chapter 3 a number of additional methods are mentioned that were previously used by other researchers for the up-scaling of flotation processes. For all of these methods it has been examined if application to the current research was possible. Unfortunately most methods require either specialized measurement techniques, for example for the bubble surface area flux (S_b) or the bubble surface load (λ_b). Also methods of computational fluid dynamics were not possible to apply, since no advanced software for numerical calculations for flotation cells were available.

Equation 3.4 gives an empirical relation to calculate the bubble surface area flux based on other operational parameters. Although the empirical constants obtained by Gorain et al. (1999) are based on other types of flotation cells, the equation is used to estimate S_b. However, relating the calculated values of S_b to the flotation rate constants does not give a clear relation between these variables, as shown in figure 5.39.
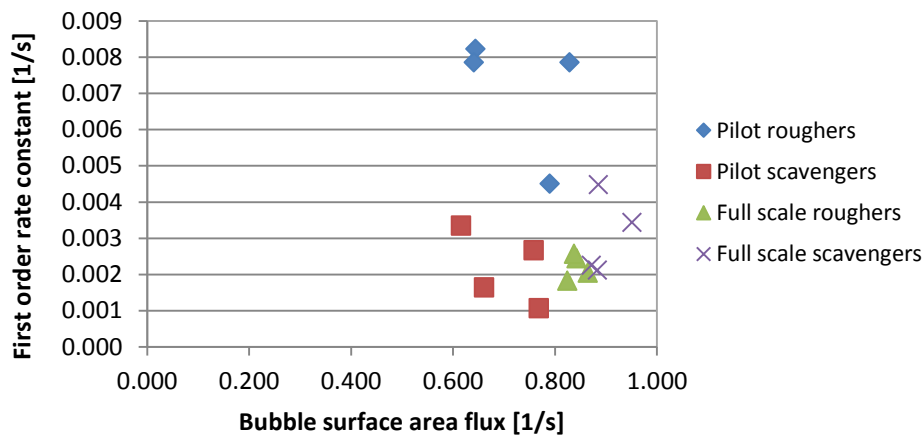

Figure 5.39: Plot of the bubble surface area flux (S_b) vs. the first order flotation rate constant (k).

6. Conclusions and recommendations

Up-scaling of the flotation process has proven to be a complicated issue, mainly as a result of the many different sub-processes that exist within a flotation cell. Previous research in literature depended in most cases on comparison of lab tests with an existing concentrator plant, or on somewhat difficult measurement methods that are generally troublesome to perform on large scale cells in a statistically confident way. The main issue is the familiar concern that each ore type is unique and absolutely no guarantee exists that any up-scaling method will be valid for another ore type. Therefore, the main research question was defined as:

How can a better estimation of industrial flotation performance be made based on lab tests?

Experience has shown that the rate at which minerals float in an industrial operation is several times slower than for the same material in a laboratory batch test. This suggests that during up-scaling certain variables are changed, causing the same material to float slower. Apart from the longer transport distances, the functioning of several flotation sub-processes forms the root of the dissimilarities. To obtain more insight on why such differences arise, the first partial research question concerned:

1. What causes the differences in results between laboratory and industrial flotation?

Comparison of batch flotation tests in cells of different volumes gave useful insight in the effects of up-scaling. Laboratory batch tests revealed a higher flotation rate constant in the smallest cell (2,5 litre), while the maximum recovery had its highest value in the largest cell (8,0 litre). The smaller quantity of total floatable minerals in the 2,5 litre cell was recovered more quickly, but was also accompanied by a higher degree of fine particle entrainment and a lower concentrate grade. This was also shown by the lower copper recoveries in the smallest flotation cell for at any value of the enrichment ratio. The cause of a higher final copper recovery in the 8,0 litre cell was unclear, although the difference with the other cells was not excessive.

With the use of a factorial design it was confirmed that not only cell size, but also operational parameters like grinding time and the weight percentage solids have significant influence on flotation performance, especially the metal grades. Since an industrial flotation plant will have variation in pulp density and fineness of the grind, for example due to alterations in ore hardness and initial fineness, this will give variation in rougher circuit performance and will therefore also lead to variable loads on the scavenger and especially cleaner circuits. Furthermore it shows that results of lab flotation tests to be used for up-scaling are susceptible to operating conditions. The contribution of entrainment was especially high for the longer flotation times when most valuable metals are recovered, indicating that the selection of the point of time at which a comparison between lab and industrial flotation is made is important.

Cell characterization and comparison of flotation on batch, pilot and industrial scale uncovered that one of the main differences between laboratory and industrial flotation is the behaviour of fine particles. Both the maximum recovery and flotation kinetics of fine minerals were evidently better in batch flotation, while the industrial cells showed to have zones of fine material segregation below the froth phase. The main problem with the pilot plants was the sensitivity of the mass pull to the air flow rate; the change in air flow between no concentrate flow and a relatively large concentrate flow was minimal. If more consistency can be found in pilot plant test results, it may provide a good link between lab and industrial flotation, since the kinetics and time-recovery profile are much closer to lab flotation, assuming the pilot plant results in this research are representative.

The second partial research question concerned:

2. What are the influences of the different sub-processes of the flotation cell on its performance?

Sampling of the industrial flotation equipment as a profile of depth showed a number of distinct zones within the cells, while most models generally assume the pulp zone to be perfectly mixed. The lower half of the cell was well mixed as a result of the turbulence caused by the impeller zone. On the other hand, the low turbulent zone in the upper cell half showed effects of accumulation of fine particles and copper minerals under the froth zone.

It is believed that a part of the differences in results between lab and industrial scale can be attributed to the more turbulent nature of the batch flotation cell as a whole, which promotes particle-bubble collisions. The laminar flow regime in the quiescent zone of the industrial flotation cell is too low energetic to collect hydrophobic particles that – for any reason – have not been recovered by the froth zone into the concentrate. However, the low downward gravitational force of fine particles and predominantly upward flow regime prevent the recirculation to the high energetic mixing zone, where particle-bubble collisions can recollect the material, or where the material can reach the tailing outlet.

Moreover, the laboratory cell lacks the presence of a quiescent zone, while the froth zone, which is already thin compared to industrial flotation, acts as the only real upgrading zone. This leads to much faster recovery of the floatable minerals, but is also associated with the recovery of more gangue minerals. The pulp zone and froth zone of the industrial cells seem to work as a stronger separation mechanism than those of the laboratory flotation cell.

An important question is if the presence of the accumulation zones will aggravate when even larger cells are used, and thus for an equal recovery the concentrate flow has to increase. This could increase the upward flow velocity, causing more material with low hydrophobicity to reach the upper part of the pulp zone. This brings forward the third partial research question:

3. What could happen during further up-scaling of industrial flotation cells?

In total, up-scaling of a flotation cell brings forward a number of important considerations. Firstly, a proportional scale-up will lead to a net reduction in surface area per volume of flotation capacity, since surface area is related to the square and volume to the third power of the cell dimensions. Meanwhile, the lip length is related to the first power of the cell dimensions.

Figure 6.1 gives the net loss of lip length and surface area during a proportional scale-up. The reduced cell surface area and lip length can lead to increased froth velocities, both vertical and horizontal, since more material needs to be transported per unit of froth surface area, and this material on average will have a longer transport distance to the launder. Internal launders may help to remedy this problem, but the vertical froth velocity will nevertheless increase. A higher froth velocity generally makes the froth less selective, leading to lower concentrate grades. For compensation the froth thickness can be increased to create a similar froth residence time, which would go at the cost of the flotation volume.
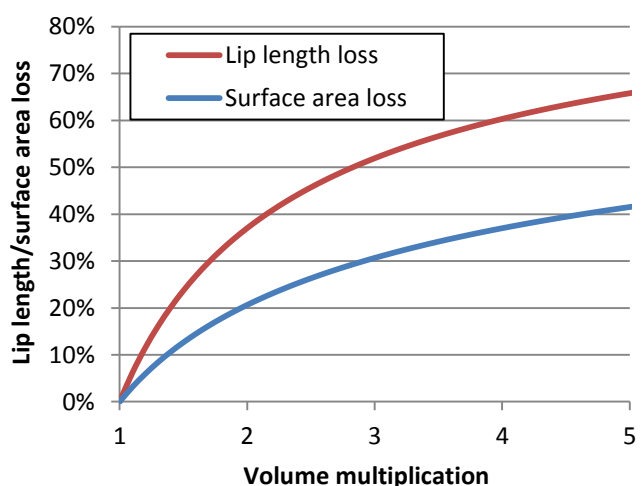

Figure 6.1: Net loss of lip length and surface area during scale-up.

73

Table 3.1 even showed an increasing trend in the height/diameter ratio of Outotec TankCell designs, meaning that even less surface area and lip length is available per mass unit of floatable material than during a proportional scale-up. Additionally, cells with a reduced surface area per volume have the risk of reaching a limitation of the carrying capacity in the first rougher cells or in cleaner flotation, where much floatable material is available and bubble surfaces are maximally covered.

Increasing transport velocities in the pulp zone and froth zone can also be at the cost of selectivity. A higher pulp velocity may enhance the upward transport of weakly hydrophobic particles that cannot be recovered by the froth zone, and could intensify the formation of an accumulation zone as was found in this research. Such an effect can however only be speculated and not be predicted with certainty, but since it seems to be related to large flotation cells, it can be one of the consequences of up-scaling.

Varying of the height and width of a flotation cell design brings forward a number of advantages and disadvantages. Flotation cells of equal volume, reduced height and increased width are reported to have a larger risk of solid sedimentation near the cell walls, due to the low turbulence in these zones. This may lead to a loss of effective flotation volume and reduced metallurgical performance caused by sediments obstructing the proper flow paths. Since sedimentation is not an uncommon problem at the Aitik concentrator, the choice for such cells should be well-substantiated for any similar ore.

Altogether, these considerations can be used to answer the main research question and give a number of recommendations on how a better estimations of industrial flotation performance can be made based on laboratorial test work.

How can a better estimation of industrial flotation performance be made based on lab tests?

Based on the differences that have been identified between lab and industrial flotation, the research can be continued with tests that may provide new insight in up-scaling of flotation. One of the main differences was found in the behaviour of fine particles. The recovery, enrichment and selectivity of particles larger than 45 μm were found to differ much less between the different scales, although the pilot plant test results lack confidence.

It is advised to henceforth use the 8,0 litre cell for laboratory tests, unless this is not possible or when the available amount of ore is limited. This cell has shown to give the lowest amount of entrainment and the highest maximum recovery, although the cause of this last observation is not well understood. Furthermore this cell has a slightly higher and slimmer design, which presumably gives a zone with lower turbulence in the upper part of the cell, creating a small quiescent zone to give extra selectivity in comparison to the smaller batch cells. Finally, the larger pulp volume will be less sensitive to inaccuracies in chemical addition and sampling time intervals assigned to different concentrates.

The froth recovery has been reported by Finch and Dobby (1990) to be near 100% in batch flotation, and in the range of 50-80% in industrial flotation. Although in this research no measurements of froth recovery were done, it is also likely that differences in froth recovery exist for different particle sizes. Especially the fine material showed accumulation zones under the froth, indicating a relatively low froth recovery. Since the froth of an industrial cell is much thicker than the froth of a lab cell, the residence time of particles in the froth is also much longer. A method to determine froth recovery can separate the enrichment sub-processes of the collection zone and the froth zone. One method to measure froth recovery was described by Rahman et al. (2013).

An alternative is a measurement of the bubble load. Such a measurement would allow calculation of carrying rate and carrying capacity within flotation cells of different sizes, and give the possibility of investigating a possible relationship between carrying rates and metal recovery, while varying a factor like the air flow rate. Moreover, the bubble load measurement allows calculation of the froth recovery, since the recovery of the pulp zone can be determined, and the product of pulp zone recovery and froth

recovery is equal to the total cell recovery. Figure 6.2 shows the mass flow rate of copper minerals in different size classes on the bubble load surface and in the cell concentrate. It can be observed that a good correlation exists, and that the concentrate mass flow is slightly lower due to a froth recovery under 100%. A method to measure bubble loads in the pulp zone of an industrial flotation cell was described by Seaman et al. (2004).
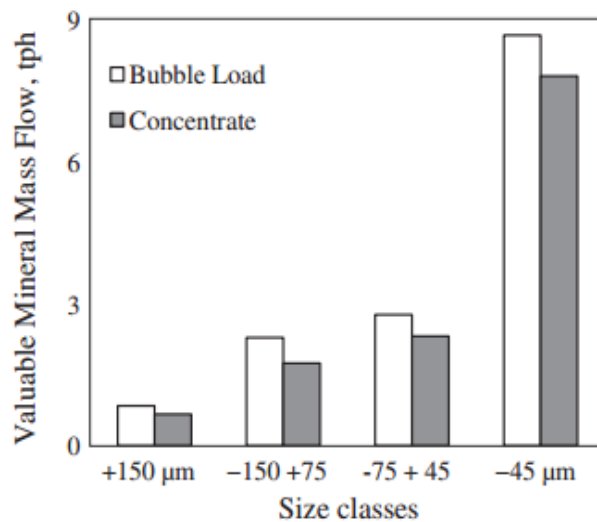

Figure 6.2: Mass flow rate of copper minerals on bubble surfaces and in cell concentrate (Yianatos et al., 2014).

Plans have been mentioned by Bolin (2014b) to create a pilot size flotation cell with the possibility of an adjustable cell height. Since the impeller dimensions will be fixed, the size of the mixing zone will also be constant. Minor changes in turbulence can arise from varying impeller speed and air flow rate, but these factors are normally constant when they are not subject of investigation. The remainder of the cell above the mixing zone will therefore function as quiescent zone or froth zone, depending on the pulp level.

Especially effects of segregation in the quiescent zone, as observed in the industrial cells, are thought to be of interest. A cell that is fairly high and narrow will have low turbulence under the froth zone, and accumulation zones could develop. By varying the cell height and pulp level, several combinations can be tested where the volume fractions of the mixing zone, quiescent zone and froth zone are different, and the influence of each of these zones on the flotation cell transport and accumulation phenomena can be determined. Additionally, the bubble load measurement can be used to evaluate the recovery of valuable minerals, but also gangue minerals over the specific sections of the cell.

7. References

Ahmed, N., Jameson, G.J., 1989, *Flotation Kinetics*, Mineral Processing and Extractive Metallurgy Review 5, pp. 77-99.

Aitik iPAK, 2014, Boliden's internal Aitik processing plant information system [Accessed 13-05-2014].

Arbiter, N., 2000, *Development and scale-up of large flotation cells*, Mining Engineering, Vol. 52, No. 3, pp. 28-33.

Ata, S., 2012, *Phenomena in the froth phase of flotation – A review*, International Journal of Mineral Processing 102-103, pp. 1-12.

Ata, S., Jameson, G., 2013, *Recovery of coarse particles in the froth phase – A case study*, Minerals Engineering 45, pp. 121-127.

Barreto, H., Howland, F.M., 2006, *Introductory Econometrics: Using Monte Carlo simulation with Microsoft Excel*, Cambridge University Press, Chapter 23: Bootstrapping, pp. 709-728, Available (including Excel add-ins) at: <http://www3.wabash.edu/econometrics/index.htm> [Accessed 27-01-2014].

Boliden, 2008, *Outotec TankCell-160 Tank Assembly Scheme for Boliden Aitik*.

Boliden, 2014, Company website, <http://www.boliden.com> [Accessed 13-05-2014].

Bolin, N.J., 2014a, *Aitik Strategy – Study of flotation capacity in the rougher scavenger flotation*, Boliden Technology internal report.

Bolin, N.J., 2014b, Boliden, Personal communication.

Burstein, M., Filippov, L., 2010, *Scale-up of flotation processes*, Computational Science & Engineering Faculty and Students Research Articles, San Diego State University.

Crawford, R., Ralston, J., 1988, *The influence of particle size and contact angle in mineral flotation*, International Journal of Mineral Processing, Vol. 23, No. 1-2., pp. 1-24.

Derjaguin, B.V., Dukhin, S.S., 1961, *Theory of flotation of small and medium size particles*, Transactions of the Institution of Mining and Metallurgy, Vol. 70, pp. 221-246.

Dobby, G.S., Savassi, O.N., 2005, *An advanced modeling technique for scale-up of batch flotation results to plant metallurgical performance*, Proceedings of the Centenary of Flotation Symposium, Brisbane, Australia, pp. 99-104.

Dowling, E. C., Klimpel, R.R., Aplan, F.F., 1985, *Model discrimination in the flotation of a porphyry copper ore*, Minerals and Metallurgical Processing, pp. 87.

Duan, J., Fornasiero, D., Ralston, J., 2003, *Calculation of the flotation rate constant of chalcopyrite particles in an ore*, International Journal of Mineral Processing, Vol. 72, pp. 227-237.

Eriksson, L., Johansson, E., Kettaneh-Wold, N., Wikström, C., Wold, S., 2000, *Design of Experiments, Principles and Applications*, Umetrics AB, Umeå, Sweden, ISBN: 9197373001.

Espinoza-Gomez, R., Finch, J.A., Yianatos, J.B., Dobby, G.S., 1988a, *Flotation column carrying capacity: particle size and density effects,* Minerals Engineering, Vol. 1, No. 2, pp. 77-79.

Espinoza-Gomez, R., Finch, J.A., Johnson, N.W., 1988b, Column *flotation of very fine particles*, Minerals Engineering 1, pp. 3-18.

Euston, J., 2011, *Engineering and science in flotation cell design*, Metallurgical Plant Design and Operating Strategies, MetPlant August 2011, Perth, pp. 292-311.

Evans, G.M., Doroodchi, E., Lane, G.L., Koh, P.T.L., Schwarz, M.P., 2008, *Mixing and gas dispersion in mineral flotation cells*, Chemical Engineering Research and Design, Vol. 86, pp. 1350-1362.

Finch, J.A., Dobby, G.S., 1990, *Column flotation*, chapter 3, 1st edition, Pergamon Press, London, UK.

Finch, J.A., Xiao, J., Hardie, C., Gomez, C.O., 2000, *Gas dispersion properties: bubble surface area flux and gas holdup*, Minerals Engineering 6, pp. 365-372.

Gorain, B.K., Franzidis, J.P., Manlapig, E.V., 1997, *Studies on impeller type, impeller speed and air flow rate in an industrial scale flotation cell*, Minerals Engineering 10, pp. 367-379.

Gorain, B.K., Harris, M.C., Franzidis, J.P., Manlapig, E.V., 1998, *The effect of froth residence time on the kinetics of flotation*, Minerals Engineering 11, pp. 627-638.

Gorain, B.K., Franzidis, J.P., Manlapig, E.V., 1999, *The empirical prediction of bubble surface area flux in mechanical flotation cells from cell design and operating data*, Minerals Engineering, Vol. 12, No. 3, pp. 309-322.

Gorain, B.K., 2007, Design*, Operating principles and optimization of mechanical flotation cells*, In: *Froth Flotation: A Century of Innovation*, SME, pp. 637-656.

Govender, D., Meadows, D., Lelinski, D., Traczyk, F., 2014, *Large flotation cells in copper processing: Experiences and considerations*, Mining Engineering, February 2014, pp. 24-32.

Grau, R., 2006, *An investigation of the effect of physical and chemical variables on bubble generation and coalescence in laboratory scale flotation cells*, Doctoral Thesis, Helsinki University of Technology.

Greet, C.J., 2010, *The Eureka mine – An example of how to identify and solve problems in a flotation plant*, chapter 1 in: Greet, C.J. (ed.), *Flotation plant optimisation – A metallurgical guide to identifying and solving problems in flotation plants,* pp. 1-33.

Grönstrand, S., Niitti, T., Rinne, A., Turunen, J., Bourke, P., 2006, *Designing flotation cells for optimized flow dynamics,* Metallurgical Plant Design and Operating Strategies, MetPlant September 2006, Perth, pp. 140-159.

Gupta, A., Yan, D.S., 2006, *Mineral Processing Design and Operation*, Elsevier Science & Technology Books, 1st edition, ISBN: 9780444516367, chapter 16: Flotation, pp. 555-603.

Gy, P.M., 1979, *Sampling of Particulate Materials: Theory and Practice*, Elsevier Scientific Publishing Company, ISBN: 0444418261, chapter 4: Sampling Processes, pp. 33-38.

Harbort, G., Schwarz, S., 2007, *Cell Characterisation and Mass Balances at the Boliden Aitik Concentrator*, Boliden internal report, JKTech flotation optimization study commissioned by Boliden Mineral AB.

Harcus, M., 2010, *Economies of Scale*, article in *Mining Magazine* [09-11-2010], available at: <http://www.miningmagazine.com/equipment/economies-of-scale>, [Accessed 23-04-2014].

Harris, C.C., Mensah-Biney, R.K., 1977, *Aeration characteristics of laboratory flotation machine impellers*, International Journal of Mineral Processing 4, pp. 51-67.

Heiskanen, K., 2013, *Flotation research – does advancement require a paradigm shift?,* Proceedings of the 6th International Flotation Conference, Cape Town, South Africa, pp. 1-18.

Imaizumi, T., Inoue, T., 1965, *Kinetic considerations of froth flotation*, Proceedings of the 6th International Mineral Processing Congress, Roberts, A. (ed.), Pergamon Press, Oxford, pp. 581-593.

Jameson, G.J., 2012, *The effect of surface liberation and particle size on flotation rate constants,* Minerals Engineering 36-38, pp. 132-137.

JKTech, 2007, Seminar on flotation, *Measurement, modeling and simulation of flotation circuits*, JKMRC.

Jowett, A., 1974, *Resolution of flotation recovery curves by a differential plot method,* Transactions of the American Society of Mining and Metallurgical Engineers, No. 85, pp. 263–266.

Kalapudas, R., 1985, *A study on scaling-up of laboratory batch flotation data to industrial size flotation*, Proceedings of the 15th International Mineral Processing Congress, Vol. 2, pp. 112-121.

Kelsall, D.F., 1961, *Application of probability assessment of flotation systems*, Transactions of the Institution of Mining and Metallurgy, No. 70, pp. 191-204.

King, R.P., 2001, *Modeling & simulation of mineral processing systems*, Butterworth-Heinemann, 1st edition, ISBN: 0750648848, chapter 9: Flotation, pp. 289-350.

Koh, P., Schwarz, P., 2011, *A novel approach to flotation cell design*, SME Annual Meeting Denver 2011.

Kowalczuk, P.B., Sahbaz, O., Drzymala, J., 2011, *Maximum size of floating particles in different flotation cells*, Minerals Engineering 24, pp. 766-771.

Lambert, A.S., 2003, *Flotation cell choice in mineral flotation*, in: Ralston, J., Miller, J.D., Rubio, J. (ed.), *Flotation and Flocculation*, pp. 221-228.

Lelinski, D., Redden, L.D., Nelson, M.G., 2005, *Important considerations in the design of mechanical flotation machines,* Centenary of Flotation Symposium, Brisbane, pp. 217-223.

Mori, S., Okamoto, H., Hara, T., Aso, K., 1985, *Kinetic studies of fluorite flotation*, Proceedings of the 15th International Mineral Processing Congress, pp. 154.

Morrison, R., 2010, *Mass Balancing Flotation Data*, chapter 3 in: Greet, C.J. (ed.), *Flotation plant optimisation – A metallurgical guide to identifying and solving problems in flotation plants,* pp. 65-81.

Napier-Munn, T.J., 2012, *Statistical methods to compare batch flotation grade-recovery curves and rate constants*, Minerals Engineering 34, pp. 70-77.

Napier-Munn, T.J., 2014, Personal correspondence.

Nelson, M.G., Traczyk, F.P., Lelinski, D., 2002, *Design of mechanical flotation machines*, chapter 8 in: Mular, A.L., Halbe, D.N., Barratt, D.J., *Mineral Processing Plant Design, Practice and Control*, SME, pp. 1179-1203.

Nelson, M.G., Lelinski, D., Grönstrand, S., 2009, *Design and operation of mechanical flotation machines*, chapter 5 in: Malhotra, D., Taylor, P., Spiller, E., LeVier, M., *Recent Advances in Mineral Processing Design*, SME, pp. 168-189.

Nesset, J.E., Hernandez-Aguilar, J.R., Acuna, C., Gomez, C.O., Finch, J.A., 2006, *Some gas dispersion characteristics of mechanical flotation machines*, Minerals Engineering 19, pp. 807-815.

Newcombe, B., Bradshaw, D., Wightman, E., 2012, *The hydrodynamics of an operating flash flotation cell*, Minerals Engineering 41, pp. 86-96.

Newell, R., Grano, S., 2007, *Hydrodynamics and scale up in Rushton turbine flotation cells: Part 1 – Cell hydrodynamics*, International Journal of Mineral Processing, Vol. 81, pp. 224-236.

Outotec, 2014, Company website, <www.outotec.com/> [Accessed 13-05-2014].

Polat, M., Chandler, S., 2000, *First order flotation kinetics models and methods for estimation of the true distribution of flotation rate constants*, International Journal of Mineral Processing 58, pp. 145-166.

Rahman, R.M., Ata, S., Jameson, G.J., 2012, *The effect of flotation variables on the recovery of different particle size fractions in the froth and the pulp*, International Journal of Mineral Processing, Vol. 106-109, pp. 70-77.

Rahman, R.M., Ata, S., Jameson, G.J., 2013, *Froth recovery measurement s in an industrial flotation cell*, Minerals Engineering 53, pp. 193-202.

Rinne, A., Peltola, A., 2008, *On lifetime costs of flotation operations*, Minerals Engineering 21, pp. 846-850.

Rodrigues, W.J., Leal Filho, L.S., Masani, E.A., 2001, *Hydrodynamic dimensionless parameters and their influence on flotation performance of coarse particles*, Minerals Engineering, Vol. 14, No. 9, pp. 1047-1054.

Rosin, P., Rammler, E., 1933, *The laws governing the fineness of powdered coal*, Journal of the Institute of Fuel, No. 7, pp. 29-36.

Runge, K., 2010, *Laboratory Flotation Testing – An Essential Tool for Ore Characterisation,* chapter 10 in: Greet, C.J. (ed.), *Flotation plant optimisation – A metallurgical guide to identifying and solving problems in flotation plants,* pp. 155-173.

Savassi, O.N., Alexander, D.J., Franzidis, J.P., Manlapig, E.V., 1998, *An empirical model for entrainment in industrial flotation plants*, Minerals Engineering, Vol. 11, No. 3, pp. 243-256.

Schubert, H., Bischofberger, C., 1998, *On the microprocesses air dispersion and particle-bubble attachment in flotation machines as well as consequences for scale-up*, International Journal of Mineral Processing, Vol. 52, pp. 245-259.

Schulze, H.J., 1982, *Dimensionless number and approximate calculation of the upper particle size of floatability in flotation machines*, International Journal of Mineral Processing, Vol. 9, No. 4, pp. 321-328.

Schwarz, S., Alexander, D., 2006, *Gas dispersion measurements in industrial flotation cells, Minerals Engineering*, Vol. 19, pp. 554-560.

Seaman, D.R., Franzidis, J.P., Manlapig, E.V., 2004, *Bubble load measurement in the pulp zone of industrial flotation machines – A new device for determining the froth recovery of attached particles*, International Journal of Mineral Processing, Vol. 74, pp. 1-13.

Szatkowski, M., Freiberger, W.L., 1985, *Kinetics of flotation with fine bubbles,* Transactions of the Institute of Mining and Metallurgy, Vol. 94, pp. 61-70.

Tao, D., Luttrell, G.H., Yoon, R.H., 2000, *A parametric study of froth stability and its effect on column flotation of fine particles*, International Journal of Mineral Processing, Vol. 59, No. 1, pp. 25-43.

Trahar, W.J., 1981, *A rational interpretation of the role of particle size in flotation*, International Journal of Mineral Processing, Vol. 8, No. 4, pp. 289-327.

Truter, M., 2010, *Scale-up of mechanically agitated flotation processes based on the principles of dimensional similitude*, MSc Thesis, University of Stellenbosch, South-Africa.

Wills, B. A., 2006, *Mineral Processing Technology*, Elsevier Science & Technology Books, 7th edition, ISBN: 0750644508, chapter 4: Particle size analysis, pp. 90-107, and chapter 12; Froth Flotation, pp. 267-352.

Xia, J., Rinne, A., Grönstrand, S., 2009, *Effect of turbulence models on prediction of fluid flow in an Outotec flotation cell,* Minerals Engineering 22, pp. 850-885.

Yianatos, J.B., Bergh, L.G., Condori, P., Aguilera, J., 2001, *Hydrodynamic and metallurgical characterization of industrial flotation banks for control purposes*, Minerals Engineering 14, pp. 1033-1045.

Yianatos, J.B., Bergh, L.G., Aguilera, J., 2003, *Flotation scale-up: use of separability curves*, Minerals Engineering 16, pp. 347-352.

Yianatos, J.B., Bergh, L.G., Diaz, F., Rodriguez, J., 2005a, *Mixing characteristics of industrial flotation equipment*, Chemical Engineering Science 60, pp. 2273-2282.

Yianatos, J.B., Henríquez, F.D., Oroz, A.G., 2005b, *Characterization of large size flotation cells*, Minerals Engineering 19, pp. 531-538.

Yianatos, J.B., Henríquez, F.D., 2006, *Short-cut method for flotation rates modeling of industrial flotation banks*, Minerals Engineering 19, pp. 1336-1340.

Yianatos, J.B., Moys, M.H., Contreras, F.A., Villanueva, A., 2008a, *Froth recovery of industrial flotation cells,* Minerals Engineering 21, pp. 817-825.

Yianatos, J.B., Larenas, J.M., Moys, M.H., Diaz, F.J., 2008b, *Short time mixing response in a big flotation cell*, International Journal of Mineral Processing, Vol. 89, pp. 1-8.

Yianatos, J.B., Bergh, L., Tello, K., Diaz, F., Villanueva, A., 2008c, *Froth mean residence time measurement in industrial flotation cells*, Minerals Engineering, Vol. 21, pp. 982-988.

Yianatos, J.B., Bergh, L.G., Vinnett, L., Contreras, F.A., Diaz, F., 2010a, *Flotation rate distribution in the collection zone of industrial cells,* Minerals Engineering 23, pp. 1030-1035.

Yianatos, J.B., Contreras, F.A., Diaz, F., 2010b, *Gas holdup and RTD measurement in an industrial flotation cell*, Minerals Engineering 23, pp. 125-130.

Yianatos, J.B., Contreras, F.A., Morales, P., Coddou, F., Elgueta, H., Ortiz, J., 2010c, *A novel scale-up approach for mechanical flotation cells,* Minerals Engineering 23, pp. 877-884.

Yianatos, J.B., Contreras, F.A., 2010a, *Particle entrainment model for industrial flotation cells*, Powder Technology 197, pp. 260-267.

Yianatos, J.B., Contreras, F.A., 2010b, *On the carrying capacity limitation in large flotation cells*, Canadian Metallurgical Quarterly, Vol. 49, No. 4, pp. 345-352.

Yianatos, J.B., Carrasco, C., Bergh, L., Vinnett, L., Torres, C., 2012, *Modelling and simulation of rougher flotation circuits*, International Journal of Mineral Processing, Vol. 112-113, pp. 63-70.

Yianatos, J.B., Carrasco, C., Vinnett, L., Rojas, I., 2014, *Pyrite recovery mechanisms in rougher flotation circuits*, Minerals Engineering online (article currently in press).

Zheng, X., Franzidis, J.P., Johnson, N.W., 2006, *An evaluation of different models of water recovery in flotation*, Minerals Engineering 19, pp. 871-882.

Additional reading

Coleman, R., Dixon, A., 2010, *Tried, tested and proven – 300 m³ flotation cells in operation*, Proceedings of the 25th International Mineral Processing Congress, pp. 3429-3440.

NEW BOLIDEN

8. Appendices

Appendix A: Derivation of carrying capacity equation

Szatkowski and Freiberger (1985) described the bubble surface coverage φ_s by equation A1, in which B is the mass transport of minerals by true flotation, d_B is the Sauter mean bubble diameter, d_P is the Sauter mean particle diameter, ρ_P is the solid density, and Q_G is the gas flow rate.

$$\varphi_s = \frac{B \cdot d_B}{\pi \cdot \rho_P \cdot d_P \cdot Q_G} \qquad (A1)$$

The mass transport is estimated by the product of the bubble load λ_B and the gas flowrate Q_G.

$$B = \lambda_B \cdot Q_G \qquad (A2)$$

Combining equations A1 and A2 gives:

$$\varphi_s = \frac{\lambda_B \cdot d_B}{\pi \cdot \rho_P \cdot d_P} \qquad (A3)$$

The superficial gas velocity J_G is defined as the gas flowrate Q_G divided by the cross-sectional area A_C.

$$J_G = \frac{Q_G}{A_C} \qquad (A4)$$

The carrying rate is equal to the mineral mass transport B divided by the cells cross-sectional area at the froth-pulp interface, A_C.

$$C_R = \frac{B}{A_C} \qquad (A5)$$

Substituting equations A2 and A4 into equation A5 gives:

$$C_R = \lambda_B \cdot J_G \qquad (A6)$$

The equation for the bubble surface area flux is given by:

$$S_B = 6 \cdot \frac{J_G}{d_B} \qquad (A7)$$

By substituting equations A3 and A7 into equation A6, the following relation for carrying rate is obtained:

$$C_R = \varphi_s \cdot \frac{\pi}{6} \cdot S_B \cdot d_P \cdot \rho_p \qquad (A8)$$

The carrying capacity C_A is defined as the maximum carrying rate, or in other words when the bubble surface coverage is maximal. Since part of the minerals in mechanical cells will be recovered by entrainment, also the froth recovery R_F has to be taken into account. Adapting equation A8 gives:

$$C_A = \varphi_{S,max} \cdot \frac{\pi}{6} \cdot S_B \cdot d_P \cdot \rho_P \cdot R_F \qquad (A9)$$

NEW BOLIDEN

Appendix B: Boliden Aitik flotation plant flow sheet

NEW BOLIDEN
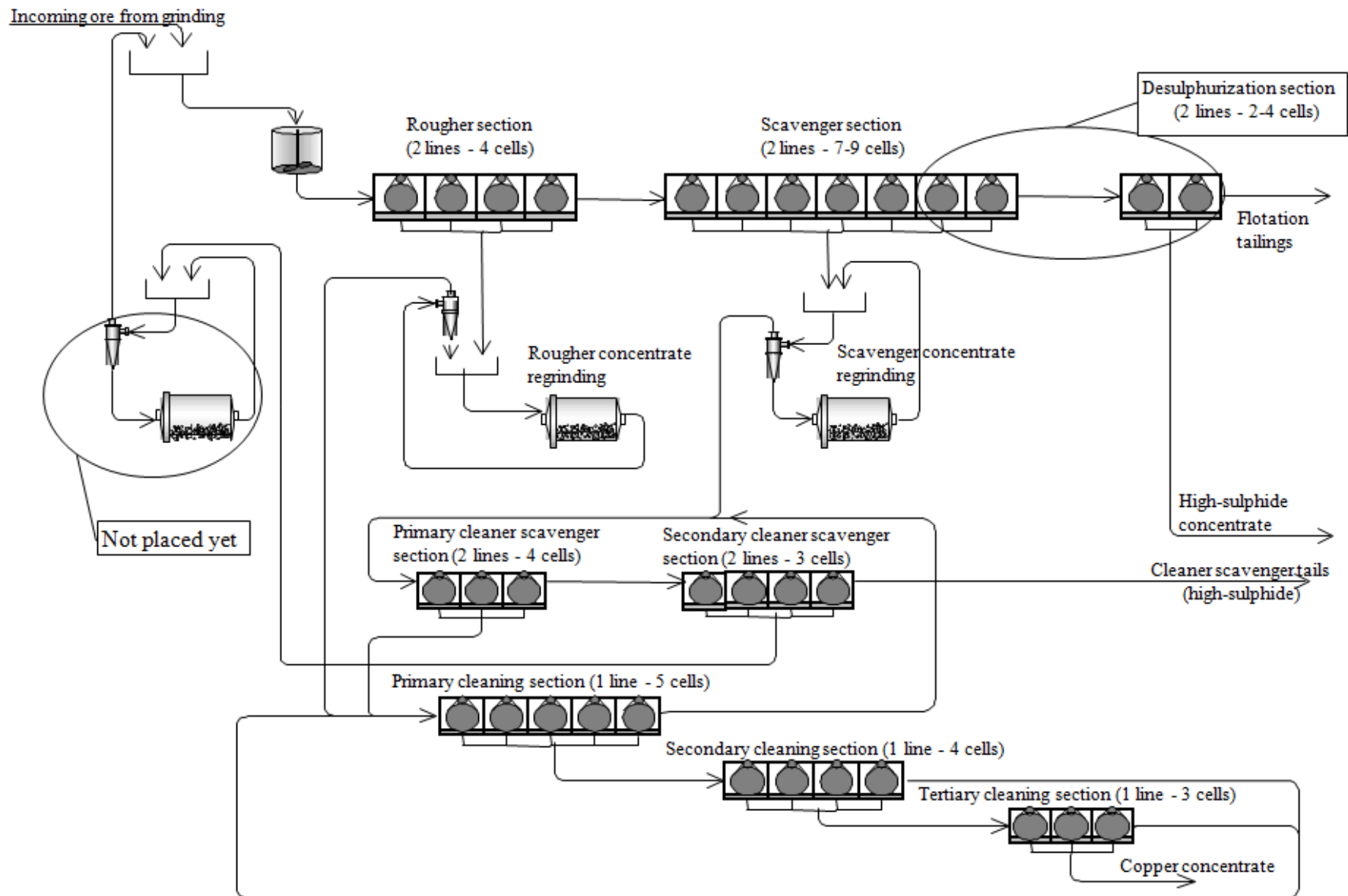
Appendix C: Statistical appendix

Data fitting

The *sum of squares* (*SS*) of two parameters x and y, for example of test data and modelled data, is defined as:

$$SS = \sum_{i=1}^{n}(x_i - y_i)^2 \qquad\qquad (C1)$$

in which x_i are the individual test data points, y_i are the data points predicted by the model equation, and *n* is the total number of data points. The *standard error of the fit* is then given by:

$$SE = \sqrt{\frac{SS}{n-p}} \qquad\qquad (C2)$$

in which *p* is the number of parameters to be fitted to the model. The value of n-p is also named the *degrees of freedom*, and gives the number of values that are free to vary during the regression calculation.

The success of a regression fit can be quantified by a number of parameters. All these parameters are equal to 1 in an ideal case. The R^2 value is named the *coefficient of determination*, and indicates the *goodness of fit* to the linear model (Eriksson et al., 2000). A disadvantage of the R^2 value is that it can be made arbitrarily close to 1, for example by including more tests into the model. R^2 is calculated by:

$$R^2 = 1 - \frac{SS_{res}}{SS_{tot}} \qquad\qquad (C3)$$

in which SS_{res} is the *residual sum of squares*, i.e. the sum of squares between the original data and the modelled data, and SS_{tot} is the total sum of squares of the test data, i.e. the sum of squares between the test data and their average value.

The Q^2 value indicates the *goodness of prediction*, and estimates the predictive power of the model, which is based on the residual sum of squares between the responses and the model. Q^2 gives a lower estimate and R^2 an upper estimate of how well the model predicts outcomes of new experiments. Q^2 is calculated as:

$$Q^2 = 1 - \frac{SS_{press}}{SS_{tot}} \qquad\qquad (C4)$$

in which SS_{press} is the *predictive residual sum of squares*.

Analysis of variation (ANOVA) table

Analysis of variation (ANOVA) tables are used to construct a statistical test in order to determine if the means of specific data sets are equal or different. For example, when two data sets are compared, a specified model is fitted to both data sets individually, and to the combined data set as a whole. An example of an ANOVA table is given in figure 5.10 on page 51.

Several parameters are given from left to right in the ANOVA table. The first are the *degrees of freedom* (DF), which is the number of values in a calculation that is free to vary, equal to the amount of tests minus the amount of variables to be fitted. Secondly, the sum of squares (SS) of the original data and the modelled data is given, as explained above and as defined in equation E1. For the shared data the sums of squares of both data sets are added up. The *mean square* (MS) is another term for the variance, and can be calculated as the sum of squares divided by the degrees of freedom (SS/DF). The *F*-parameter is used to compare factors of the total deviation according to an F-distribution. The F-distribution is used because it uses the ratio of two scaled sums of squares. The *p*-parameter gives the chance that the regression fit is different from the test data, and for a 95% confidence interval, p has to be smaller than (100-95)/100% = 0,05. If this criterion is not satisfied, the model fit is insufficient, and thus the model of the combined data sets is unreliable, meaning that the data sets are proved to be statistically different.